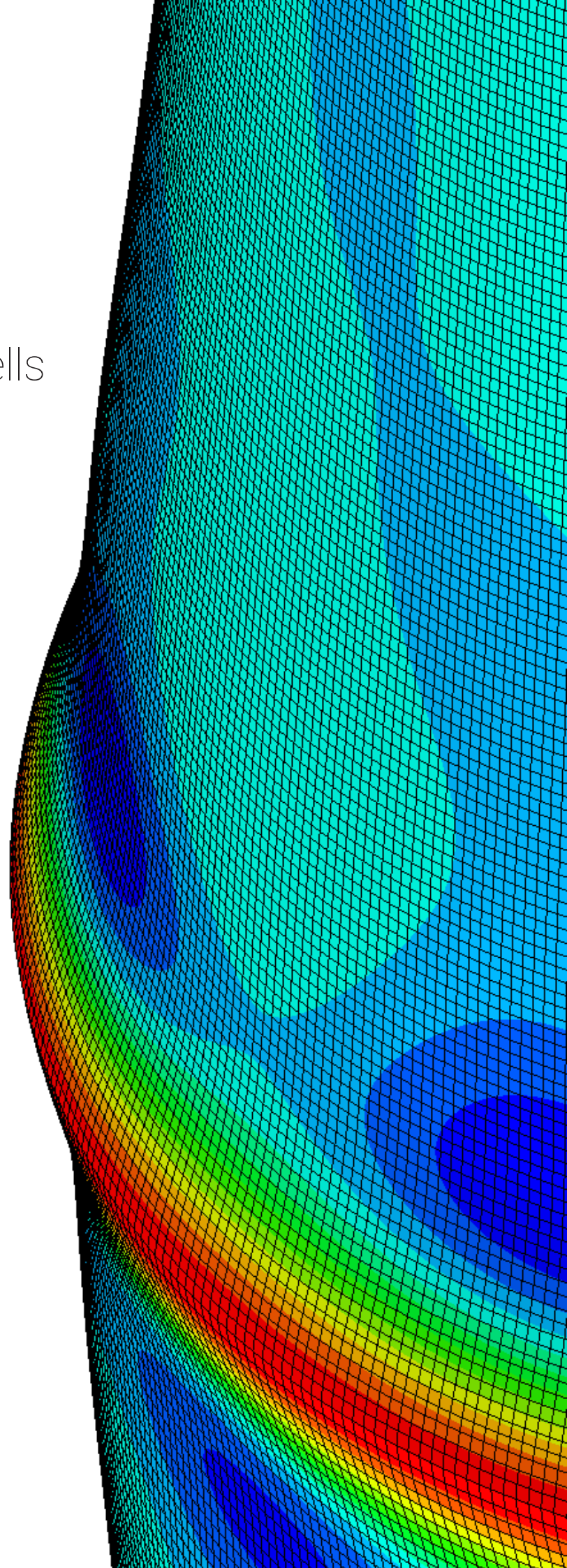


# Buckling analysis of sandwich composite cylindrical-conical shells

T.K. Bolton





# Buckling analysis of sandwich composite cylindrical-conical shells

by

T.K. Bolton

to obtain the degree of Master of Science  
at the Delft University of Technology,  
to be defended publicly on Tuesday Februari 11, 2020 at 12:30.

Student number:	4282752
Project duration:	Januari 14, 2019 – Februari 11, 2020
Thesis committee:	Prof. dr. C. Bisagni      Chair
	Dr. S. G. P. Castro,      First
	Dr. D. M. J. Peeters,    Second
	Ir. M. T. Rudd,          Third

An electronic version of this thesis is available at <http://repository.tudelft.nl/>.



# Abstract

Cylindrical shells and conical shells have been analysed and tested separately for the last decade. However, due to new manufacturing techniques and the use of composite material systems more complex structures can be made. By combining a cylindrical shell and a conical shell one structural component can be created: a cylindrical-conical shell. This is a potential design solution for launch vehicle structures, but there is limited research available about it. Not much is known about the buckling behaviour or imperfection sensitivity of these structures, especially not for sandwich composite shells. Moreover, there are no design guidelines for the buckling of sandwich composite cylindrical-conical shells. SP-8007 and SP-8019 are commonly used guidelines for the design of launch vehicle structures; however, these are only valid for cylindrical shells and conical shells separately. These guidelines also only address composite shells and do not account for sandwich composite shells. The buckling behaviour and imperfection sensitivity has to be fully understood in order to develop new guidelines for sandwich composite cylindrical, conical, and cylindrical-conical shells. Therefore, the purpose of this research is to better understand the buckling behaviour and imperfection sensitivity of sandwich composite cylindrical, conical, and cylindrical-conical shells.

The research focuses on using finite element analysis to study the buckling behavior and imperfection sensitivity of the shells. Models are created of the sandwich composite cylindrical shell, conical shell, and cylindrical-conical shell. Different modelling techniques are compared to find out how to represent a sandwich composite shell. This is done by performing an element study, a mesh convergence study, and a study on the analysis parameters. Moreover, the buckling behavior of the individual shells are compared with the buckling behavior of the combined structure. Different shell geometries such as height of the cone, angle of the cone, and radius of curvature at the transition are used for the comparison. To further investigate the difference between the shells, both linear and non-linear analyses are performed. A comparison is made between the buckling loads, mode shapes, and force-displacement graphs. To investigate the imperfection sensitivity of the different shells, axisymmetric and eigenmode imperfections are added using different amplitudes based on a percentage of the wall thickness.

From the results it could be observed that the buckling behavior of the sandwich composite cylindrical and conical shells without initial imperfections can be captured by both the eigenvalue analysis and the dynamic implicit analysis. However, for the sandwich composite cylindrical-conical shell the eigenvalue analysis is not able to accurately capture the highly non-linear behavior. This can be explained due to the large radial displacement happening at the transition area for the dynamic implicit analysis. The result of this is that the dynamic implicit analysis model is less stiff compared to the eigenvalue analysis model resulting in a lower buckling load. In order to investigate if the non-linear behavior at the interface (location where the conical shell intersects with the cylindrical shell) can be mitigated, a radius of curvature was added to the structure. This was done in order to create a smooth transition at the interface. From the results it could be seen that by adding a radius of curvature the difference between the eigenvalue analysis and dynamic analysis decreased. Moreover, a reinforcement was added to the structure to stiffen the structure at the interface. The results show that this indeed mitigates the non-linear behavior and can give a dynamic implicit buckling load close to the eigenvalue analysis buckling load. From these results it can be concluded that if the non-linear effects are mitigated, the eigenvalue analysis is able to give a buckling load prediction of the sandwich composite cylindrical-conical shell. Moreover, the imperfection sensitivities were compared for the different shells. A similar imperfection sensitivity to geometrical imperfections was observed for the cylindrical shell and conical shell. However, when looking at the imperfection sensitivity of the cylindrical-conical shell it could be seen that the shell is not as sensitive to geometrical imperfections. This can be explained by the fact that the behavior at the transition is dominating the buckling behavior of the whole structure. The results obtained from the thesis show the importance of the non-linear behavior at the transition for the sandwich composite cylindrical-conical shell. This means that for further research it is important that the non-linear effects are included when analysing such a structure.



# Contents

<b>Abstract</b>	<b>iii</b>
<b>List of Figures</b>	<b>vii</b>
<b>List of Tables</b>	<b>xi</b>
<b>Nomenclature</b>	<b>xiii</b>
<b>Acknowledgements</b>	<b>xv</b>
<b>1 Introduction</b>	<b>1</b>
<b>2 Literature study</b>	<b>3</b>
2.1 Buckling tests . . . . .	3
2.1.1 Test setup . . . . .	3
2.1.2 Difference between the theoretical and experimental buckling load . . . . .	5
2.2 Imperfection analysis . . . . .	9
2.2.1 Knockdown factor using the NASA design guidelines . . . . .	9
2.2.2 Perturbation methods . . . . .	10
2.2.3 Measured imperfections . . . . .	13
2.2.4 Stochastic methods . . . . .	20
2.2.5 Discussion of the methods . . . . .	23
2.3 Modelling techniques . . . . .	23
2.3.1 Cylindrical shell . . . . .	24
2.3.2 Conical shell . . . . .	27
2.3.3 Buckling analysis in Abaqus . . . . .	28
2.3.4 Type of elements . . . . .	30
<b>3 Aim, objective, and research questions</b>	<b>33</b>
<b>4 Sandwich composite cylindrical shell and conical shell</b>	<b>35</b>
4.1 Linear analyses of the sandwich composite cylindrical shell . . . . .	35
4.1.1 Modelling technique . . . . .	36
4.1.2 Mesh convergence study . . . . .	37
4.1.3 Results of linear static analysis and eigenvalue analysis . . . . .	39
4.2 Dynamic analysis of the sandwich composite cylindrical shell . . . . .	43
4.2.1 Sensitivity to displacement rate . . . . .	43
4.2.2 Results of the dynamic implicit analysis . . . . .	44
4.3 Linear analyses of the sandwich composite conical shell . . . . .	46
4.3.1 Modelling techniques . . . . .	46
4.3.2 Mesh convergence study . . . . .	47
4.3.3 Results of linear static analysis and eigenvalue analysis . . . . .	48
4.4 Dynamic analysis of the sandwich composite conical shell . . . . .	52
4.5 Sensitivity to conical height . . . . .	53
<b>5 Sandwich composite cylindrical-conical shell</b>	<b>57</b>
5.1 Modelling techniques . . . . .	57
5.2 Linear analyses . . . . .	58
5.3 Dynamic analysis . . . . .	59
5.4 Mesh comparison . . . . .	60
5.5 Sensitivity to conical height . . . . .	61
5.6 Sensitivity to semi-vertex angle . . . . .	64

<b>6</b>	<b>Investigation of the non-linear behavior of the sandwich composite cylindrical-conical shell</b>	<b>67</b>
6.1	Verification of the dynamic implicit analysis . . . . .	67
6.2	Difference in radial deformation of linear analyses and non-linear analyses . . . . .	69
6.3	Difference in strains right before buckling of linear analyses and non-linear analyses . . . . .	70
6.4	Preloading structure before eigenvalue analysis. . . . .	77
6.5	Buckling load of cylindrical part same as conical part. . . . .	79
6.6	Aluminum cylindrical-conical shell. . . . .	82
6.7	Composite cylindrical-conical shell. . . . .	84
6.8	Effect of radius of curvature at the interface. . . . .	87
6.9	Reinforcing the sandwich composite cylindrical-conical shell by using extra plies at the interface . . . . .	90
<b>7</b>	<b>Sensitivity to geometrical imperfections</b>	<b>95</b>
7.1	Computational time study . . . . .	95
7.2	Axisymmetric imperfection . . . . .	97
7.2.1	Cylindrical shell . . . . .	97
7.2.2	Conical shell . . . . .	99
7.2.3	Cylindrical-conical shell . . . . .	100
7.3	Eigenmode imperfection . . . . .	103
7.3.1	Eigenmode imperfection without preload . . . . .	103
7.3.2	Eigenmode imperfection with preload. . . . .	105
<b>8</b>	<b>Conclusion and recommendations</b>	<b>109</b>
8.1	Conclusion . . . . .	109
8.2	Recommendations . . . . .	111
	<b>Bibliography</b>	<b>113</b>



# List of Figures

2.1	CTA 8.1 test setup [47]. . . . .	4
2.2	The test facility (left) and a scematic representation of the test setup (right) [35]. . . . .	5
2.3	Comparison of the load shortening curves generated by the finite element model and the test result [30]. . . . .	6
2.4	Influence of the imperfections on the normalized buckling load of a quasi-isotropic shell. $W$ = imperfection amplitude scale factor for the geometric imperfection, $T$ = imperfection amplitude scale factor for the thickness variation, and $D$ = imperfection amplitude scale factor for the loading imperfection [24]. . . . .	7
2.5	The ply pieces plotted on the conical shell surface including fiber orientation in degrees [35]. . . . .	8
2.6	Semi-vertex angle of a conical shell. . . . .	9
2.7	Test data for isotropic cylinders subjected to axial compression including the lower bound curve [61]. . . . .	10
2.8	Proposed perturbation methods [55]. . . . .	11
2.9	Buckling load due to perturbation [39]. . . . .	11
2.10	SBPA thresholds and empirical data [55]. . . . .	12
2.11	Load vs. displacement curves for the CTA 8.1 using FEM and experimental test [47]. . . . .	14
2.12	Geometrical imperfection of the sandwich composite barrel [46]. . . . .	15
2.13	Numerical and experimental results of three composite cylindrical shells [23]. . . . .	16
2.14	Measured radial imperfection pattern of the CTA 8.1 [48]. . . . .	17
2.15	conical shell with imperfection pattern and 10x amplitude [48]. . . . .	17
2.16	Measured imperfection surface of conical shell scaled by a factor 100 [35]. . . . .	18
2.17	Thickness plot of the conical shell [35]. . . . .	18
2.18	Load vs. displacement graphs for the conical shells [35]. . . . .	19
2.19	Different ply angle imperfections used for the K08 cone [35]. . . . .	20
2.20	Block diagram of the probability based methodology [11]. . . . .	21
2.21	Predicted bounds of the buckling load of a composite cylindrical shell [23]. . . . .	22
2.22	CTA 8.1 finite element model [47]. . . . .	24
2.23	Sketch of FE model including load introduction and degrees of freedom [14]. . . . .	26
2.24	FE model of conical shell with degrees of freedom [48]. . . . .	28
2.25	Post buckling shape of the experimental test [10]. . . . .	29
2.26	Post buckling shape of the numerical model [10]. . . . .	29
4.1	Through the thickness mesh of the different element models. . . . .	37
4.2	Finite element model of the sandwich composite cylindrical shell with reference points. . . . .	37
4.3	Regular mesh of the sandwich composite cylindrical shell using a mesh size of 20 mm. . . . .	38
4.4	First buckling mode shapes of the sandwich composite cylindrical shell using different mesh sizes. For generating the figures a scaling factor of 30 was employed. . . . .	39
4.5	Force-displacement graphs of the sandwich composite cylindrical shell using a displacement rate of 10 mm/s, 5 mm/s, 2 mm/s, and 1 mm/s. . . . .	44
4.6	Force-displacement graph of the sandwich composite cylindrical shell. Whereas, (a), (b), (c), and (d) represent the different phases of deformation. . . . .	45
4.7	Deformation shapes in radial direction of the sandwich composite cylindrical shell with a scaling factor of 1. Whereas, (a), (b), (c), and (d) represent the different phases of deformation and $U_1$ denotes the out of plane deformation. . . . .	45
4.8	Finite element model of the sandwich composite conical shell with reference points. . . . .	46
4.9	Problem with the cone edges when extruding the S4R model. . . . .	47
4.10	Regular mesh of the sandwich composite conical shell using a S4R element and a mesh size of 20 mm. . . . .	47

4.11	First buckling mode shapes of the sandwich composite conical shell using different mesh sizes. For generating the figures a scaling factor of 30 was employed. . . . .	48
4.12	Force-displacement graph of the sandwich composite conical shell. Whereas, (a), (b), (c), and (d) represent the different phases of deformation. . . . .	52
4.13	Deformation shapes in radial direction of the sandwich composite conical shell with a scaling factor of 1. Whereas, (a), (b), (c), and (d) represent the different phases of deformation and U1 denotes the out of plane deformation. . . . .	53
4.14	First buckling mode shape of the sandwich composite conical shells with different heights. For generating the figures a scaling factor of 30 was employed. . . . .	54
4.15	Force-displacement graphs of the sandwich composite conical shells with a height of 800 mm, 600 mm, 400 mm, and 200 mm using the SC8R element model. . . . .	54
5.1	First three buckling mode shapes of sandwich composite cylindrical-conical shell using the S4R element model. For generating the figures a scaling factor of 30 was employed. . . . .	59
5.2	Force-displacement graph of sandwich composite cylindrical-conical shell. Whereas, (a), (b), (c), and (d) represent the different phases of deformation. . . . .	60
5.3	Deformation shapes in radial direction of the sandwich composite cylindrical-conical shell with a scaling factor of 1. Whereas, (a), (b), (c), and (d) represent the different phases of deformation and U1 denotes the out of plane deformation. . . . .	60
5.4	First buckling mode shapes of the sandwich composite cylindrical-conical shell with different conical heights. For generating the figures a scaling factor of 30 was employed. . . . .	62
5.5	Force-displacement graphs of the sandwich composite cylindrical-conical shell with different conical heights. . . . .	63
5.6	Deformation shapes right before buckling of the sandwich composite cylindrical-conical shell with different conical heights. For generating the figures a scaling factor of 1 was employed. . . . .	63
5.7	First buckling mode shapes of the 1200 mm sandwich composite cylindrical-conical shell with different semi-vertex angles. For generating the figures a scaling factor of 30 was employed. . . . .	64
5.8	Force-displacement graphs of the 1200 mm sandwich composite cylindrical-conical shell with different semi-vertex angles. . . . .	65
5.9	Deformation shapes right before buckling of the 1200 mm sandwich composite cylindrical-conical shell with different semi-vertex angles. For generating the figures a scaling factor of 1 was employed. . . . .	66
6.1	Force-displacement graphs obtained by the non-linear Riks analysis and dynamic implicit analysis of the sandwich composite cylindrical-conical shell. . . . .	68
6.2	Force-displacement graphs obtained by the dynamic implicit analysis using the S4R element model and the SC8R element model of the sandwich composite cylindrical-conical shell. . . . .	69
6.3	Radial deformation of the sandwich composite cylindrical-conical shell at a displacement of -7.12 mm in axial direction. For generating the figures a scaling factor of 20 was employed. . . . .	70
6.4	Strain distribution of the first ply in different directions of the dynamic implicit analysis and linear static analysis. . . . .	74
6.5	Strain distribution of the second ply in different directions of the dynamic implicit analysis and linear static analysis. . . . .	75
6.6	Strain distribution of the third ply in different directions of the dynamic implicit analysis and linear static analysis. . . . .	76
6.7	Force-displacement graph of the sandwich composite cylindrical-conical shell including the eigenvalue analysis points obtained after adding a preload. . . . .	78
6.8	First buckling mode shape of the sandwich composite cylindrical-conical shell determined after adding a preload. For generating the figures a scaling factor of 30 was used. . . . .	78
6.9	First buckling mode shape of sandwich composite cylindrical-conical shell using modified material properties. For generating this figure a scaling factor of 30 was employed. . . . .	79
6.10	Force-displacement graphs of the sandwich composite cylindrical-conical shell using the modified material properties and using the original material properties for the cylindrical shell. . . . .	80
6.11	Radial deformation shape right before buckling of the sandwich composite cylindrical-conical shell using modified material properties. For generating this figure a scaling factor of 1 was employed. . . . .	80

6.12	First buckling mode shape of sandwich composite cylindrical-conical shell using modified material properties. For generating this figure a scaling factor of 30 was employed. . . . .	81
6.13	Force-displacement graphs of the sandwich composite cylindrical-conical shell using the modified material properties and using the original material properties for the cylindrical shell. . . .	82
6.14	First mode shapes of aluminum cylindrical and conical shell. For generating this figure a scaling factor of 30 was employed. . . . .	83
6.15	Force-displacement graph of aluminum cylindrical-conical shell. . . . .	84
6.16	Deformation shapes obtained by the eigenvalue analysis and dynamic implicit analysis of the aluminum cylindrical-conical shell. . . . .	84
6.17	First mode shapes of the 1600 mm and 1200 mm composite cylindrical-conical shell. For generating this figure a scaling factor of 30 was employed. . . . .	86
6.18	Force-displacement graphs of the composite cylindrical-conical shells. . . . .	86
6.19	Radial deformation shapes right before buckling of the 1600 mm and 1200 mm cylindrical-conical shell. For generating this figure a scaling factor of 1 was employed. . . . .	87
6.20	First buckling mode shape of the model including a radius of curvature of 380mm. Scaling factor is equal to 30. . . . .	87
6.21	Force-displacement graphs of the sandwich composite cylindrical-conical shell model with and without radius of curvature. . . . .	88
6.22	Mesh of the 1200 mm shell including different radii of curvature. . . . .	88
6.23	First mode shape of the cylindrical-conical shell using different radii of curvature. A scaling factor of 30 was used. . . . .	89
6.24	Force-displacement graphs of the 1200 mm sandwich composite cylindrical-conical shell model with and without radius of curvature with different values. . . . .	90
6.25	Radial deformation shapes right before buckling for the 1200 mm shell including different radii of curvature. For generating this figure a scaling factor of 1 was employed. . . . .	90
6.26	First mode shape of the reinforced cylindrical-conical shell. For generating this figure a scaling factor of 30 was employed. . . . .	91
6.27	Force-displacement graph of the reinforced cylindrical-conical shell. The linear static and eigenvalue buckling point are included in the model. . . . .	92
6.28	Radial deformation right before buckling of cylindrical-conical shell with a reinforcement of 200 mm. A scaling factor of 1 was used. . . . .	92
6.29	Force-displacement graph of the cylindrical-conical shell including a reinforcement of 300 mm. . . . .	93
6.30	Radial deformation right before buckling of cylindrical-conical shell with a reinforcement of 300 mm. A scaling factor of 1 was used. . . . .	93
7.1	Force-displacement graphs of the sandwich composite cylindrical-conicals shell using 5 cases with different dynamic implicit parameters. . . . .	96
7.2	Shells including an axisymmetric imperfection with an amplitude of 300% and 12 half waves. . . . .	97
7.3	Force-displacement graphs of the sandwich composite cylindrical shell with axisymmetric imperfection. . . . .	98
7.4	Force-displacement graphs of the sandwich composite conical shell with a height of 800 mm including axisymmetric imperfection. . . . .	99
7.5	Force-displacement graphs of the sandwich composite conical shell with a height of 400 mm including axisymmetric imperfection. . . . .	100
7.6	Force-displacement graphs of cylindrical-conical shell with a height of 1600mm including axisymmetric imperfection. . . . .	102
7.7	Force-displacement graphs of the sandwich composite cylindrical-conical shell with a height of 1200mm including axisymmetric imperfection. . . . .	103
7.8	Force-displacement graphs of the sandwich composite cylindrical-conical shell with a height of 1600 mm including mode 1 imperfection shape with different amplitudes. . . . .	104
7.9	Force-displacement graphs of the sandwich composite cylindrical-conical shell with a height of 1200 mm including mode 1 imperfection shape with different amplitudes. . . . .	105
7.10	Force-displacement graphs of the sandwich composite cylindrical-conical shell with a height of 1600 mm including mode 1 imperfection shape after performing a preloading of the structure. . . . .	106

---

7.11 Force-displacement graphs of the sandwich composite cylindrical-conical shell with a height of 1200 mm including mode 1 imperfection shape after performing a preload to the structure with different amplitudes. . . . .	107
--------------------------------------------------------------------------------------------------------------------------------------------------------------------------------------------------------------------------------	-----

# List of Tables

2.1	Knockdown factors for different imperfection types for the sandwich cylindrical shell [3]. . . . .	21
4.1	Geometrical properties of the sandwich composite cylindrical shell. . . . .	35
4.2	Material properties of IM7/8552. Material properties taken from [16]. . . . .	35
4.3	Material properties of Rohacell 300 WF. Material properties taken from [1]. . . . .	36
4.4	First three force eigenvalues and CPU times of the sandwich composite cylindrical shell using different mesh sizes. . . . .	38
4.5	Analytical buckling loads calculated for the sandwich composite cylindrical shell using different methods. . . . .	40
4.6	Displacement of the sandwich composite cylindrical shell due to a force of 900 kN in axial direction. . . . .	40
4.7	First three force eigenvalues and CPU times for the sandwich composite cylindrical shell using different element models. . . . .	41
4.8	First three displacement eigenvalues and CPU times for the sandwich composite cylindrical shell using different element models. . . . .	41
4.9	First three buckling mode shapes of the sandwich composite cylindrical shell using different element models. For generating the figures a scaling factor of 30 was employed. . . . .	42
4.10	Buckling loads, CPU times, and difference with respect to 1 mm/s for the sandwich composite cylindrical shell using different displacement rates. . . . .	44
4.11	Geometrical properties of the sandwich composite conical shell. . . . .	46
4.12	First three force eigenvalues and CPU times of the sandwich composite conical shell using different mesh sizes. . . . .	47
4.13	Displacements of the sandwich composite conical shell due to a force 900 kN in axial direction. . . . .	48
4.14	First three force eigenvalues and CPU times for the sandwich composite conical shell using different element models. . . . .	49
4.15	First three displacement eigenvalues and CPU times for the sandwich composite conical shell using different element models. . . . .	49
4.16	First three buckling mode shapes of the sandwich composite conical shell of different element models. For generating the figures a scaling factor of 30 was employed. . . . .	51
4.17	First three force eigenvalues of the conical shell with different conical heights using the SC8R element model. . . . .	53
4.18	Buckling loads of the different height models determined by the dynamic analysis. . . . .	55
5.1	Displacement of the sandwich composite cylindrical-conical shell due to a force of 900 kN in axial direction. . . . .	58
5.2	First three force eigenvalues and CPU times of sandwich composite cylindrical-conical shell using a S4R element model and a SC8R element model. . . . .	58
5.3	First three force eigenvalues and CPU times of the sandwich composite cylindrical-conical shell using different meshes. . . . .	61
5.4	First three force eigenvalues of the sandwich composite cylindrical-conical shells with different conical heights. . . . .	62
5.5	Buckling loads of the sandwich composite cylindrical-conical shell with different conical heights determined by the dynamic analysis. . . . .	63
5.6	First three force eigenvalues of the 1200 mm cylindrical-conical shell with different semi-vertex angles. . . . .	64
6.1	Maximum radial displacement of the sandwich composite cylindrical-conical shell at a displacement of -7.12 mm in axial direction. . . . .	70

6.2	Micro strains of the dynamic implicit analysis at a load of -440 kN. Ply1 - Ply3 are the strains of the inner face sheet. Ply4 - Ply6 are the strains of the outer face sheet. . . . .	71
6.3	Micro strains of the non-linear Riks analysis at a load of -440 kN. Ply1 - Ply3 are the plies of the inner face sheet. Ply4 - Ply6 are the plies of the outer face sheet. . . . .	71
6.4	Difference between the strains of the dynamic implicit analysis and non-linear Riks analysis in percentages. Ply1 - Ply3 are the plies of the inner face sheet. Ply4 - Ply6 are the plies of the outer face sheet. . . . .	71
6.5	Micro strains of the linear static analysis at a load of -440 kN. Ply1 - Ply3 are the plies of the inner face sheet. Ply4 - Ply6 are the plies of the outer face sheet. . . . .	71
6.6	Difference between the strains of the dynamic implicit analysis and linear static analysis in percentages. Ply1 - Ply3 are the plies of the inner face sheet. Ply4 - Ply6 are the plies of the outer face sheet. . . . .	72
6.7	Failure strains of the composite IM7/8552 material in micro strain [16]. . . . .	77
6.8	Buckling loads obtained by the eigenvalue analysis after performing a preload of the sandwich cylindrical-conical shell and difference with respect to the dynamic buckling load. . . . .	77
6.9	Material properties set 1 of sandwich composite cylindrical shell [50]. . . . .	79
6.10	Material properties set 2 of sandwich composite cylindrical shell. . . . .	81
6.11	Material properties of aluminum 2024-T4 [49]. . . . .	82
6.12	Buckling loads of the cylindrical shell and conical shell using eigenvalue analysis. . . . .	82
6.13	Buckling loads of the eigenvalue analysis and dynamic implicit analysis. . . . .	83
6.14	Buckling loads of the composite cylindrical shell and conical shells calculated using the SP-8007 and SP-8019 guidelines. . . . .	85
6.15	Buckling loads of a quasi-isotropic cylindrical-conical shell with a length of 1600 mm and 1400 mm. . . . .	85
6.16	Buckling loads of the composite cylindrical-conical shells with a height of 1600 mm and 1200 mm obtained by the dynamic implicit analysis and difference w.r.t. the eigenvalue analysis buckling load. . . . .	86
6.17	Buckling loads obtained by the dynamic analyses of the models with and without radius of curvature. . . . .	88
6.18	Force eigenvalues of the 1200 mm cylindrical conical shell with a semi-vertex angle of 5° using different radii of curvature at the transition. . . . .	89
6.19	Buckling loads obtained by the dynamic analyses of the models with and without a reinforcement. . . . .	91
7.1	The dynamic implicit parameters used for the 5 cases analysed for the computational time study of the sandwich composite cylindrical-conical shell. . . . .	96
7.2	Buckling loads, CPU times, and difference with respect to the reference case of the sandwich composite cylindrical conical shells using different dynamic implicit parameters. . . . .	97
7.3	Buckling loads of the sandwich composite cylindrical shell including axisymmetric imperfection. . . . .	98
7.4	Buckling loads of the sandwich composite conical shell with a height of 800 mm including axisymmetric imperfection. . . . .	99
7.5	Buckling loads of the sandwich composite conical shell with a height of 400 mm including axisymmetric imperfection. . . . .	100
7.6	Buckling loads of cylindrical-conical shell with a height of 1600 mm including axisymmetric imperfections. . . . .	101
7.7	Buckling loads of the sandwich composite cylindrical-conical shell with a height of 1200mm including axisymmetric imperfection. . . . .	102
7.8	Buckling loads of the sandwich composite cylindrical-conical shell with a height of 1600 mm including mode 1 imperfection shape. . . . .	104
7.9	Buckling loads of the sandwich composite cylindrical conical shell with a height of 1200 mm including mode 1 imperfection shape with different amplitudes. . . . .	105
7.10	Buckling loads of sandwich composite cylindrical-conical shell with a height of 1600 mm including mode 1 imperfection shape obtained after performing a preloading of the structure. . . . .	106
7.11	Buckling loads of the sandwich composite cylindrical-conical shell with a height of 1200 mm including mode 1 imperfection shape obtained after preloading of the structure with different amplitudes. . . . .	107

# Nomenclature

<b>AFP</b>	Automated Fiber Placement
<b>ATL</b>	Automated Tape Laying
<b>BC</b>	Boundary Condition
<b>DIC</b>	Digital Image Correlation
<b>DOF</b>	Degree Of Freedom
<b>FE</b>	Finite Element
<b>KDF<sub>i</sub></b>	Knockdown Factor due to imperfections
<b>KDF</b>	Knockdown Factor
<b>LVDT</b>	Linear Variable Differential Transformer
<b>SBPA</b>	Single Boundary Perturbation Approach
<b>SLS</b>	Space Launch System
<b>SPDA</b>	Single Perturbation Displacement Approach
<b>SPLA</b>	Single-Perturbation Load Approach
<b>U1</b>	Radial out of plane deformation
<b>WMPLA</b>	Worst Multiple Perturbation Load Approach





# Acknowledgements

My thesis would not have been possible without the help of several people. In this chapter I would like to take the opportunity to thank these people for helping me throughout this period of obtaining my master degree. First of all, I would like to thank my supervisor, Chiara Bisagni, for the advise and supervision she gave me during the thesis. Her experience with research projects really helped me achieving the best result possible. Moreover, she gave me the opportunity to work together with NASA, which I am really thankful for.

I would also like to thank Michelle Rudd from NASA for all the advise she gave me during the thesis. She always found the time to help me out and I appreciate all the valuable feedback she gave me about my results. Moreover, I really appreciate all the discussions we had over skype, she always kept me sharp towards my results.

Besides my supervisors, I would also like to thank Chiara's PhD students, Luc and Kevin, for being my 24/7 Abaqus help desk. I really appreciate all the time they spent on explaining me how Abaqus works and how to interpret my results. Even with the smallest questions they found the time to help me out. Without them I would have not been as good in Abaqus as I am now. Next to providing me with the professional knowledge, they also became good friends in which I am grateful for.

I would also like to give a special thanks to my parents and sister. I could have not finished my aerospace studies without them. They helped me through so many emotional breakdowns and were always there supporting me. I cannot even remember how often I said that I would quit my studies and they always convinced me to push through in which I am now thankful for.

Furthermore, I would like to thank my boyfriend Kelbey. I am very proud to say that we started aerospace engineering together and are finishing it together. I am thankful for all the confidence you have given me throughout the years and for always helping me out with assignments. Because of you I kept challenging myself and achieving the best possible result.

Last but not least, I would like to thank all my friends from the faculty. All the coffee breaks and beers at bouwpub really helped me in clearing my mind. It was really nice working with all of you and am grateful for the friendships we built up throughout the past year.





# Introduction

Sandwich composite structures are used in many launch vehicles such as the Delta II, Delta IV, Atlas V and the Ariane 5 [46], [22]. The main structural components are cylindrical shells and conical shells; these structures are loaded in heavy compression when launched. This loading condition makes buckling one of the main considerations during the design process due to the decrease in loading capability after buckling. Cylindrical shells and conical shells are very sensitive to imperfections when axially loaded. This is because these shells have high radius over thickness ratios. Due to the uncertainty during the manufacturing process and testing of sandwich composite structures, imperfections can arise which result in a lower buckling load when compared to the pristine structure buckling load. Therefore, during the design process imperfections have to be taken into account. However, the buckling behavior and imperfection sensitivity of these structures is not yet fully understood which results in designs being too conservative. As a result a lot of research has been performed on this topic which includes executing buckling tests.

The research topic that has been studied during the last 50 years is the imperfection sensitivity of shell structures. Loading imperfections, geometrical imperfections, and thickness variations result in an experimental buckling load that is much lower than the theoretical buckling load. Therefore, it is important that during the design process these imperfections are taken into account when calculating the buckling load. Nowadays, the buckling load is predicted by calculating the theoretical buckling load and then multiplying it with a Knockdown Factor (KDF), which accounts for the imperfections. This KDF can be determined by using the NASA guidelines, SP-8007 for cylindrical shells [42] and the SP-8019 for conical shells [41], which are based on empirical data collected back in the 1930s. Because of the fact that since then the materials used and the manufacturing processes changed, the KDFs calculated by the NASA guidelines are outdated and often result in conservative designs [59]. For that reason, new KDFs are needed that take into account sandwich composite materials and the new manufacturing processes.

Moreover, sandwich composite cylindrical shells and sandwich composite conical shells have been manufactured and tested separately for the last decade. However, due to new manufacturing techniques and the use of sandwich composite structures, it is possible to manufacture the cylindrical shells with the conical shells together resulting in one structural component: a cylindrical-conical shell. The next step in the investigation is to test and study these 3D structures. However, the buckling behavior of such a structure is not yet fully understood and also the modelling techniques are not yet fully explored.

Therefore, the aim of the thesis is to investigate the buckling behavior of sandwich composite cylindrical shells, conical shells, and cylindrical-conical shells including imperfections. The thesis focuses on the numerical aspect of the determination of the buckling behavior of these structures and implementation of the imperfections and imperfection sensitivity. The goal is to compare the buckling behavior and imperfection sensitivity of a sandwich composite cylindrical and conical shell alone with the buckling behavior and imperfection sensitivity of a sandwich composite cylindrical-conical shell.

The structure of the report is as follows: Chapter two describes the literature study performed at the beginning of the project. Within this study the research that has already been done is elaborated on. The focus of the literature study is to better understand the buckling behavior of cylindrical and conical shells and to find out how an imperfection sensitivity study is performed. The main focus lies on using numerical methods to analyse the behavior. After that, the research objective and research questions are developed and are explained in chapter 3. This is followed by a chapter about investigating the buckling behavior of sand-

wich composite cylindrical and conical shells. This chapter includes determining which elements are best for modelling sandwich composite shells and performing mesh convergence studies. The buckling behavior is analysed by using both linear and non-linear analyses. After knowing the buckling of the separate shells, the buckling behavior of the sandwich composite cylindrical-conical shell is explained. Within this chapter the way in which a cylindrical-conical shell can be modelled best is explained. Moreover, linear and non-linear analyses are performed. An indepth explanation and interrogation of the results from chapter 5 will be investigated in chapter 6. Chapter 6 focuses on using different materials, looking at the deformations and strains, changing the material properties, and using different types of analyses. Moreover, it is investigated how to give a more realistic representation of the structure: by adding a radius of curvature and by adding a reinforcement. After that, the imperfection sensitivity of the sandwich composite cylindrical, conical, and cylindrical-conical shell is elaborated on. The focus lies on adding geometrical imperfections to the shells and to compare the imperfection sensitivity of the shells. At the end conclusions and recommendations are given about the thesis project.

# 2

## Literature study

This chapter describes the literature study performed at the beginning of the thesis project. This study was needed in order to better understand the thesis topic and to investigate the gaps in literature. As already pointed out in the introduction the thesis focuses on the buckling behavior and imperfections sensitivity of cylindrical and conical shells. It should be noted that the focus lies on sandwich composite shells however, the research performed is limited. Therefore, also papers are included that only cover composite cylindrical and conical shells. Moreover, there is no to little research about buckling analysis of sandwich composite cylindrical-conical shells and therefore, in this literature study the focus lies on understanding the buckling behavior and modeling techniques of sandwich composite cylindrical and conical shells.

The structure of this chapter is as follows: the first section describes the buckling tests of cylindrical and conical shells and touches upon the differences between the test results and numerical results. After that, the different ways in which an imperfection analysis can be performed are described. This is followed by a section about how to model a cylindrical and conical shell in finite element software.

### 2.1. Buckling tests

The buckling tests contribute to the understanding of the buckling behavior of sandwich composite cylindrical shells and conical shells. By executing these tests, the prediction methods for determining the imperfections can be validated and new guidelines can be established. This section discusses the test setup, tests performed, and the difference between the theoretical and experimental buckling load of both cylindrical shells and conical shells.

#### 2.1.1. Test setup

The tests of sandwich composite cylindrical shells and conical shells under axial compression are described in this subsection. The first part of this subsection shows the test setup of sandwich composite cylindrical shells under axial compression. The second part of this subsection discusses the test setup used for the buckling tests of composite conical shells. The reason for describing the test setup used for the testing of composite conical shells is that the explanations of the buckling tests of sandwich composite cylinders are not detailed enough. Baker [7], Bert et al. [9], and Abramovich [2] performed buckling tests on sandwich composite cones and it could be seen that the same test setup is used as for composite cones. Therefore, it is assumed that the same test setup applies for the compression tests of sandwich composite conical shells.

#### Cylindrical shell

In order to contribute to the development of the new design guidelines for the knockdown factors, Schultz et al. [47] tested a full-scale 2.4m sandwich composite cylinder (CTA 8.1). The specimen consist out of a honey-comb core and composite face sheets. Before executing the buckling tests, the CTA 8.1 was subjected to measurement tests in order to establish the imperfections. Visual inspection, flash thermography, and vacuum shearography were used to determine voids, delaminations, and areas of dry fibers. Structural light scanning was needed to determine thickness variations and mid-surface imperfections.

The cylinder was tested at the NASA Marshall Space Flight Center which has a test facility that is able to apply a maximum compression load of 1,500,000 lb, the test facility can be seen in figure 2.1. As can be seen

in the figure, the test facility has two load introduction platforms at the top and bottom of the specimen, and the load is applied using eight loading trusses which consist of hydraulic actuators and load cells. The test article was placed between the top and the bottom plates by potting the edges into the end-ring channels. In order to add redundancy to the clamping system, bolts were inserted through the end rings and shell of the cylinder. To make sure that there is a proper load introduction into the specimen, padups were secondarily bonded to the top and the bottom of the specimen. When the specimen was placed within the structure, pure compression was applied.

The buckling behavior of the sandwich composite cylindrical shell was monitored during the test. The strains and displacements of the specimen were determined using eight low speed Digital Image Correlation (DIC) systems, 28 electric displacement transducers, 256 strain gauges, and 16000 fiber-optic strain sensor locations. Microphones and video cameras were used to observe the buckling behavior.

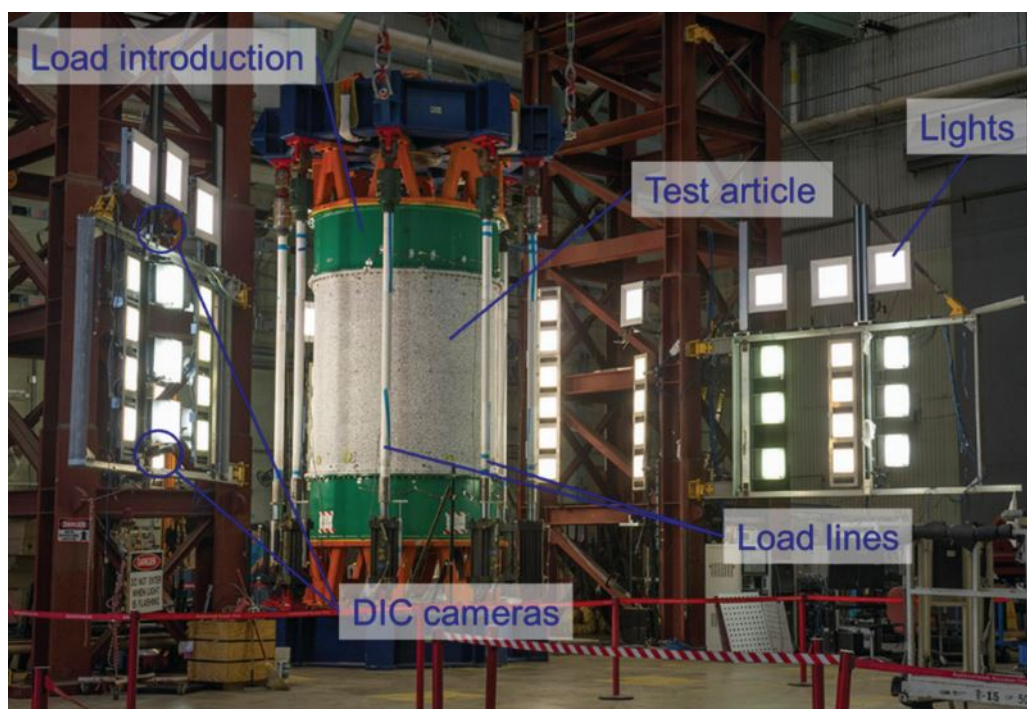


Figure 2.1: CTA 8.1 test setup [47].

### Conical shell

The conical shells have a similar test setup as presented for the cylindrical shells. Khakimova et al. [35] performed tests on three composite conical shells under axial compression. Before the axial compression tests were performed, the specimens were measured in order to inspect the specimen for imperfections. Automatic ultrasonic testing using water split coupling was used to detect thickness variations. Moreover, the actual shape of the conical shells were established by using an optical 3D digitizing measurement system which is based on photogrammetry. The initial geometric imperfections were determined by using a best-fit procedure.

The buckling tests were performed using the test facility at the Institute of Composite Structures and Adaptive Systems of DLR. The test setup was as follows: the conical shell was clamped between one axially supported plate on top and one drive plate on the bottom. The top plate was able to move in vertical direction in order to account for different cone heights. The load was applied in a displacement controlled manner using three load cells. The test setup can be seen in figure 2.2.

In order to evenly apply the load into the specimen and to clamp the specimen within the test setup, metal rings were assembled to the top and the bottom of the conical shell. Within the metal rings a circular groove with a trapezoidal cross-section was present in order to precisely fit the edges of the specimen. The specimen were placed within the metal rings using potting, which was done by an epoxy resin system. Moreover, between the metal rings and the supporting plates thin equalized layers of epoxy concrete was applied to make sure that the load was equally introduced into the metal rings.

During the tests the loads and axial displacements were registered using three displacement transducers

placed at  $90^\circ$ ,  $180^\circ$  and  $270^\circ$ . Moreover, the strains were measured using 18 strain gauges which were placed in back to back configuration. A digital correlation system was used to determine the deformations.

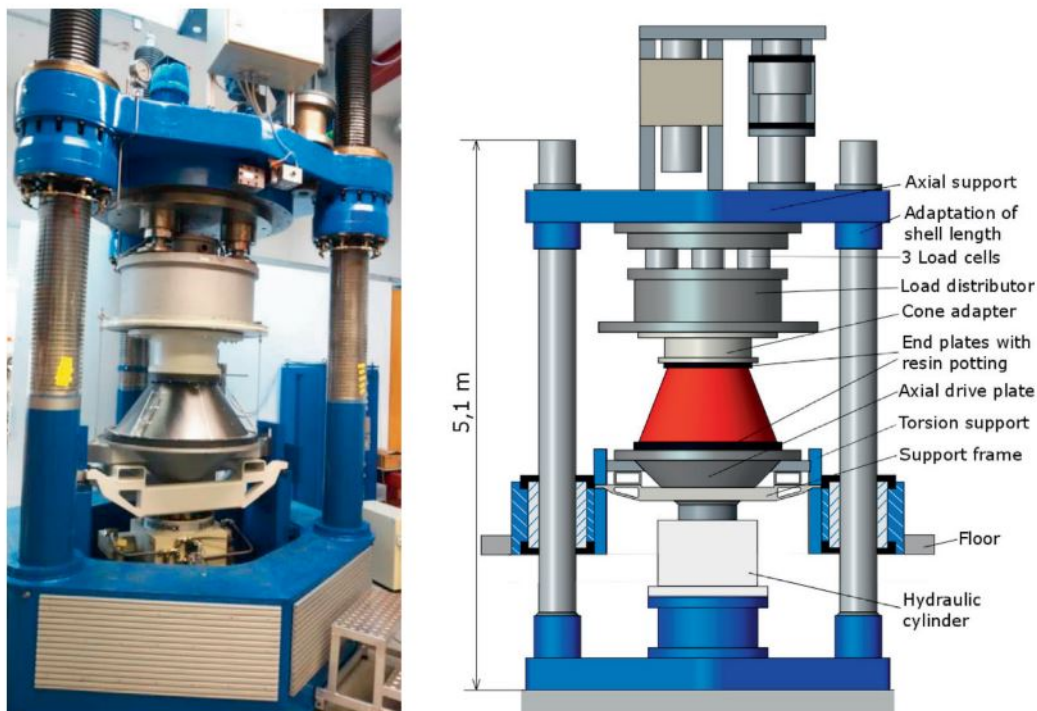


Figure 2.2: The test facility (left) and a schematic representation of the test setup (right) [35].

### 2.1.2. Difference between the theoretical and experimental buckling load

After performing the experiments and analysing the buckling behavior, it can be observed that the experimental buckling load of cylindrical shells and conical shells is lower than the theoretical buckling load. Therefore, it is suspected that these structures are sensitive to imperfections. This subsection investigates the different imperfections and their influence on the buckling load.

#### Cylindrical shell

During the manufacturing process imperfections can arise in the cylindrical shell. Due to mandrel imperfections, geometrical deviations in the shell radius can appear. This imperfection is studied most in literature. However, there are other type of imperfections that are less studied but are also important. This is because these imperfections can reduce the buckling load even more when compared to the the geometrical imperfection [58]. An example of such an imperfection is thickness variation. This imperfection type can arise due to variations in the resin content or due to ply gaps. For sandwich composite structures, this imperfection is introduced due to thickness variation in the core. Another less studied imperfection is the material imperfection, which emerges due to the probabilistic values of the material properties given by the manufacturer or provided in literature. During the testing phase, also imperfections can arise. As described in subsection 2.1.1, the specimen has to be potted into the testing equipment using epoxy. This introduces an elastic boundary condition which can result in a non uniform boundary. This imperfection is called the boundary imperfection. Besides the fact that during the buckling tests a lot of attention is paid to the load introduction as described in subsection 2.1.1, non uniform load introduction can still arise resulting in loading imperfections. The imperfection types described above, all have a different influence on the buckling load of cylindrical shells. Below, first the imperfection sensitivity of composite cylindrical shells is presented and after that the imperfection sensitivity of sandwich composite cylindrical shells is shown. This in order to see the differences.

Keppe et al. [30] studied the "influence of imperfections on axial buckling load of composite cylindrical shells". Within this study, the theoretical buckling load was compared with the experimental buckling load. Also a finite element model was created to investigate the influence of two different imperfections, geomet-

rical imperfections and thickness variation. The theoretical buckling load was found using the bifurcation load of a perfect cylindrical shell. The influence of thickness variation and geometrical imperfections were studied by implementing the measured imperfections into the finite element model. The load shortening curves of an imperfection sensitive composite cylinder with geometrical and thickness imperfections can be seen in figure 2.3. It can be seen that the difference between the perfect cylindrical shell buckling load and the experimental buckling load is almost 50%, which stresses the importance of the imperfections. It can also be seen that the cylinder is more sensitive to geometrical imperfections than thickness imperfections, and together result in an even lower buckling load. The difference between the test buckling load and the numerical buckling load of the imperfect cylindrical shell can be explained by the loading imperfections that have not been taken into account. Furthermore, by using a stochastic model also the imperfection sensitivity to material imperfections was investigated. It could be seen that the effect was negligible as expected.

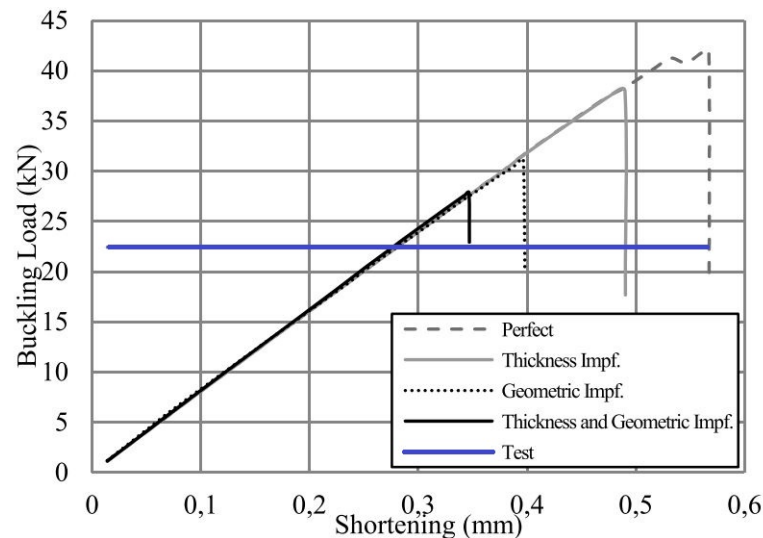


Figure 2.3: Comparison of the load shortening curves generated by the finite element model and the test result [30].

Furthermore, Hilburger and Starnes [24] investigated the influence of imperfections for composite cylindrical shells. This study focuses on the difference between lay-ups, and the influence of ply-gaps and elastic boundary condition. There were two different orthotropic laminated shells and one quasi isotropic laminated shell tested. It was observed that the quasi isotropic laminated shell was more sensitive to imperfections than the orthotropic laminated shell. Therefore, the quasi isotropic laminated shell was further investigated and the influence of each imperfection was studied. Figure 2.4 shows the normalized buckling load as result of different imperfections. If the imperfection amplitude scale is zero, no imperfection is present. From the graph it can be seen that the geometric imperfections has the biggest influence on the normalized buckling load (decrease of 11%), followed by the thickness imperfection (decrease of 4%). It can be seen that the loading imperfection has a more significant effect when the geometrical imperfection amplitude is low. When the geometrical imperfection amplitude increases the influence of the loading imperfection changes which indicates a complex non-linear coupling between both imperfections. Moreover, in this study the effect of ply-gaps and elastic boundary condition due to potting were investigated. It could be seen that these imperfections had a marginal effect on the buckling load (about 1%).

The imperfection sensitivities have also been studied for sandwich composite cylindrical shells. Bisagni and Alfano [11] performed a buckling analysis on a sandwich composite cylindrical shell using measured imperfections. In this paper a sensitivity analysis is presented for different imperfections. It could be seen that the cylindrical shell was less sensitive to geometrical imperfection when compared to thickness variations. The buckling load determined due to the thickness imperfections was 7% lower. Moreover, when the two imperfections were combined the reduction in buckling load was 15%. When comparing this buckling load reduction with the composite cylinders described above it suggests that a sandwich composite cylindrical shell is less sensitive to imperfections when compared with a composite cylindrical shell. This was also concluded by Orifici and Bisagni [39]. In this study a comparison was made between the design buckling load of two sandwich composite cylindrical shells and two composite cylindrical shells. The study showed that by using a radial perturbation, the knockdown factors for the sandwich composite cylindrical shells were higher



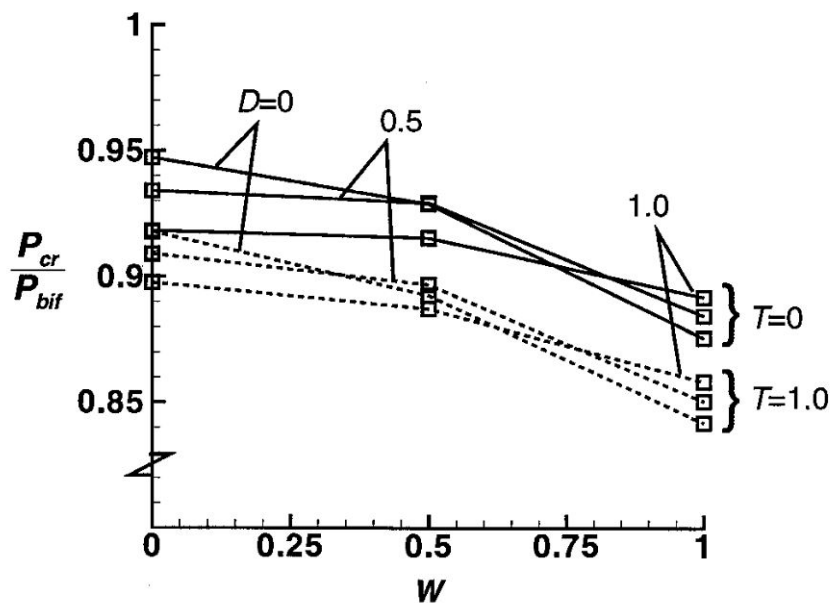


Figure 2.4: Influence of the imperfections on the normalized buckling load of a quasi-isotropic shell.  $W$  = imperfection amplitude scale factor for the geometric imperfection,  $T$  = imperfection amplitude scale factor for the thickness variation, and  $D$  = imperfection amplitude scale factor for the loading imperfection [24].

than the ones for the composite cylindrical shells. However, this does not mean that for sandwich composite cylindrical shells the imperfections do not have to be taken into account.

From these studies it can be concluded that the imperfection sensitivity depends on the type of material used, a sandwich composite cylindrical shell is less sensitive to imperfections than a composite cylindrical shell. Also the lay-up influences the imperfection sensitivity, a quasi isotropic lay-up is more sensitive to imperfections than an orthotropic lay-up. The studies presented above showed that for each cylindrical shell the influences of the imperfections differ. Therefore, it is advised to always consider the geometrical, thickness, and loading imperfections when determining the design buckling load. However, the material imperfections, ply-gap imperfections and boundary conditions imperfections have a marginal effect on the buckling load and do not have to be taken into account during the first stages of the design process. These imperfections become important during the validation process of the numerical models.

### Conical shell

The imperfections of conical shells also arise during the manufacturing process. Using filament winding with a horizontal helical winding machine and a conical steel mandrel can result in specimens with thickness deviations. By using this manufacturing process the shell thickness increases at smaller shell radius [34]. More information about the filament winding process of conical shells can be found in [8] and [21]. When using automatic fiber placement or automatic tape laying, thickness variations and fiber angle deviations can occur. This is due to overlaps and ply-gaps that are created because of the changing radius of the conical shell. Angle deviations occur due to the accuracy of the Automated Fiber Placement (AFP) and Automated Tape Laying (ATL) processes, and the finite number of plies used. Due to the higher chance of getting ply-gaps when using these processes [35], the difference in fiber volume fraction along the cone becomes another imperfection that can arise. Furthermore, an imperfect mandrel, vacuum bagging and demolding can result in geometrical imperfections. As for cylindrical shells, loading imperfections, elastic boundary condition imperfections, and material imperfections also emerge for conical shells. In the studies presented below the imperfection sensitivity of different composite conical shells are presented. This is because the research done on sandwich composite conical shells is limited.

Khakimova et al. [35] studied the imperfection sensitivity of three composite conical shells, K01, K06 and K08. Whereas, two conical shells had the same material properties except for the ply topology design and one conical shell had a different lay-up. The different ply topology designs, D1 and D3, can be seen in figure 2.5. It can be seen that D1 has less ply pieces and a higher angle deviation when compared to D3.

Within this study all the imperfections described above are taken into account. The influence of the different imperfections were studied by using finite element software. After generating the results, it could be seen that the geometrical and thickness imperfections reduce the buckling load most. It could also be observed that when the fiber volume fraction imperfection was taken into account the buckling load changed. This can be explained due to the higher or lower stiffness obtained if the fiber volume changed at certain places. However, the effect compared to the thickness variation and geometrical imperfection was small. Also the influence of the elastic boundary condition was studied, and it could be seen that the effect was marginal compared to the other imperfection types. However, implementing an elastic boundary into the model did give a better match of the numerical and experimental results.

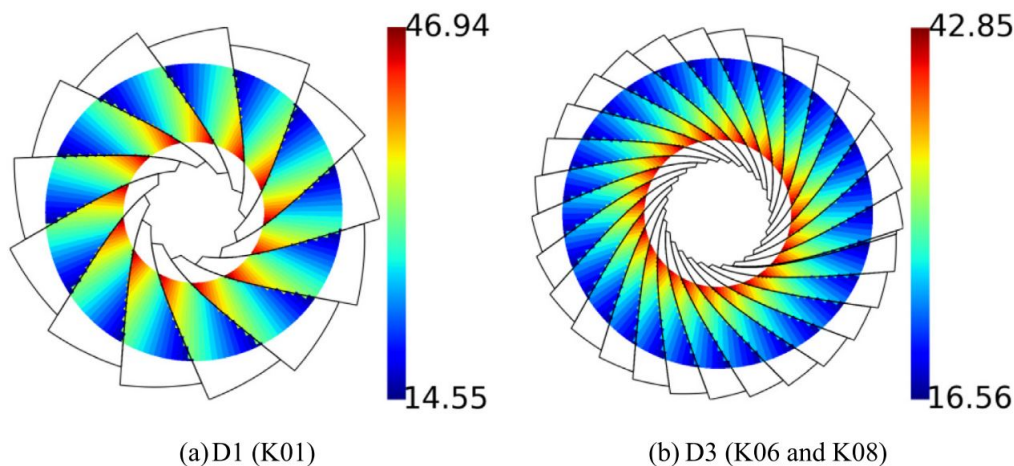


Figure 2.5: The ply pieces plotted on the conical shell surface including fiber orientation in degrees [35].

Moreover, it could be observed that the difference in ply topology design can reduce the normalized buckling load by 0.3. The conical shell with the D1 topology design had a lower buckling load than the conical shells with the D3 topology design. The reason for this is that the D1 topology design has a more pyramid like shape, which is created by using less ply pieces with a larger ply piece width compared to the D3 topology design [34]. The D1 topology design is more imperfection sensitive which results in a lower buckling load. It could be seen that for the conical shell with the D1 topology design the influence of the angle deviation was bigger when compared to the D3 topology design. The angle deviation influenced the buckling load by 15% for the D1 topology design, and a marginal effect could be observed for the D3 design. This result stresses the importance of including the ply topology design and ply angle deviation for determining the buckling load of conical shells.

It was also investigated what the effect of the conical shell shape is on the imperfection sensitivity. Khakimova et al. [32] [33] and Di Pasqua et al. [19] looked at the behavior of conical shells with different semi-vertex angles. A visual representation of the semi-vertex angle,  $\alpha$ , can be seen in figure 2.6. In [33] the influence of a radial perturbation was investigated on conical shells with different semi-vertex angles. It could be seen that the value of the knockdown factor for a semi-vertex angle of  $5^\circ$  was around 0.5 and the knockdown factor for a semi-vertex angle of  $75^\circ$  was around 1. In [32] and [19] it was also concluded that when the semi-vertex angles decreased the sensitivity to imperfections increased. This can be explained by the fact that when the value of the semi-vertex angle is low, the conical shell has a more cylinder like shape resulting in higher imperfection sensitivity. When the semi-vertex angle has a high value, the conical shell looks more like a flat plate resulting in a low imperfection sensitivity.

What can be concluded from these studies is that the imperfections that have to be taken into account for the cylindrical shells are the same for the conical shells. However, when the conical shell has a higher value of the semi-vertex angle, the structure becomes less imperfection sensitive making the imperfections less important. Furthermore, the topology design used for the conical shells is also an important parameter, since it has a big influence on the imperfection sensitivity. This stresses the importance of implementing the design topology used within the buckling load predictions. Also the fiber angle deviation has to be taken into account when the D1 topology design is used, since it has a significant influence.

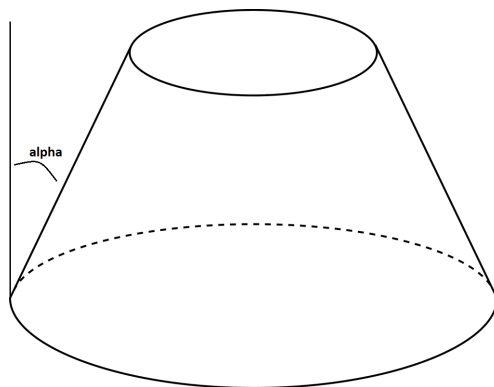


Figure 2.6: Semi-vertex angle of a conical shell.

## 2.2. Imperfection analysis

In subsection 2.1.2, the difference between the theoretical and experimental buckling load is explained. It can be seen that imperfections play a mayor roll in decreasing the buckling load and have to be considered during the design process. However, during the design process, the imperfections are unknown and these have to be predicted. The design buckling load is determined by using the bifurcation buckling load and then multiplying it by a Knockdown Factor (KDF) in order to account for the imperfections.

As already stated in the introduction, the KDFs that can be determined by using the NASA design guidelines are outdated and conservative. Therefore, there are new design guidelines for determining the KDFs needed. There are two research projects that have been investigating the possibilities: the New Robust Design Guideline for Imperfection Sensitive COMposite Launcher Structures (DESICOS) project, which is already finished, and the Shell Buckling Knockdown Factor (SBKF) project, which is still ongoing. The DESICOS project mainly focused on perturbation and stochastic methods to establish new KDFs for cylindrical shells and conical shells [4]. The methods are investigated for sandwich, isogrid, and monolithic shells with and without holes. Whereas the SBKF project is using measurement techniques to accurately predict the KDFs of metallic and composite cylindrical shells [59].

The ultimate goal of both projects is to be able to accurately predict the buckling load of shell structures such that the design of launcher structures can be improved and its weight can be reduced. This section will discuss the methods established by both projects and will give a more detailed description about the current NASA design guidelines.

### 2.2.1. Knockdown factor using the NASA design guidelines

The NASA design guidelines for cylindrical shells and conical shells were established by Peterson in 1968 [42], [41]. These guidelines use experimental data and the lower-bound curve determines the knockdown factor for different geometries. An example of the lower-bound method can be seen in figure 2.7. Since this method is based on empirical data collected back in 1968, it means that this method does not take into account the current developments. For example: the sandwich structures with composite face sheets and the higher precision of manufacturing processes are not taken into account. Therefore, the KDFs determined using these guidelines are conservative and lead to heavy designs.

The SP-8007 design guidelines can be used for isotropic unstiffened cylindrical shells, orthotropic cylindrical shells, and isotropic sandwich cylindrical shells. Since the research topic of this literature study is on orthotropic sandwich cylindrical shells, the SP-8007 has no guideline for calculating the knockdown factor. Therefore, it is assumed that an orthotropic sandwich cylindrical shell can be seen as an orthotropic cylindrical shell. The same is done by Bisagni and Alfano [11], where it is assumed that the core of the sandwich composite is part of the lay-up. When assuming this, the equations for calculating the knockdown factor,  $\gamma$ , of an orthotropic cylindrical shell can be used.

The SP-8019 design guidelines have been established to determine the KDFs for conical shells. The guidelines can be used for isotropic conical shells, orthotropic conical shells, and sandwich conical shells. From the experimental data collected for creating the SP-8019 guidelines, it could be seen that there is no clear relation between the geometry or type of the conical shell and the knockdown factor. Therefore, the lower-bound of the experimental data gives  $\gamma = 0.33$ , which does not depend on the type of conical shell. This knockdown factor is only valid for semi-vertex angles between  $10^\circ$  and  $75^\circ$  due to the limited data. When the semi-vertex

angle is lower than  $10^\circ$  the conical shell can be converted to an equivalent cylinder and the SP-8007 design guideline can be used.

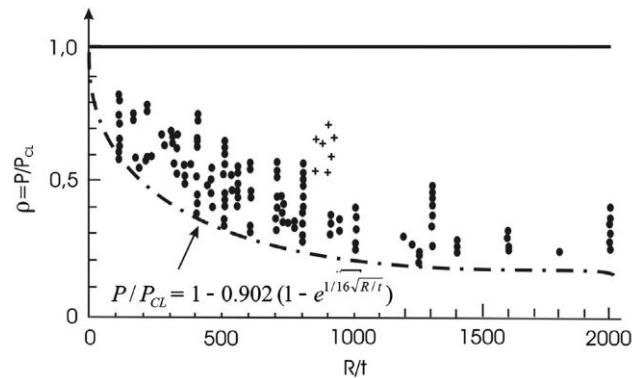


Figure 2.7: Test data for isotropic cylinders subjected to axial compression including the lower bound curve [61].

### 2.2.2. Perturbation methods

A new approach that has been developed to determine the KDFs of cylindrical and conical shells is to introduce a perturbation to the perfect geometry. Examples of perturbations are adding a lateral load, a radial displacement, and a boundary perturbation. The idea is that adding a perturbation to the perfect geometry results in the worst case imperfection. This subsection describes the perturbation methods for cylindrical shells and conical shells, respectively. It should be noted that most of the investigations on perturbation methods are based on composite cylindrical shells.

#### Cylindrical shell

The first perturbation method that was established for cylindrical shells was created by Hühne et al. [27] in 2005. Hühne et al. proposed the Single-Perturbation Load Approach (SPLA), which is based on the observation that the buckling process of a cylindrical shell starts with a single buckle. The SPLA introduces a lateral load in the middle of the cylindrical shell to create a single buckle. It can be observed that the buckling load decreases when increasing the lateral load; however, at a certain threshold the buckling load does not decrease anymore. The buckling load becomes constant after a certain value of lateral load. This constant value of the buckling load is said to be the design load by Hühne. A visual representation of the buckling load versus the lateral perturbation load can be seen in figure 2.8 (left). In this paper, the method was validated by testing six composite cylindrical shells with different lay-ups. However, one case showed irregular buckling behavior which resulted in a higher design buckling load when compared to the experiment. This suggested that more research was needed on the SPLA. The SPLA was created with the idea that it creates the worst case imperfection. Arbelo et al. [5] studied if the SPLA really imposes the worst case imperfection scenario. From the results it could be seen that the SPLA method is able to account for geometrical imperfections but not for other imperfections, which was also concluded by Khakimova et al. [37].

The studies presented above show the results of the SPLA by using composite cylindrical shells, but the method has not yet been proven for sandwich composite cylindrical shells. Therefore, Orifici and Bisagni [39] studied the SPLA on two composite cylindrical shells and two sandwich composite cylindrical shells. Figure 2.9 shows the results obtained for the SPLA for each of the cylindrical shells. It can be seen that the sandwich composite cylindrical shells and the cross-ply composite cylindrical shell do not show the same behavior as the quasi-isotropic composite cylindrical shell. This means that no buckling load could be determined for the cross-ply composite cylindrical shell and the sandwich composite cylindrical shells. For these structures the SPLA cannot be used. This graph also shows that the imperfection sensitivity of the quasi-isotropic composite cylindrical shell is higher compared to the other cylindrical shells.

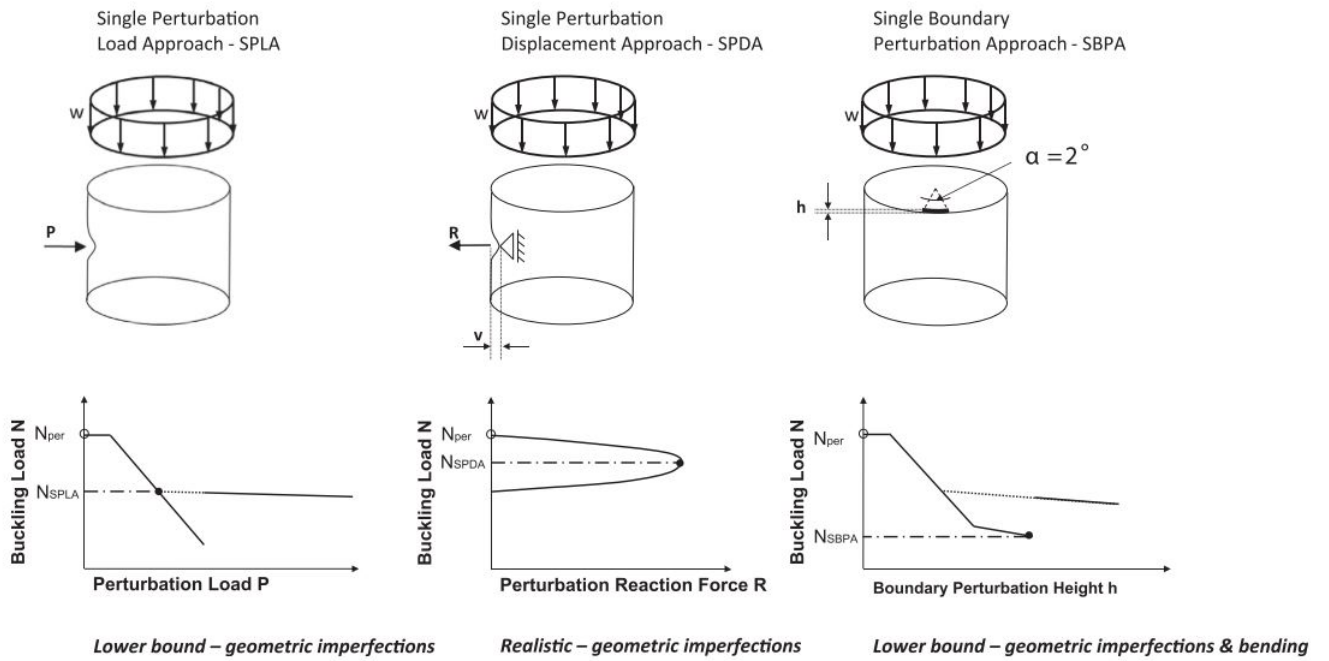


Figure 2.8: Proposed perturbation methods [55].

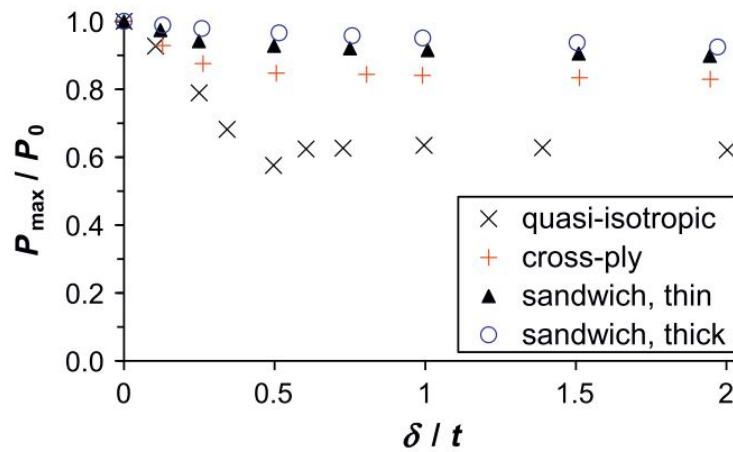


Figure 2.9: Buckling load due to perturbation [39].

Due to the shortcomings of the SPLA, Wagner et al. [53] introduced the Single Perturbation Displacement Approach (SPDA) as an improvement of the SPLA. This method introduces the single buckle to the perfect shell by using a displacement controlled loading at the middle of the shell. A limit point can be established, which cannot be done when initiating a single buckle using loading control (like the SPLA). During axial compression, the amplitude of the perturbation displacement "v" is fixed and the reaction force is determined. The process is repeated for different values of "v". It can be observed that when increasing "v" the reaction force reaches a maximum and the corresponding buckling load is the design load determined by Wagner. A visual representation of this method can be seen in figure 2.8 (middle).

From the results in [53] and [27], it could be seen that both the SPLA and SPDA could give unconservative results. It was suspected that this was because of the restricted movement of the single dimple when imposed in the middle of the shell. Therefore, Wagner et al. [56] [54] investigated the influence of the pre-buckling behavior on the motion of the single dimple. It could be seen that when imposing a single simple at the top of the shell the dimple wants to move down. However, it is not allowed to due to inherent deformation pattern of the shell. This results in a local snap through behavior resulting in a lower buckling load. Therefore, when

imposing the single dimple at the middle of the shell there is no movement of the dimple resulting in an unconservative buckling load.

Another method was proposed to capture this behavior. This method is called the Single Boundary Perturbation Approach (SBPA), which accounts for geometrical imperfections and loading imperfections. The method is based on the following procedure: a shim is introduced on the top of the shell which results in a local loading imperfection. When the cylinder is axially compressed the shim causes an additional bending moment. Due to the uneven loading, a single dimple appears beneath the shim and moves downwards to the middle of the cylindrical shell during axial compression. The buckling load has to be calculated for different shim heights and a similar graph can be made as for the SPLA. A visual representation can be seen in figure 2.8 (right). Due to the fact that the buckle is able to move downwards, more conservative results are expected. Wagner et al. [55] validated this method and established a semi-analytical expression for determining the knockdown factors obtained with the SBPA. The KDFs are valid for isotropic or quasi isotropic composite shells with  $R/t$  and  $L/R$  ratios from 90 till 500 and 1 to 5, respectively. In figure 2.10 the SBPA thresholds and empirical data can be seen. The KDFs are 10% to 200% higher than the KDFs obtained with SP-8007, which is promising.

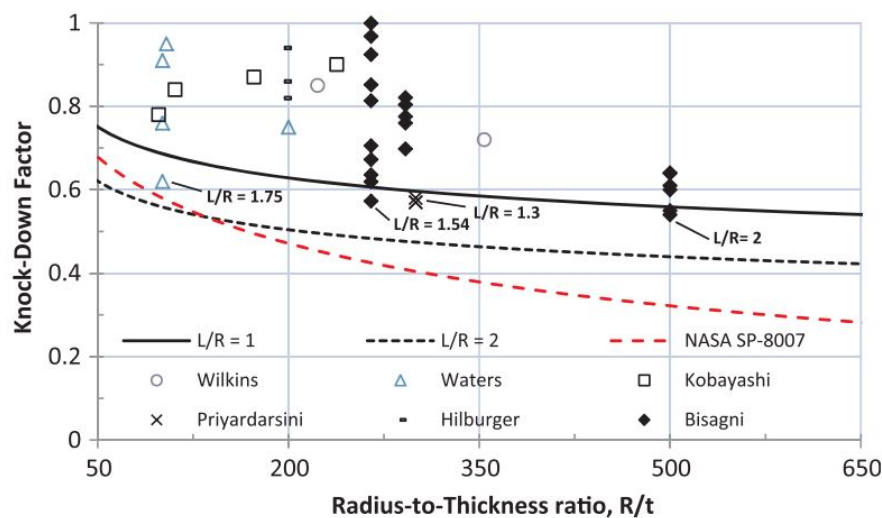


Figure 2.10: SBPA thresholds and empirical data [55].

Wang et al. [59] investigated the possibilities of an improved method of the SPLA. This method is called the Worst Multiple Perturbation Load Approach (WMPLA), which is based on using multiple lateral loads to induce multiple single dimple shape imperfections. This in order to better represent the geometrical imperfections. The number and positions of the lateral loads are determined by using an optimization process where the buckling load is minimized. When the number and positions of the lateral loads are known, the design buckling load is determined using the same process as for the SPLA. The same graph can be constructed as for the SPLA, see figure 2.8 (left). In this paper, five isotropic cylindrical shells were tested using the WMPLA. This method was able to give conservative results even if the measured imperfection amplitude increased. Wang et al. [60] also investigated the WMPLA on composite cylindrical shells with delaminations and geometric imperfections. In this paper, the WMPLA method was validated using two composite cylindrical shells.

To conclude, the SPLA and SPDA are not recommended for the design process. This is because these methods do not account for all the imperfections resulting in unconservative results. The SPLA is also not able to give a design load for sandwich composite cylindrical shells. A better option is the WMPLA which is an extension of the SPLA and can impose a worse case imperfection scenario. However, it takes a lot of time to set up the optimization and this method has not yet been validated for sandwich composite cylindrical shells. The last method proposed was the SBPA, this method is promising; however, has not yet been validated for sandwich composite cylindrical shells. This means that more research is needed before the SBPA and WMPLA can be used for the prediction of the design buckling load of sandwich composite cylindrical shells.

### Conical shell

For the conical shells, the same methods apply as described for the cylindrical shells. Within literature, the SPLA and the SBPA are investigated most, so these will be the ones that are presented here. It should be noted that no research was found related to the perturbation methods of sandwich composite conical shells.

Khakimova et al. [36] studied if the SPLA can be used as a new guideline to determine the KDF for conical shells. In this paper, the same three conical shells were used as described in section 2.1.2 [35] to see the effect of the ply topology. The perturbation load was applied at  $z/H = 0.5$ , since it gives the most conservative results [32]. The KDFs of the three cylinders were determined using the SPLA and compared to the KDFs determined by a finite element model only including the measured geometrical imperfection. It could be seen that the method does give conservative results of the 2/3 cylindrical shells, which both have the same manufacturing method. Therefore, it was proposed that the imperfections that arise for conical shells are related to the manufacturing process and there should be different guidelines for different manufacturing processes. This was also stressed in section 2.1.2.

In order to further investigate the applicability of the SPLA for conical shells, Khakimova et al. [32] investigated the SPLA method for different composite conical shells. Numerical models were made for composite conical shells having three different lay-ups: quasi isotropic, orthotropic, and cross ply together with seven different geometries: semi-vertex angles varying between  $5^\circ$  and  $75^\circ$ . The perturbation load was applied at  $z/H = 0.5$  and the same curve as in figure 2.8 (left) was created for all different configurations. For the cross ply composite conical shell, it could be observed that the figure created by the SPLA did not show the bi-linear behavior when the semi-vertex angle increased. This means that the buckling load could not be determined for these cases and show the limitations of the SPLA. This has also been concluded for cylindrical shells.

Due to the limitations of the SPLA and the promising results of the SBPA for cylindrical shells, the SBPA has also been used for conical shells. Wagner et al. proposed the SBPA in [57] for metallic conical shells and in [54] for composite conical shells. For the composite shells [54], the results were compared with the experiments of composite conical shells and showed conservative results; however, the amount of data was limited. The same was tested for metallic conical shells since more data were available. However, the SBPA method did not result in conservative buckling loads for the 26 out of 180 metallic cylindrical shells.

To conclude, there are several numerical investigations performed using the SPLA and the SBPA for composite conical shells; however, the validation data are not yet sufficient to establish these methods as guidelines. Therefore, more tests should be performed on composite conical shells. Moreover, the SBPA showed unconservative results for metallic conical shells and because composite conical shells are more complex more investigation is needed.

### 2.2.3. Measured imperfections

The most accurate way to predict the KDFs of sandwich composite shells is to use measured data of the manufactured component. By generating a Finite Element (FE) model of the perfect structure and by inserting the measured imperfections, the non-linear buckling load can be determined. This method is proven to give accurate results and is described in further detail below. This method is based on the assumption that the manufacturing process of one manufacturer produces the same imperfection signature every time a part is manufactured meaning that the measured imperfections for one shell structure can be used for multiple structures [26]. Furthermore, the equipment used to determine the measured imperfections are constantly improved to give more accurate data [40], resulting in a better match between the experimental and numerical results. This subsection describes the ways of implementing the measured imperfections into the FE models and the results obtained using this method.

However, not for all the shell structures measured imperfection data is available. Especially during the design process, when the model has not been manufactured yet. Therefore, in [43], [48], [13], a method is described to use the available measured imperfections from other shell structures. This will be described in more detail below. The setup of this subsection is as follows: first the measured imperfection method is used for cylindrical shells and after that the measured imperfection method is described for conical shells.

It should be noted that this subsection focuses on the implementation of the measured imperfections in the FE model. No attention is paid to the modelling techniques used for the shell structures and how to set up a FE model. This is described in section 2.3.

### Cylindrical shell

Not a lot of buckling tests of sandwich composite cylindrical shells have been performed yet resulting in models that have not been validated. However, the modelling techniques for implementing the imperfections are still used as a guideline.

An example of a validated FE model including the measured imperfections is presented by Schultz et al. [47]. In [47], a full-scale sandwich composite cylindrical shell was tested. The test set-up and test article are described in subsection 2.1.1 so are not repeated here. In order to predict the buckling behavior of the CTA 8.1 test article, a FE model was created. More details on the FE model can be found in section 2.3. After the model was created, the measured imperfections determined by the measurement tests were added to the model. From the tests, the geometrical imperfections and thickness variation were gathered. The geometrical imperfection data were implemented in the FE model using a user written program. This program was used to convert the data into measured imperfections at each node location. When this was known, the nodes were perturbed by the amount determined by the code and an imperfect mid surface was created. The highest imperfection measured was 0.25 mm. Also the thickness variation was added to the model. The thickness variation was assumed to come from the difference of the core thickness. Within the FE model, the core thickness was changed for each element, which was done by alternating the composite ply properties of each element (the core is represented by one single composite ply due to the small core thickness). The material properties used in the FE model were assumed material properties of the honey-comb core and composite face sheets. However, pretests were planned to determine the material properties of the CTA 8.1, but due to testing difficulties the tests were canceled. Therefore, material imperfections were introduced into the model. When the first tests of the CTA 8.1 were performed, it could be seen that the FE model gave a different response due to a different stiffness. Then it was decided that the first tests performed act as calibration tests in order to match the material properties of the FE model with the test conditions. After the right material properties were added in the FE model, the actual tests were performed. The difference between the numerical and experimental results can be seen in figure 2.11. It can be seen that the difference is less than 1% and that including the measured imperfections into the FE model gives a good correlation with the experimental results. The reasons for the differences between the results are given in subsection 2.3.1, this is due to the fact that it is not related to measured imperfections. What can be concluded from this paper is that adding the measured imperfections to the finite element model the buckling load can be predicted.

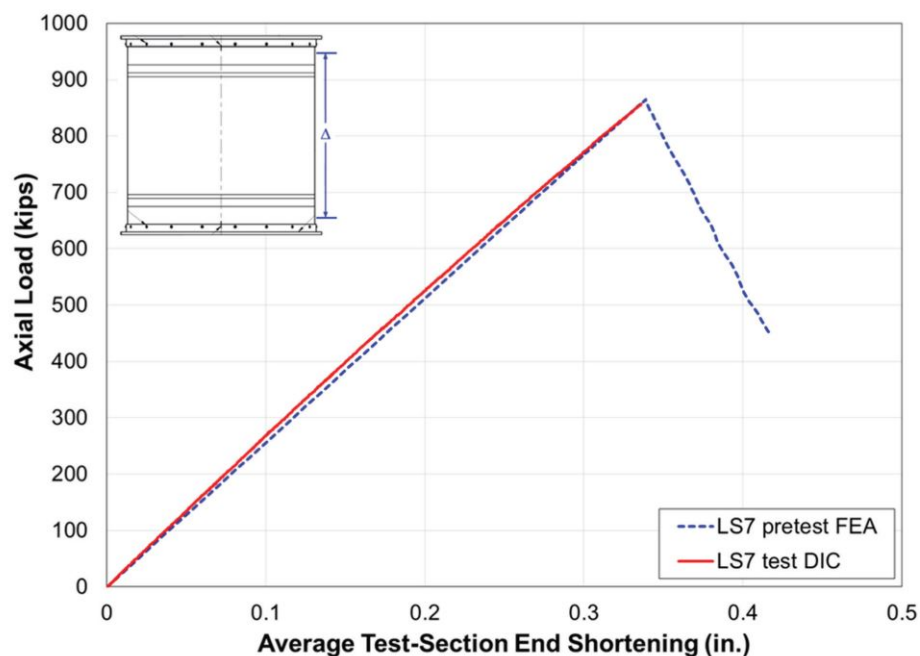


Figure 2.11: Load vs. displacement curves for the CTA 8.1 using FEM and experimental test [47].

However, measured imperfections are not always available. Since measured imperfections are the most



accurate way of implementing imperfections compared to other methods, researchers want to use this method [59]. In [46], a method is described to implement measured imperfections in the early stages of the design process. For this method, the imperfection signature of a different cylindrical shell was used. Four sandwich composite cylindrical shells were used in the analysis, the Ares V intertank and Interstage, and the Space Launch System (SLS) upper stage skirt and the Interstage. These cylindrical shells were modelled using FE software and the imperfection sensitivity was explored by adding geometrical imperfections. However, no manufacturer data were available, so the geometrical imperfection of a fluted-core sandwich composite barrel was measured. The barrel was manufactured by joining five panels including pad-ups using longitudinal scarf joints. The imperfection signature can be seen in figure 2.12.

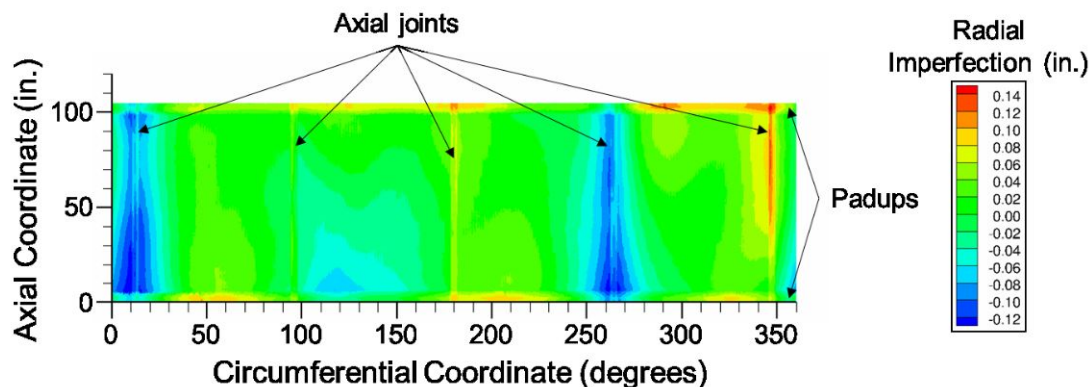


Figure 2.12: Geometrical imperfection of the sandwich composite barrel [46].

From figure 2.12, it can be seen that the largest imperfections occur at the joint and pad-up locations. Besides the fact that the actual designs do not include the joints, this imperfection signature was still used for the investigation. Due to the fact that the barrel did not have the same size as the launch vehicle structures, the measured imperfection had to be scaled to the same size. After the scaling was done, the imperfections were added to the FE models. Furthermore, the amplitude of the measured imperfection was kept as a variable and changed within the FE model. After that, analyses were run for all models with different imperfection amplitude and an imperfection sensitivity analysis was performed. The results showed that the NASA guideline was overly conservative and that depending on the structure the mass could be reduced by 4% to 19%. It should be noted that imperfection signatures of cylindrical shells that do not represent the current design well, should only be used for determining the imperfection sensitivity and the result should not be used as design buckling load.

Due to the fact that there is a lack in literature about methods to implement the imperfections into the FE model for sandwich composite cylindrical shells, the method described in [23] for composite cylindrical shells is shortly described here. This paper gives a detailed explanation on how to implement the geometrical imperfections, thickness variation, boundary condition imperfections, and loading imperfections into the STAGS software. It should be noted that the routines created in the STAGS software can also be created using python. The first step in the process was to generate a FE model with a perfect geometry. After that, the imperfections had to be added.

The geometrical imperfections and thickness variations were added to the model using subroutines. These subroutines are similar to the user written programs created by Schultz [47] as already explained above, so are not repeated here. Moreover, It should be noted that the method of implementing the geometrical imperfections has also been used in [59] and [58]. In order to account for the potting of the cylindrical shell 2D plane strain FE analyses were run. A FE model was created of the potting material including the cylindrical shell wall. These analysis were used to determine the stiffness of the potting material. When the stiffness was known the potting material was added to the total FE model by using linear spring elements at the edges of the cylindrical shell. The non uniform loading conditions were added to the finite element model by using the measured loading surface imperfections. This was done by perturbing the nodes at the load end of the shell by the measured amount.

In the paper [23], three cylindrical shells were modelled including imperfections using the subroutines described above. The specimens that were tested were 8-ply cylindrical shells with a length of 16 inch, a radius of 8 inch, and a nominal thickness of 0.04 inch. Each cylindrical shell had a different lay-up. The

numerical results and the experimental results were compared and it could be seen that the results match well. The load displacement graphs can be seen in figure 2.13. It should be noted that in this study also the uncertainty of the testing process was taken into account resulting in graphs including predictive bounds. The same author also tested three 16-ply composite cylindrical shells [25]. The buckling loads were predicted using the same software and imperfection modelling method as described above. Herein the results of the experimental test and the numerical model were similar and a similar graph was shown as in figure 2.13. The difference between the 8-ply composite cylindrical shell and the 16-ply composite cylindrical shell is that the knockdown factors are higher due to the increased thickness. These papers prove that the method of the measured imperfections give good results. This is also the case when the thickness of the shell increases, which can be related to a sandwich composite cylindrical shell.

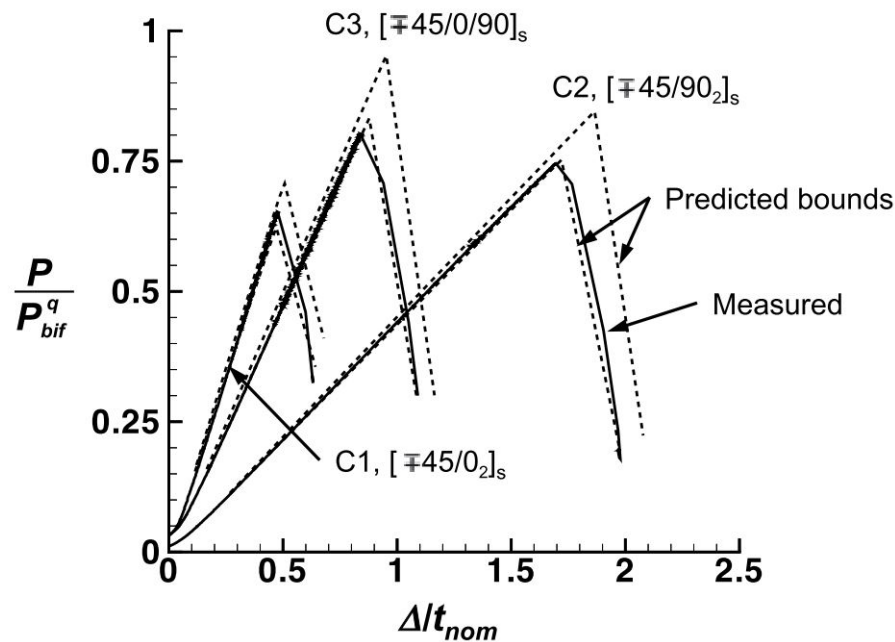


Figure 2.13: Numerical and experimental results of three composite cylindrical shells [23].

### Conical shell

This part describes the measured imperfection method for conical shells. It could be seen that when searching in literature not a lot can be found on the measured imperfection method for sandwich composite conical shells and only little can be found on composite conical shells. This also means that not a lot of test data exist. Firstly, a paper is described where a method was proposed on how to implement measured imperfections from a different structure. This paper is explained because of the use of sandwich composite material. After that, a fully validated model including measured imperfections is described for composite conical shells.

As said previously, not a lot of measured imperfection data can be found for conical shells. Therefore, Sleight et al. [48] proposed a method to still be able to inspect the imperfection sensitivity without knowing the actual imperfection pattern. Sleight studied the imperfection sensitivity of sandwich composite conical shells under axial compression. The conical shells considered were components from the Space Launch System (SLS), the Payload Attach Fitting (PAF) with a shallow semi-vertex angle and the Universal Space Adapter (USA) with a steep semi-vertex angle. The material used was a honeycomb core and composite face sheets. The imperfection sensitivity was investigated for different core thicknesses and different lay-ups. A FE model was created of the perfect conical shells. Due to the fact that no measured imperfections were available for large scale composite conical shells, the measured imperfections of the CTA 8.1 were used. The geometrical imperfection pattern of the CTA 8.1 was scaled both in length and circumferential direction in order to apply it to a conical shape. The amplitude of the measured imperfection was varied from 1x to 10x. The scaled imperfection pattern was applied to the FE model in a stress-free state. In figure 2.14 the imperfection pattern from the CTA 8.1 can be seen and in figure 2.15 the scaled imperfection pattern can be seen on the conical shell with an amplitude of 10x the measured imperfection. For all different configurations and amplitudes

analysis were performed.

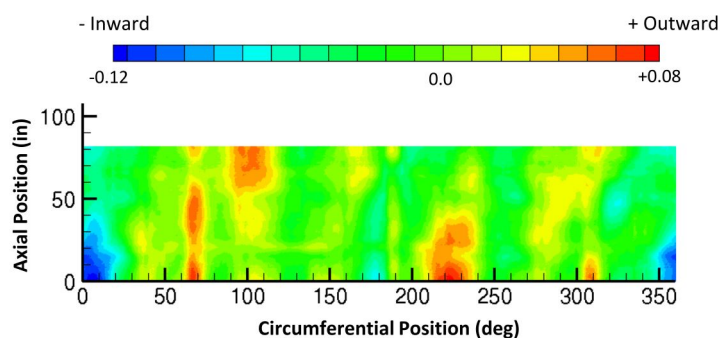


Figure 2.14: Measured radial imperfection pattern of the CTA 8.1 [48].

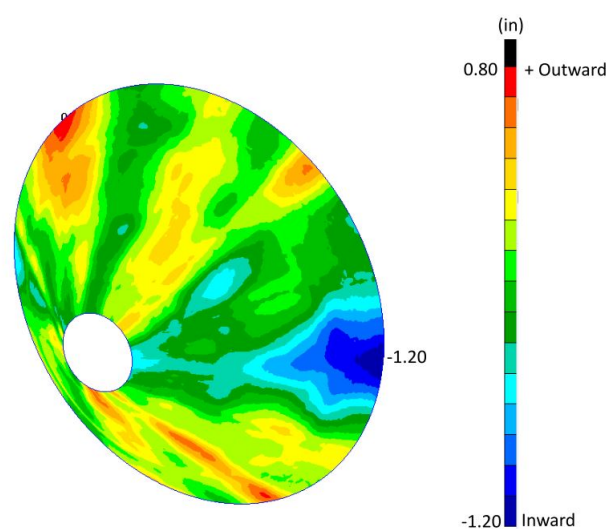


Figure 2.15: conical shell with imperfection pattern and 10x amplitude [48].

From the results it could be seen that for both of the conical shells with different core thicknesses and lay-ups, the knockdown factor was above 0.6 except for two cases. These two cases had a knockdown factor of around 0.5 and belong to the cases where the core thickness was 0.5 inch and the imperfection amplitude was 10x. From these results it can be observed that all values are above the NASA knockdown factor of 0.33, which proves that these guidelines are conservative. This report also proves that without knowing the actual pattern of the measured imperfection of the conical shell still the imperfection sensitivity can be investigated. It should be noted that an imperfection amplitude of 10x will only happen in extreme cases. During the manufacturing process, only small imperfections can arise due to regulations. However, during the assembly of the specimen to the testing equipment mishandling can take place resulting in high amplitude imperfections, since the chance that this will happen is low, an amplitude of 10x is still considered conservative. This means that taking the design knockdown factor of the value belonging to an amplitude of 10x will result in a conservative prediction.

Furthermore, a validated finite element model was presented using the measured imperfection method by Khakimova et al. In [35], a study is presented where the KDFs are predicted for three composite conical shells using measured imperfections. This study is performed to prove that the SP-8019 guidelines are conservative. The test setup and a short description of the test articles have already been given in subsection 2.1.1 and 2.1.2, and is not repeated here. A FE model was set up for all the three cones in Abaqus Standard 6.14 and the imperfections were modelled as accurately as possible. The imperfections considered in this paper were the mid-surface imperfections, the thickness variation, fiber volume fraction, and ply piece imperfection.

The FE model created was assumed to have a perfect conical shape. However, the actual shape of the

conical shells is not perfectly conical. Therefore, the cones were subjected to measurement tests and the 3D-scanning system ATOS was used to determine the geometrical imperfections. The measurement system created a data file that was the input for the GOM inspect software. This software package fits a conical shell through the data points resulting in a reference configuration. Then the measured data together with the reference configuration is used to determine the deviations. These were then transported to a text file in order to load them in the DESICOS ABAQUS-plugin. The plugin was able to read the data and calculated the perturbation that was needed for each node of the FE model using a weighted interpolation technique. These calculated perturbations were added to the nodes and the final surface can be seen in figure 2.16. The same method of adding the geometrical imperfection is presented in [20] using a different software package.

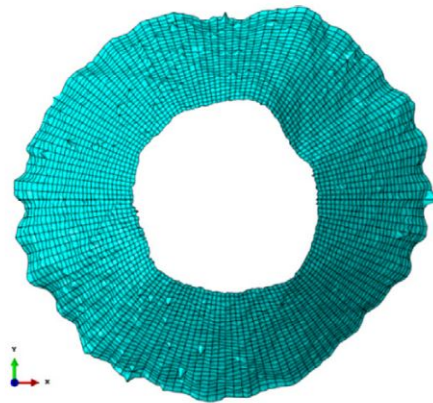


Figure 2.16: Measured imperfection surface of conical shell scaled by a factor 100 [35].

The next imperfection that had to be added was the thickness variation. Ultrasonic scanning was used to determine the difference between the inner and outer surface. The data were processed in a similar way as described above for the geometrical imperfections. For the thickness variation, the thickness and coordinates had to be saved to a text file. This text file was then added to the FE model resulting in a thickness plot, which can be seen in figure 2.17.

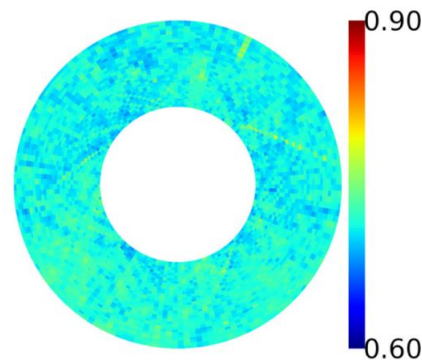


Figure 2.17: Thickness plot of the conical shell [35].

This method of adding the thickness variation to the model has some limitations. As what can be seen in figure 2.17 the thickness is assigned to each element. By using this procedure the assumption is made that the thickness is the same for the whole element. Moreover, it is assumed that within each element the plies have the same thickness. However, the thickness deviation occurs due to ply gaps and overlaps which makes this assumption not valid. Furthermore, the range of true thickness values for each element is enormous and in order to keep it manageable, a list of thicknesses with corresponding lay-up is used. This results in that the closest value with respect to the true thickness is chosen from the list resulting in a small error.

As said above, the material properties stay the same for each element. However, in order to better represent the material properties of the conical shell, it was assumed that the thickness variation is the result of the

change in the amount of matrix volume with the amount of fibers staying constant. For each element the new volumes are calculated and by using the composition rule and the corrected composition rule by Chamis [15] the material properties can be calculated for each element. For implementing the material properties into the FE model the same process as for the thickness imperfection is used; however, for each element also new material properties had to be defined.

The final imperfection that had to be added was the ply piece imperfection. In the FE model created the fiber angle is constant. However, as described in subsection 2.1.2, the lay-up is performed with a finite number of ply pieces which results in fiber angle deviations. The process that was used to add this deviation in the FE model is as follows: first the ply topology had to be determined accurately, and then for each ply piece and element, the fiber orientation had to be changed to the right value. This had to be done for each element. The limitations of this method is that the fiber angles are determined by using the as to be built structure, which means that production mistakes are not taken into account. Moreover, at the edges of the cone there are no fibers present resulting in a weak spot. However, this is not implemented in the FE model.

After the imperfections were implemented in the FE models, the analyses could be performed. The buckling loads of the FE models were compared with experimental data. A good correlation with the experimental results can be seen for two out of the three conical shells as shown in figure 2.18. The deviation of the K08 cone can be explained by the fact that the angle deviations have not been taken into account accurately enough. This is because there have not been a method proposed yet how to accurately measure the ply angle deviations. In order to overcome this problem a worst and best case scenario of the ply angle imperfections have been implemented. Figure 2.19 shows the improved graph and it can be seen that the gap between the experimental and FE results is closed. This also means that the ply topology is an important factor to implement accurately into the FE model. It could also be seen that all three composite conical shells had knockdown factors of above 0.6, which is much higher than the value of 0.33 obtained using the SP-8019 guidelines.

To conclude, It can be seen that by using the measured imperfection method a design buckling load can be determined. Since the FE models have been validated it proves to be a good method to include the imperfections. It is assumed that the method presented herein for composite conical shells can also be used for sandwich composite conical shells. The difference lies in the implementation of the thickness variation. For sandwich structures it can be assumed that the thickness deviation occurs due to variations in the core meaning that no new material properties have to be determined for each element. In order to apply the thickness variation to the core, the thickness of the ply representing the core has to be changed. This process has already been explained above. Furthermore, the implementation of the ply angle deviation should be done correctly in order to match the experimental with the FE results. However, for that to improve first the measurement techniques to detect ply angle deviations on conical shells should be upgraded.

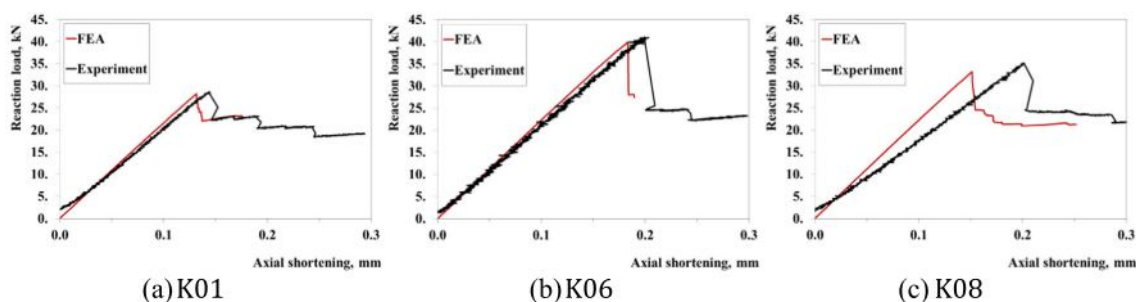


Figure 2.18: Load vs. displacement graphs for the conical shells [35].

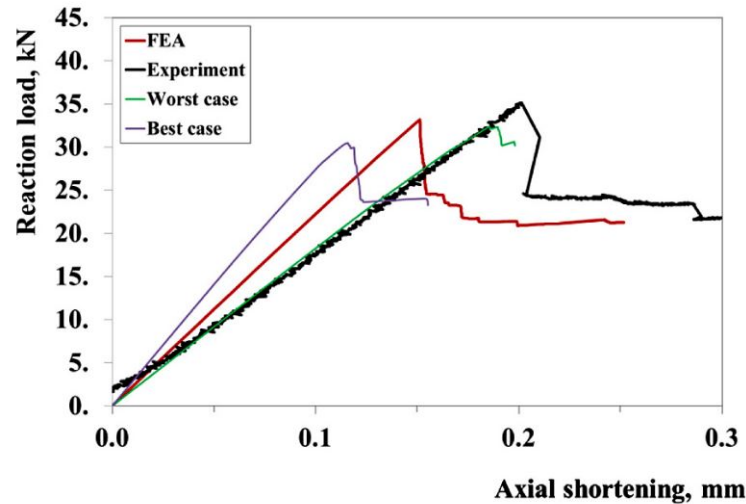


Figure 2.19: Different ply angle imperfections used for the K08 cone [35].

#### 2.2.4. Stochastic methods

It is important that the modelled imperfections represent the real imperfections. In order to check if the modelled imperfections are accurate, buckling tests are needed. When realistic imperfections are modelled it results in less conservative designs, cost-efficient, and light weight structures. However, it would take a lot of time to manufacture and test every shell structure. In the early stages of the design process it is not even possible to manufacture the shell structure but still an imperfection estimate is needed.

Therefore, the DESICOS project explored the probabilistic methods to determine new KDFs for shell structures. These methods use the measured imperfections gathered during the tests for a probabilistic analysis. It is assumed that when the shell structures are manufactured at one manufacturer the imperfections stay within probabilistic bounds when producing a new shell structure. In this way only a few shell structures have to be manufactured and measured. The imperfection pattern obtained including a probabilistic analysis can be used for other shells manufactured at the same manufacturer. In the end a guideline can be established for determining the KDFs for different manufacturers. This subsection describes the probabilistic methods that are proposed. Due to the fact that the probabilistic methods are not yet explored for conical shells, this subsection focuses on the methods developed for the cylindrical shells.

Arbocz and Hilburger [6] proposed a probabilistic approach to determine a new lower bound for composite cylindrical shells. In this paper the first-order second-moment (FOSM) method was explained and compared to the Monte Carlo method. The Monte Carlo method uses the characteristics of the statistical input variables for making samples. Then for each of the samples the buckling load is determined and a statistical evaluation is performed on the buckling loads obtained. The FOSM method uses a database containing properties of a number of shells such as the geometry, material properties, and geometrical imperfections. This data base is then used to predict the reliability function and to obtain improved knockdown factors. The results of the FOSM were validated using the experimental buckling loads of nine composite cylindrical shells. It could be seen that the methods gave conservative results for every cylindrical shell. After the results were presented, also a comparison between the methods was made. The major differences between the FOSM method and the Monte Carlo method are that the FOSM method takes less computational time and that approximations are introduced.

Due to the fact that methods are needed that do not require approximations but are based on actual data, Bisagni and Alfano presented several papers on new probabilistic approaches that do not require approximations. In [3], a method is presented where the Monte Carlo Method is combined with Latin Hypercube sampling.

Within this paper, three cylindrical shells were used as test articles, two composite shells and one sandwich composite shell. Different imperfections were studied: uncertainty of longitudinal Young's Modulus, uncertainty of ply orientation, loading imperfection, and geometrical imperfections. For each of the imperfections the method was used to determine the best fit probability density functions and the knockdown factors. The knockdown factors obtained for the sandwich composite cylindrical shell can be seen in 2.1. It

can be seen that the Young's modulus and the geometrical imperfections have to most influence on the buckling load. It was also observed that the knockdown factor obtained using the probability method was higher when compared to the value of the NASA SP-8007 guidelines. This method was proposed to investigate the effect of the input parameters on the buckling load. Therefore, it is advised to use this method only during the intermediate stage of the design process.

Table 2.1: Knockdown factors for different imperfection types for the sandwich cylindrical shell [3].

Imperfection	Knockdown factor
Young's Modulus	0.83
Ply orientation	0.96
Loading imperfection	0.92
Geometrical imperfection	0.7
All	0.53

Bisagni and Alfano [11] presented another probabilistic method to analyse the buckling behavior of sandwich composite cylindrical shells. This method is able to account for geometrical imperfections, thickness variation, ply misalignment, and boundary imperfections. The Stress-Strength Interface Method and the Latin Hypercube Method were both used for the analysis. This method was used to analyse the buckling behavior of the scaled Dual Launch System (SYLDA) of the Ariane 5 launcher. The cylindrical shell consist out of a foam core with composite face sheets and was manufactured to measure the geometrical imperfections and the thickness variation along the shell surface. These imperfections were the inputs for the probabilistic approach. A block diagram of the process can be seen in figure 2.20.

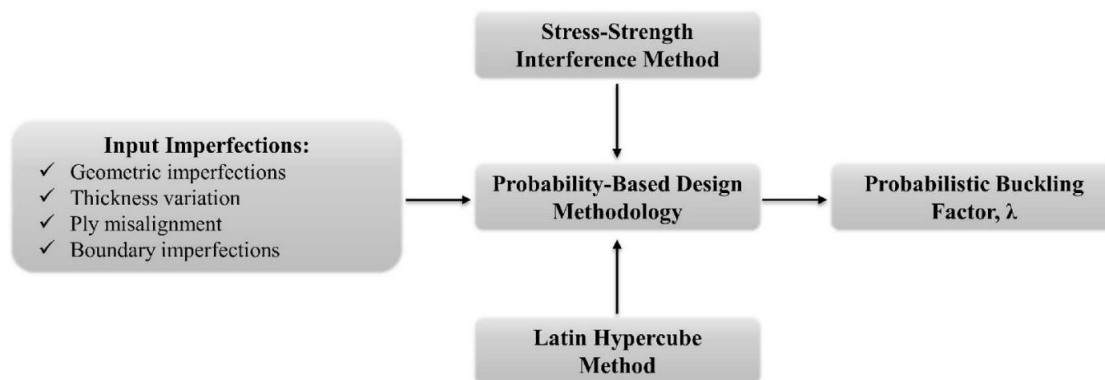


Figure 2.20: Block diagram of the probability based methodology [11].

Since the measured imperfections were needed for the probabilistic approach, the SYLDA was exposed to measurement tests. LVDTs were used to determine the geometrical imperfections. A best-fit cylinder approach was used on the data. The thickness variation was determined by calculating the difference between the inner and outer surface measurements.

The measurements were used to determine the input parameters for the probabilistic analysis. In past researches [6], [31], [58], it was discovered that the geometrical imperfections have a specific pattern, which can be represented by a half-wave cosine double Fourier series. The measured data of the geometrical imperfections were used to determine a half-wave cosine double Fourier series with imperfection amplitude and imperfection phase. A multivariate Gaussian distribution was then employed to vary the imperfection amplitudes and imperfection phases. The same process was used for determining the input of the thickness variation. The ply misalignment was assumed to be normally distributed. Since no data were available for the boundary condition imperfections, a one dimensional Gaussian random field was used to create the boundary condition imperfections.

After the input parameters were known, a FE model was created of the sandwich cylindrical shell. S4R elements were used to represent the structure and fixed boundary conditions were employed. The imperfections were added by perturbing the nodes in the FE model using a user written MATLAB program.

After executing the probabilistic analysis, the knockdown factor obtained was 0.75 for 99% probability.

The knockdown factor calculated using the SP-8007 was 0.57, which is much lower. Moreover, in [4], Alfano and Bisagni presented the same probabilistic method and analysed another sandwich composite shell, the Interstage Skirt Structure (ISS) of the Ariane 5. The knockdown factor determined by this method was 0.79 for 99% probability. Again, the KDF determined by the SP-8007 guideline was much lower and equal to 0.64. Besides the fact that the method shows promising results more identical shells to the SYLDA and the ISS have to be manufactured in order to create a large data set. More data make the probability approach more reliable and eventually a lower bound for determining the knockdown factors for these particular shells can be generated.

Another approach that was proposed was to generate a manufacturing signature of the geometrical imperfections, which could be used for different cylindrical shells manufactured at the same manufacturer. In [23] the measured geometrical imperfections were used and rewritten as a double Fourier series using the same approach as described above. However, in order to establish a manufacturing process specific imperfection signature the Fourier coefficients had to be determined by using geometrical imperfection data of several cylinders in order to be reliable. By using the data of several cylinders, the Fourier coefficient were determined by using a probability distribution. The result was a mean imperfection shape and a corresponding standard deviation that were based on the measured data. Now by using the imperfection signature and implementing them in the FE model a buckling load range could be obtained. This was tested for one composite cylindrical shell and the result can be seen in figure 2.21. What can be seen that the as-measured result lies within the bounds of the prediction. It should be noted that this approach results in a lower bound for determining the knockdown factors for a specific manufacturing process if validated with more test data.

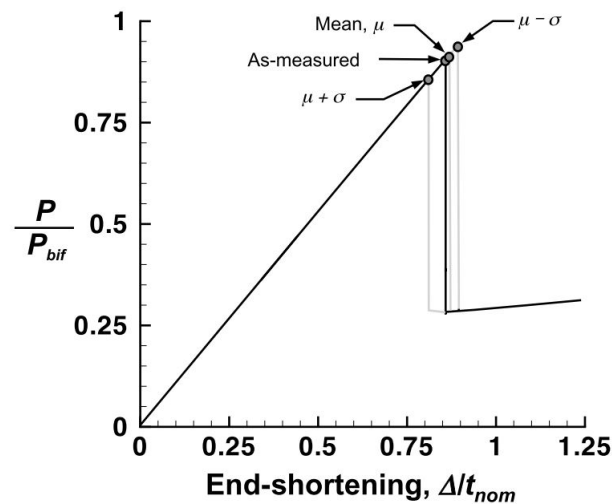


Figure 2.21: Predicted bounds of the buckling load of a composite cylindrical shell [23].

A different way of using a probabilistic approach is to only use it for the imperfections that are unknown. This approach combines the measured imperfections with probability based imperfections. This means that the unknown imperfections will be assumed using a probability density function. In [17] such an approach is presented. In this study the loading imperfections and material imperfection were assumed with probability distributions. In order to create the different samples the Monte Carlo method was used. The samples generated were modelled using FE software. The buckling loads were calculated for each shell and a probability density function could be determined. The results were then compared to experimental results and showed promising results. However, the author stresses the importance of the choice of probability density function for the unknown imperfections. Such an approach was also used in [24] where the uncertainties that arise during the buckling test were unknown. Examples are imperfect measurements, the fiber volume fraction, and variations in the applied load. These were assumed using a lower and upper bound. By implementing the minimum and maximum values in the FE model a margin could be found for the buckling load. When the experimental and probability based results were compared it could be seen that the experimental results lied within the probability bounds. This means that this method is able to account for the uncertainties during the manufacturing and testing processes. These two methods ensure that without having all the measured data the buckling loads still can be approximated by taking into account all the possible imperfections.

The probabilistic methods proposed in this subsection show promising results. However, in order to make



a probabilistic approach reliable a lot of test data are needed. When more data are available a lower bound for determining the KDFs can be obtained. Another way of implementing a probability approach in predicting the KDFs of shells is by assuming a probability density function for the unknown imperfections. By using this approach all the imperfections can be taken into account.

### 2.2.5. Discussion of the methods

In this subsection three ways of determining new guidelines for calculating the KDFs have been presented. This subsection will discuss the differences between the perturbation methods, measured imperfection methods, and stochastic methods. For each of the methods the advantages and disadvantages will be given.

An advantage of the perturbation methods is that these methods can be used in the early stages of the design process since no test data are required. The implementation of this method is also easy since the only requirement is a finite element model. A disadvantage of this method is that it is not known if these methods can impose the real imperfections if no test data are used. It has already been proven that these methods are able to only account for geometrical imperfections and loading imperfections. If a shell is sensitive for thickness variation this will not be taken into account and non conservative results will be obtained. Furthermore, the methods presented in this subsection have only been tested and validated using composite cylindrical shells and conical shells. It is not yet proven that these methods also work for sandwich composite cylindrical shells and conical shells. As can be seen in subsection 2.2.2, poor results are obtained for two sandwich composite cylindrical shells using the SPLA method. Since these methods have not yet been validated for sandwich composite cylindrical shells these cannot be used during the thesis.

Furthermore, the measurement technique methods are proven to give good results if the modelling is done correctly. By using actual measurement data the imperfections can be modelled accurately and the FE element software can predict the buckling load well when compared to the experimental results. However, for this method the design has to be manufactured and measured in order to gain the measured imperfections. It is possible to use the measured imperfection of different shells if the measured imperfections of the current design are not available. In order to do this it is required that the shell is similar to the current design and should have the same manufacturer if the purpose is to predict the buckling load. If only the imperfection sensitivity has to be determined any imperfection signature can be used. The methods presented in this subsection are a good option to be used during the thesis since there are measured imperfection available of the CTA 8.1 test article, which is a similar cylindrical shell that also will be used during the thesis.

The last methods that have been proposed are the probabilistic approaches. For these approaches the measured imperfections of a series of identical cylindrical shells are used to determine the lower bound of the knockdown factors. These methods are based on the assumption that a manufacturer has its own imperfection signature resulting in the same imperfection pattern every time. This method shows promising results; however, for it to be used as a guideline a lot of test data are required. The test data have to be obtained using measurement tests of similar shells. Since this takes a lot of time and cost, the probabilistic approaches that have been proposed do not have enough data yet to be reliable. Since during the thesis project no data set is available for the measured imperfections of similar shells, these methods cannot be used.

## 2.3. Modelling techniques

The thesis focuses on analysing the buckling behavior and imperfection sensitivity of sandwich composite cylindrical shells and conical shells by using numerical methods. For the purpose of the thesis, Finite Element (FE) models have to be created and analysed. Therefore, this section investigates the different modelling approaches in Abaqus to accurately represent the buckling tests of cylindrical shells and conical shells. It should be noted that for the modelling of the imperfections of sandwich composite shells similar techniques can be used as for composite shells when buckling is investigated. However, if the failure of the sandwich composite shells becomes a phenomena of interest, different modelling techniques are needed due to the difference in failure modes. Moreover, there are different solvers available within Abaqus and this section is meant to explore them. The structure of the section is as follows: the first subsection explains the modelling techniques used to create sandwich composite cylindrical shells in FE software, and after that the modelling techniques employed for sandwich composite conical shells are discussed. This is followed by a comparison between the solvers that can be used to perform buckling analyses. The last subsection covers the type of elements that can be used for the modelling of sandwich composite structures.

### 2.3.1. Cylindrical shell

This subsection describes the modelling techniques used to accurately represent the buckling tests of sandwich composite cylindrical shells. First, a paper is presented that shows a validated FE model and after that, two papers are described that investigate the need of incorporating the whole test setup in the FE model.

Schultz et al. [47] compared experimental results with numerical results using a FE model generated in Abaqus 6.14. This paper investigated how the buckling tests can be modelled best and the goal was to perfectly match the experimental results with the numerical results. The specimen and the test setup used have already been discussed in subsection 2.1.1 and will not be repeated here.

In order to accurately represent the experimental buckling test performed, the whole test setup was modelled using FE software. A visual representation can be seen in figure 2.22. Within the FE model the specimen including pad-ups, load introduction struts, load introduction platforms, and end rings were realized. Within the FE model the specimen was realised using S4 four noded general purpose shell elements and a combination of the S4 shell and B31 shear-flexible beam elements were used for the adjacent structure. After the model was built, a convergence study was carried out to determine the amount of elements needed.

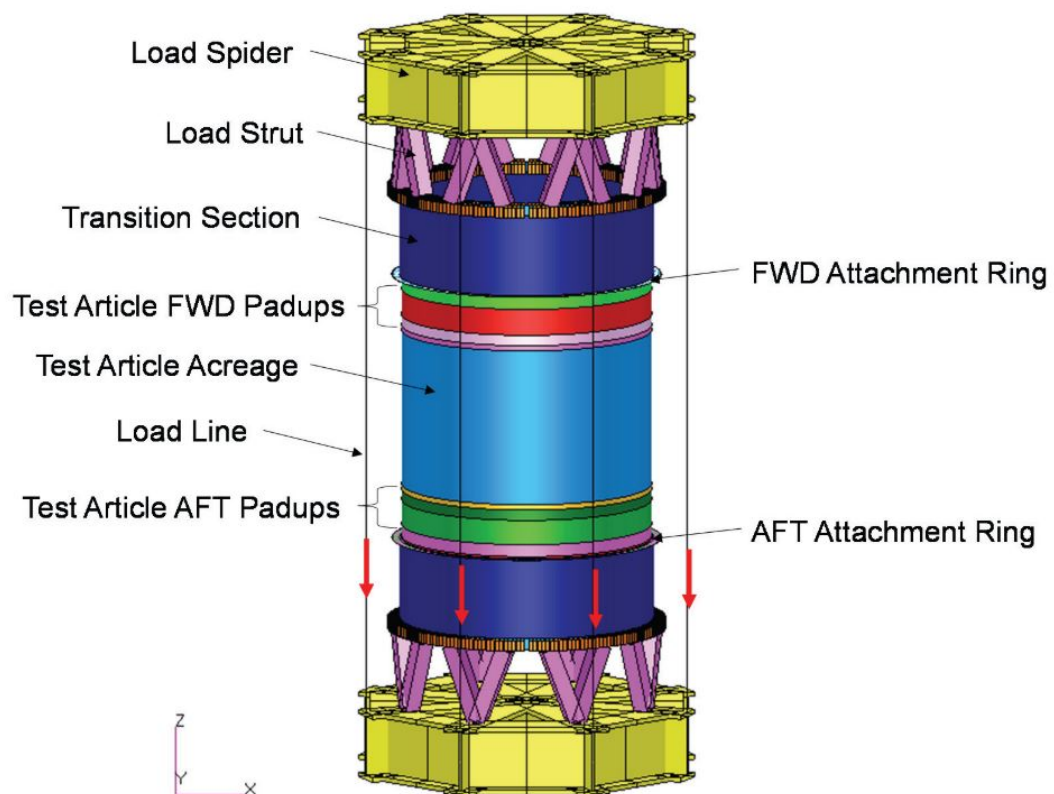


Figure 2.22: CTA 8.1 finite element model [47].

Not only the test setup was modelled as accurately as possible but also a detailed model of the specimen was created. Attention was paid to the way in which the sandwich composite material, imperfections, and pad-ups were modelled. The sandwich composite material was implemented in the FE model by using plies. Within the Abaqus software there is a composite material option available where all the plies can be specified. It should be noted that the core was represented by one ply with the material properties of the core material. The face sheets were implemented individually in the lay-up. As stated in subsection 2.1.1 the CTA 8.1 test article was subjected to measurement tests in order to determine the imperfections. These imperfections were implemented in the FE model as described in subsection 2.2.3. Moreover, the pad-ups were also modelled by using the exact lay-up and ply drops.

After the modelling was done, the boundary conditions and the loading conditions could be added to the model. The load was introduced by using eight load points placed at the end of the loading beams. The bottom load platform was fixed by constraining the translational and rotational directions. The top load plat-

form was also fixed except for the axial direction, this in order to allow axial displacement of the specimen. The load applied is visualized in figure 2.22 by the red arrows. The analyses that were run used displacement control, since this is also used during actual buckling tests. In order to determine the buckling load and to investigate the final point of failure, non-linear static analysis and non-linear transient analysis were used. The non-linear static analysis performed the buckling analysis until the load was 80% of the predicted buckling load. After that, the non-linear transient analysis continued the analysis to determine the buckling load and the post buckling behavior. By looking at the load vs. displacement graph the buckling load could be determined.

In order to match the numerical results with the experimental results pre tests were performed to examine the material properties used by the FE model. It could be seen that in order to match the stiffness of the experimental results the material properties assumed had to be increased by 8.7%. After this adjustment the buckling load differed 1%, the load vs. displacement graph can be seen in figure 2.11. However, when looking at the graph before buckling still a small difference between the results can be observed. It can be seen that the material behavior before buckling was non-linear instead of linear which was not incorporated in the FE model. Moreover, the buckling initiation side was not identical for the experimental result and the numerical result. Due to these differences a post test analysis was needed. The first step was to investigate the reason for these deviations. The stiffness difference could be explained by the thickness of the experimental ply laminates, which was 9% thicker than expected. The non-linearity could be explained by non-linear material properties. In order to remove the difference and capture the non-linear behavior before buckling a non-linear relationship of the material properties was established. Moreover, the buckling initiation site differed between the experimental and numerical results due to imperfect loading. By implementing these adjustments the differences between the results were solved and an accurate representation of the buckling test was created. To conclude, a validated FE model was created for this test article. This means that FE models are able to capture the behavior of sandwich composite cylindrical shells under axial compression.

Since it takes a lot of time to model the whole test setup, it is investigated if this is really needed. Przekop et al. [43] presented a paper where the design of large-scale sandwich composite cylindrical shells for the SKBF project is explained and where different FE models are created. Within this paper designs are proposed which were generated using analytical equations and nondimensional parameters. These results were verified by using FE models. Within this paper two different FE models of the buckling tests were created and compared in order to explore the modelling techniques. The specimens that were used consisted of a honeycomb core with composite face sheets. Different lay-ups and thicknesses were used for the analyses. For all the specimens detailed FE models were created using Abaqus, the reason for this is that the closed-form solution of the initial test article had limitations. By only using analytical expressions the pad-ups, load introductions rings, and imperfections could not be taken into account.

For the buckling analyses two different models were created, one model consisting out of the specimen including pad-ups and end rings and one model including the specimen and the surrounding structure. This was done in order to verify the assumption that adding the whole loading introduction structure does not change the output of the results much. The first model was created using S4R reduced integration shell elements. The sandwich structure was modelled by representing the core as one single ply within the composite stacking sequence. Furthermore, the face sheets were individually added as plies within the model. By using the manufacturing files of the materials used, the material properties could be determined.

The second model created included the surrounding structure. This includes: the loading spider, struts, and load lines. The FE model looked similar to the FE model presented in figure 2.22. This model was created by adding the surrounding structure to the first model described above. The loading introduction cylinders were implemented using the S4R shell elements with a coarser mesh when compared to the mesh of the specimen. Modelling of the load spider and struts was done by using B31 beam elements with an even coarser mesh. The load lines were modelled using one T3D2 truss element for each line.

After the modelling was done, a linear eigenvalue analysis was performed to verify the closed-form buckling calculations. In order to account for the non-linear behavior in the pre buckling regime, the quasi-static linear and geometrically non-linear static analyses were used. Another reason for doing non-linear analyses was because of the design of the pad-ups. By using the results, the pad-ups could be altered and optimized. An implicit transient geometrically non-linear analysis was performed to determine the state at buckling and to analyse the post-buckling regime. First, the analyses were performed on the perfect models and it could be seen that some perfect cylinders showed a load plateau meaning a very good stability. However, in reality this would never happen so the mesh was somewhat perturbed in axial and radial direction. It should be noted that when this is done the shape of the perfect cylindrical shell should be retained. The loading plateau has to

be removed because the results should represent the actual behavior of cylindrical shells. After that, analyses were run including imperfections. Furthermore, the results of the FE model including the whole test setup and the FE model without the whole test setup were compared. It could be seen that the difference between the buckling loads was 0.31%, which shows that using a simplified model is good enough for predicting the buckling load.

Another paper that investigated the need of implementing the whole test setup in the FE models was presented by Cha and Schultz. Cha and Schultz [14] created two FE models of a honeycomb-core composite cylindrical shell, whereas one model consist of the free length of the cylindrical shell where the end rings were modelled as boundary conditions and the other model included the end rings with load introduction cylinders. The purpose of the paper was to compare both models. The cylindrical shell was modelled as a single shell with the honeycomb-core as an extra ply, this method is only valid for thin-walled sandwich structures. The load introduction cylinders were made out of steel, so the material properties of steel were used for the modelling. Throughout the model, S4 elements were used. The boundary conditions for the model without the loading introduction cylinders were applied at the edges of the cylinder, whereas the potting was simulated by fixing the nodes in the potting region in all directions except for the axial direction. The edge of the cylinder was fixed at one edge and on the other edge the compression load is applied. A rigid body link was used to tie the nodes along the edge to a reference point. Compression was applied to the reference point. This modelling technique imposes that the loading introduction was done by a rigid plate.

The second model created consisted of three parts, the cylindrical shells with the end rings and the steel cylindrical load introduction cylinders. Important to note is that the load introduction cylinders did not have the same size as the cylindrical shell. All three parts were modelled using shell elements. In order to simulate the buckling test, one load introduction cylinder was constraint in all directions and one load introduction cylinder was constraint in all directions except for the axial direction. As described for the model above the load was applied using a reference point which was connected to the end nodes of the load introduction cylinder. A sketch of the modelled load introduction can be seen in figure 2.23.

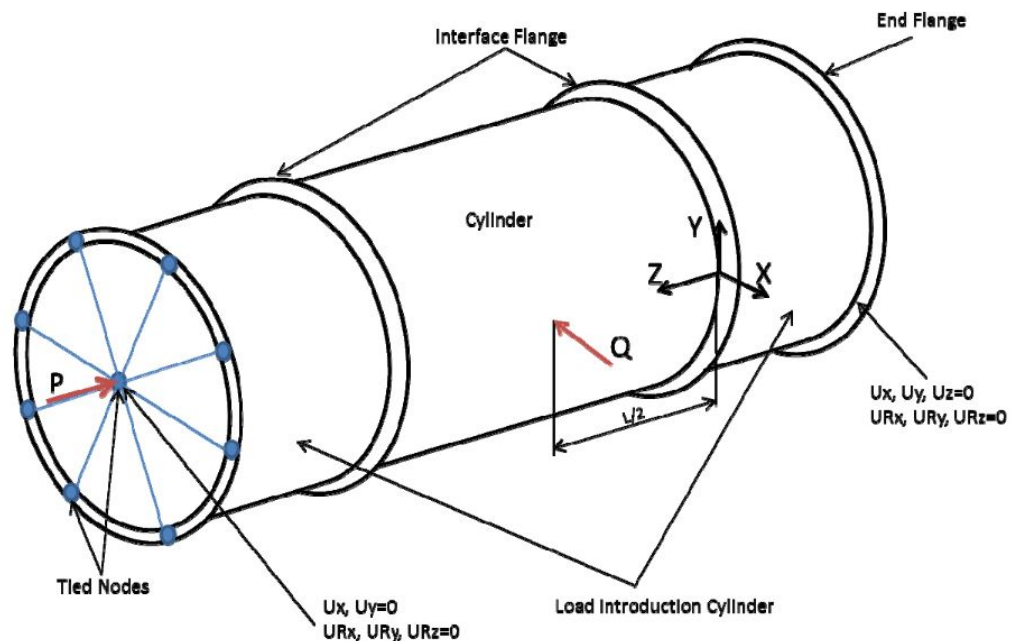


Figure 2.23: Sketch of FE model including load introduction and degrees of freedom [14].

After the modelling was done, a convergence study was performed for both models. This was followed by a linear eigenvalue buckling analysis and a non-linear analysis. Geometrical imperfections were introduced using the SPLA. The linear eigenvalue buckling analysis results of both models were similar, the difference between the buckling loads was 0.02% and the buckling shapes were the same. These results were checked with an analytical model. For the non-linear analysis the results were also close to each other and the difference between the buckling loads was 2.6%. After that, the geometrical imperfections were added to the models.

For the model including the loading introduction cylinders the KDF was 0.64 and for the other model the KDF was 0.67. This means that the difference is small and that without modelling the loading cylinders the result is still accurate. Another observation was done when looking at the results of both models. In the model where the loading cylinders were added, an additional rotation could be seen at the interface of the load introduction cylinder and the cylindrical shell. This could be explained by the misalignment between the radius of the specimen and the load introduction cylinders, resulting in an extra rotation when compared to the model without the load introduction cylinders. For the model without the load introduction cylinders this rotation is constraint due to the boundary conditions applied to the model. This additional rotation can be seen as an error in how the load introduction cylinders have been modelled. Therefore, care should be taken when implementing the load introduction structure of the buckling tests.

### 2.3.2. Conical shell

This subsection presents the modelling techniques used for sandwich composite conical shells and composite conical shells, because no literature could be found on validated sandwich composite conical shell models. In this subsection, one paper is presented where the modelling of sandwich composite conical shells is explained; however, no validation is presented for these models. After that, another paper is presented where the validation of the FE models of three composite conical shells is discussed.

Sleight et al. [48] presented a study where the buckling imperfection sensitivity was investigated for sandwich composite conical shells. Two conical shells were analysed which were based on space launch systems, whereas one had a low value of the semi-vertex angle and the other one had a high value of the semi-vertex angle. Within this study, FE models were created with different geometrical imperfections. The program that was used for generating the FE models was Abaqus 6.14. It was chosen to select the number of elements in axial direction depending on the aspect ratio at the mid height of the conical structure. An aspect ratio of 1:1 was striven for. The elements used were the S4R four-node, quadrilateral shell elements with reduced integration and a large-strain formulation. The boundary conditions were applied by using a center node in the middle of the top and bottom of the cones. The center nodes were connected to the edges of the cone by using multi-point constraints to the nodes located on the edges. The bottom was constraint in all translational and rotational degrees of freedom and the top was constraint in all translational and rotational degrees of freedom except for the axial degree of freedom. The compression load was applied using displacement control at the center node located at the top of the conical shell. The final model created can be seen in figure 2.24. After the modelling was done, the buckling loads of the perfect structures were determined using linear buckling analysis. For the imperfect structure, non-linear static and non-linear transient analyses were performed. The non-linear static analysis was used to load the structure up to 80% of the predicted buckling load for the perfect cylinder and after that the non-linear transient analysis was used to simulate the buckling and post buckling phase. These analyses were performed for different imperfection amplitudes and different cone geometries. The results are not presented here because it is not related to FE modelling. This paper is presented to give an example of how a sandwich composite conical shell can be modelled and analysed. It should be noted that for the modelling of sandwich composite conical shells the same methods are used as for sandwich composite cylindrical shells.

Khakimova et al. [35], [36] validated FE models with measured imperfections by the use of experiments. The test setup and the conical shells employed were already described in subsection 2.1.1, so will not be repeated here. The FE models were created using ABAQUS Standard 6.14 (implicit) together with a plugin that was developed during the DESICOS project. The conical shells were modelled using S8R elements which is a quadratic thin shell with 8 nodes per element and six degrees of freedom. The reason for using these elements is explained in [20] and [19], where a trade-off is presented between the accuracy of the results and computational cost. It should be noted that both papers use composite conical shells as specimens. Moreover, reduced integration was incorporated. The number of elements was determined by a convergence study. Furthermore, the boundary conditions were applied using fixed constraints at the bottom of the shell, resulting in a clamped boundary condition. At the top of the shell the translations were constraint in all directions except for the axial direction, the rotations were constraint around all the axes. The load was applied by using a reference point in the middle of the top of the conical shell. This reference point is linked to the nodes along the top edge using pin constraints, constraining all translations. The loading is applied to the reference point using a time varying axial displacement. For determining the buckling load, the Newton-Raphson iterative solver with artificial damping was employed due to the good results obtained in [13], [5], [17]. By incorporating the measured imperfections, the buckling loads of the experiments were matched with the buckling loads of the FE models. The load vs. displacement graphs can be seen in figure 2.18. It can be seen that the results

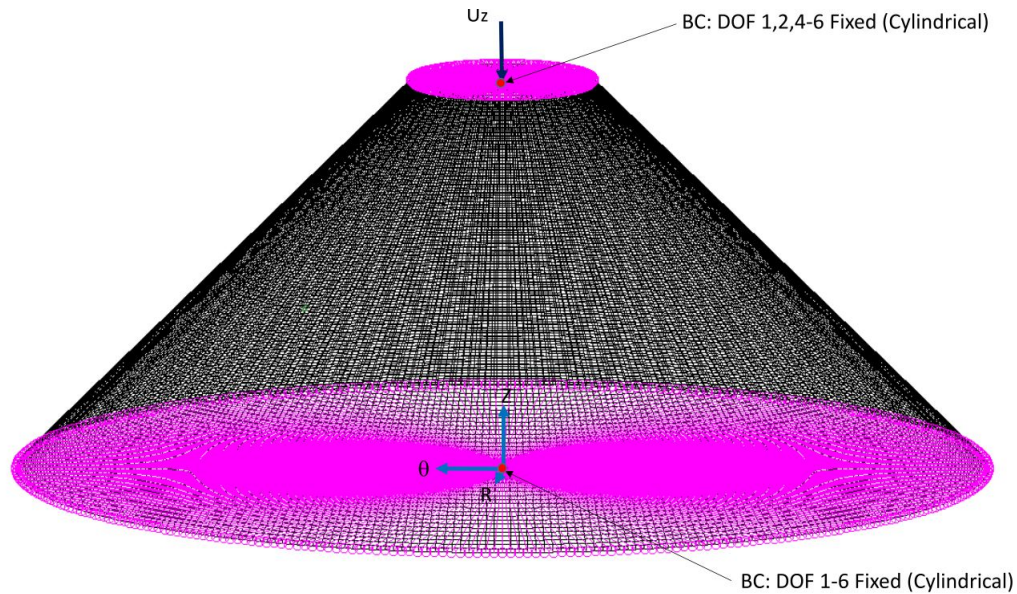


Figure 2.24: FE model of conical shell with degrees of freedom [48].

are similar for two out of the three cones. In order to close the gap between the experimental and numerical results, the resin rings were added to the FE model to see if it affects the load-displacement curves. It could be seen that the change in buckling load is negligible and the change in stiffness is only 6%. This closed the gap of K01 and K06; however, the deviation between the results for the K08 conical shell was still large and could be explained by the fiber angle deviation between the FE model and the experimental specimen as described in subsection 2.2.3. The present paper proves that by using FE models the buckling behavior of conical shells can be predicted.

### 2.3.3. Buckling analysis in Abaqus

When the sandwich composite cylindrical shell and conical shell are modelled, the buckling behavior has to be analysed. This can be done by using different solvers in ABAQUS. The solvers that are mostly discussed in literature are the eigenvalue solver, the non-linear Riks method, and a dynamic analysis. Bisagni [10] presented a paper where these methods are compared. It should be noted that the solvers used in this paper are applicable for sandwich composite structures.

The specimens that were used in the paper presented by Bisagni were composite cylindrical shells with a length of 700 mm. At the bottom and the top of the specimens, tabs were added in order to attach them to the loading rings. However, these tabs were not included in the model resulting in a free length of 540 mm. Moreover, the material properties as determined during the tests were used. For the modelling, S4R elements were used which have six degrees of freedom and use bending strain measures. They do not have the problem of inter shear locking and have no unconstrained hourglass mode. The constraints used on the specimen forced the top and the bottom of the specimens to remain plane and circular and to maintain the circular radius. Moreover, the geometrical imperfections were measured and added to the model.

The first step in the buckling analysis was to compute the bifurcation buckling load, which can be done by using a perfect model and the eigenvalue analysis option provided in Abaqus. It should be noted that this method does not take into account any non-linearity. Executing a non-linear buckling analysis is important because a linear analysis cannot take into account material and geometrical non-linearities, the behavior after buckling, and imperfections. The eigenvalue analysis was performed in the paper and after executing a mesh convergence study the difference between the numerical model and the analytical model was 2-4%. During the analysis it was observed that the buckling pattern highly depended on the lay-up used. In order to account for the imperfections, a non-linear analysis is needed. The non-linear Riks method as implemented in the ABAQUS/Standard edition was employed, which is based on the arc length method. After performing the analysis, the difference between the numerical model and the analytical model was 4%. However, as reported by Bisagni, the solution of the non-linear Riks method is sensitive to the values of the artificial stiffness and structural damping. Therefore, these parameters have to be determined carefully when this solver

is used.

Moreover, a dynamic analysis was performed. This was done by using an assigned displacement to simulate the compression, which is also done when performing an actual buckling test. The dynamic behavior of the model is determined by using the explicit central difference formula which is integrated in ABAQUS/Explicit. The buckling loads were also calculated by using an implicit integration operator which can be found in ABAQUS/Implicit. When comparing these methods it could be seen that the computation using the implicit integration operator takes more CPU time when compared to the explicit integration operator with no difference in buckling behavior. Therefore, for these shells ABAQUS/Explicit is preferred. It should be noted that the CPU time of the ABAQUS/Implicit and ABAQUS/Explicit depend on the shell tested, which means that when a different shell is used ABAQUS/Implicit can be faster. The results obtained differ with 2% from the analytical results and were able to follow the load displacement curves even in the post-buckling regime.

For further comparison experimental results were compared with the numerical results and it could be seen that the difference was 15-20%, which could be explained by the manufacturing process. During curing the mandrel can expand which result in the fibres going towards the inner surface, which reduces the bending stiffness resulting in an overestimation of the buckling loads. Despite the difference in the buckling loads, it could be seen that the dynamic analysis was able to follow the experimental curve in the post buckling regime which cannot be done when using the non-linear Riks method. Also the post buckling shape obtained showed a similar result to the the experimental one, see figures 2.25 and 2.26.

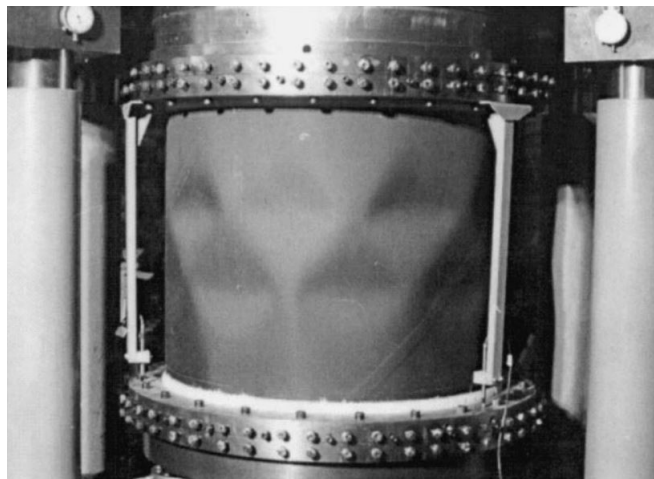


Figure 2.25: Post buckling shape of the experimental test [10].

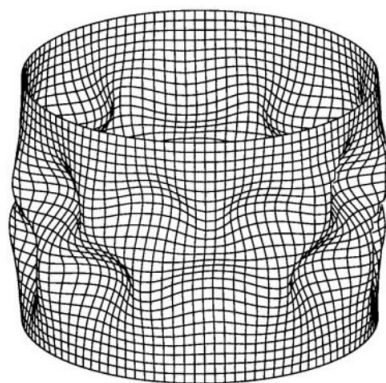


Figure 2.26: Post buckling shape of the numerical model [10].

However, Arbelo et al. [5] argued that the drawbacks of using the dynamic analysis are the computational time needed and its ability to handle the instability phenomena when approaching the buckling load. This

was also observed in [38], where the dynamic analysis was giving negative eigenvalues for a sandwich composite curved panel with measured imperfections. The results were unreliable and could be resolved by using the non-linear Riks method. Therefore, the non-linear Newton Raphson method including artificial damping or the non-linear Riks method is used in most papers. A drawback of these methods is that parameters have to be determined manually in order to get accurate results, as example the time integration step, damping factor, and number of increments. Since these parameters are not based on physical phenomena these parameters have to be determined using convergence studies. This process can be time consuming.

In [13], a detailed explanation is given on how to determine these parameters. The most important aspects of this paper are given below. In ABAQUS, the damping factor is set to  $1e-4$  as default value; however, it is not recommended to use this value if the structure experiences an abrupt change between the pre- and post buckling states. This is due to the fact that the default value results in an overdamped solution with a higher buckling load. To prevent obtaining non conservative solutions it is recommended to start with a value of  $1e-7$  and increase it until convergence is achieved. Furthermore, the values that are used in most papers are described below. For the initial, min and max increment size the values are  $10e-3$ ,  $10e-6$ ,  $10e-3$ , respectively. The max number of increments is  $10e5$ .

### 2.3.4. Type of elements

In literature the elements used for modelling shell structures are mostly the conventional shell elements, such as S4R, S4, and S8R. However, within the Abaqus analysis guide [18], more type of elements are available and might be a better choice for the modelling of sandwich composite structures. When modelling sandwich composite structures, transverse shear becomes an important phenomena that has to be captured. Therefore, it is required that the elements used are able to account for transverse shear. It should be noted that Abaqus just released new elements that are able to better represent this behavior.

The S4 and S4R elements are 4 node elements that have 6 degrees of freedom. These elements are able to account for large strains and transverse shear. Reduced integration and hourglass mode control are incorporated in the S4R element. The general-purpose elements (S4R and S4) are able to adjust the solving behavior depending on the thickness of the shell. When the thickness of the shell increases the thick shell theory is used for the computation and if the thickness of the shell is small the Kirchhoff shell theory is used. This is due to the fact that the transverse shear deformation can be neglected for thin shells, which means that another theory can be used. Since these elements are able to take into account transverse shear, the general purpose elements can be used to represent sandwich composite structures. However, if transverse shear flexibility and second order interpolation is required the S8R should be used. This happens for thick shells (when the thickness is larger than  $1/15$  of the length).

In [13], a study is presented where the different general-purpose elements are compared. In this study different elements were used to model composite cylindrical shells. Castro conducted a comparison study using the S4R, S4R5, S8R, and S8R5 element models based on mesh refinement and computational time. It should be noted that the S4R5 and S8R5 use the Kirchhoff theory, so cannot be used for thick shells. When looking at the results it could be seen that the S8R and S8R5 showed better convergence compared to the linear S4R and S4R5 elements. Moreover, the S8R elements had a higher computational cost than the S8R5 elements. This can be explained by the fact that the S8R5 has one degree of freedom less per node. On the other hand, the linear elements had less computational cost compared to the parabolic elements. When deciding on which elements to use a trade-off has to be made between the accuracy of the results and experimental costs.

Apart from the conventional shell elements, there are other type of shell elements that can be used. Such a shell element is the continuum shell element, SC8R. This element uses the first-order layer-wise composite theory and can be stacked in order to get a more precise through-thickness result. However, when this element is employed it should be checked if the overall deformation determined comply with the layer-wise plane stress assumption. This assumption yields that the response of the structure is dominated by bending and that the change in thickness is less than 10%. If this does not happen regular three-dimensional solid elements should be used.

If a three-dimensional constitutive material behavior is needed for the shell structure the continuum solid shell element, CSS8, is advised. This element contains seven incompatible modes which results in a better bending behavior when compared to other elements. Moreover, locking is diminished by using an assumed strain. This element is mostly used for thin structures where a three-dimensional constitutive response is required, like composite structures. This element uses only displacement degrees of freedom and full integration. Hourglassing is not a problem for this element.

As described above, not only the conventional shell elements can be used to determine the behavior of



---

sandwich composite shells. The SC8R and the CSS8 elements might also be a good choice for the modelling, since the transverse shear can be taken into account more accurately. Another option is to use a combination of elements, for example by using different elements for the face sheets and core. Also the number of elements through the thickness can be varied to improve the transverse shear behavior of sandwich composite structures. It should be noted that choosing the type of elements and mesh is a trade-off between the accuracy of the results and computational time.



# 3

## Aim, objective, and research questions

The aim of the thesis has already been briefly described in the introduction and is defined as "to investigate the buckling behavior of sandwich composite cylindrical shells, conical shells, and cylindrical-conical shells including imperfections". From the aim, the following research objective is established:

*The research objective is to contribute to the investigation on the buckling behavior of sandwich composite shells by comparing the buckling behavior and imperfection sensitivity of a sandwich composite cylindrical shell and conical shell alone with the buckling behavior and imperfection sensitivity of a sandwich composite cylindrical-conical shell using finite element analysis.*

When looking at the objective, three different sub objectives can be derived. The first sub objective is to find a modelling technique to accurately model a sandwich composite cylindrical shell and conical shell, this includes determining which elements to use and performing convergence studies. This is followed by including the imperfections in the finite element models and by doing an imperfection sensitivity analysis for each model. The final sub objective is to compare the buckling behavior of a sandwich composite cylindrical shell and conical shell alone with the buckling behavior of a cylindrical-conical shell. For the last step it is important to understand the relation between the separate shell models and the cylindrical-conical shell model.

From the objective, three main aspects have been derived that need to be investigated during the thesis; the modelling techniques, the imperfection sensitivities, and the comparison between the different models. From these three aspects the research questions have been derived and are presented below. It should be noted that when the sub questions are answered the main research question is answered as well.

1. What is the most promising method to model buckling tests of sandwich composite cylindrical shells, conical shells, and cylindrical-conical shells, with and without imperfections, using finite element analysis?
  - (a) Which elements are able to represent the behavior of sandwich composite structures?
  - (b) What modelling techniques are needed to combine a cylindrical shell with a conical shell?
  - (c) What modelling techniques are required to implement imperfections in the sandwich composite finite element models?
2. What is the imperfection sensitivity of the sandwich composite cylindrical shell, conical shell, and cylindrical-conical shell?
  - (a) Which imperfections are important for sandwich composite structures?
  - (b) How do the imperfections change the buckling behavior of the sandwich composite cylindrical shell, conical shell, and cylindrical-conical shell?

3. What is the relation between the sandwich composite cylindrical shell and conical shell alone and the cylindrical-conical shell?
  - (a) What are the similarities between the buckling behavior of the separate shells and combined shell?
  - (b) What are the similarities between the load vs. displacement graphs of the separate shells and combined shell?
  - (c) What are the differences between the imperfection sensitivities of the separate shells and combined shell?

# 4

## Sandwich composite cylindrical shell and conical shell

This chapter is meant to explore the modelling techniques in Abaqus and to gain more knowledge about the buckling of sandwich composite shells. Before performing analyses on the sandwich composite cylindrical-conical shell, first analyses are performed on a sandwich composite cylindrical shell and conical shell separately. This in order to better understand the behavior of both shells alone and to investigate if there is any relation between the shells separately and the cylindrical-conical shell as a whole. Since this thesis project is in collaboration with NASA, the sandwich composite cylindrical shell material properties, dimensions, and lay-up were used as described in [52]. The design of a sandwich composite conical shell is still in the early stages of the design process and no buckling tests have been performed yet. Since the design of the conical shell is still in progress, for now the material properties and lay-up of the sandwich composite cylindrical shell were used. For the dimensions of the conical shell the maximum mandrel dimensions were taken. In this chapter, first the linear analyses and dynamic analysis of the sandwich composite cylindrical shell are presented and after that the linear analyses and dynamic analysis of the sandwich composite conical shell are shown. Not only the buckling loads and mode shapes are presented, but also an element comparison is given. This in order to investigate which elements are able to represent a sandwich composite shell structure.

### 4.1. Linear analyses of the sandwich composite cylindrical shell

The sandwich composite cylindrical shell considered in this section has the geometrical properties as shown in table 4.1. It should be noted that the length is a bit longer than specified in [52], this in order to be consistent with the cylindrical-conical mandrel design presented later on. Moreover, the lay-up that is shown in the table is the lay-up for one face sheet.

Table 4.1: Geometrical properties of the sandwich composite cylindrical shell.

Length [mm]	Diameter [mm]	Lay-up [deg]	Core thickness [mm]
800	800	[56,0,-56]	1.9

The materials used for the shell are composite face sheets and a foam core. For the face sheets the composite IM7/8552 was used and the material properties can be seen in table 4.2.

Table 4.2: Material properties of IM7/8552. Material properties taken from [16].

$E_{11}$ [MPa]	$E_{22}$ [MPa]	$\nu$ [-]	$G_{12}$ [MPa]	$t_{ply}$ [mm]	$\rho$ [kg/m <sup>3</sup> ]
140928	9721	0.356	4688	0.175	1580

For the core the Rohacell 300 WF foam was used and the material properties can be seen in table 4.3.

Table 4.3: Material properties of Rohacell 300 WF. Material properties taken from [1].

<b>E [MPa]</b>	<b><math>\nu</math> [-]</b>	<b>G [MPa]</b>	<b><math>\rho</math> [kg/m<sup>3</sup>]</b>
578	0.3	364	300

The first step in analysing the buckling behavior of the sandwich composite cylindrical shell was to do a linear static analysis and an eigenvalue analysis. These analyses already give insight into the behavior of the sandwich composite cylindrical shell. The linear static analysis is used in order to get a stiffness estimate of the cylindrical shell, which can be useful for further dynamic analysis. An eigenvalue analysis is performed in order to get the linear buckling load and the buckling mode shape.

In this section also the different type of elements that can be used to model a sandwich composite cylindrical shell are compared. The elements considered are the S4R, SC8R, CSS8, and the C3D8R element. These elements all behave differently and this section is meant to explore which elements are best to represent the behavior of a sandwich composite cylindrical shell. It should be noted that it might be better to represent the model by using more elements through the thickness or a combination of different elements. In this section first the modelling techniques used are discussed. This is followed by a mesh convergence study to determine the mesh size. Then the results of the linear static analysis and eigenvalue analysis are given for different element models.

#### 4.1.1. Modelling technique

For the creation of the model, four different elements were used: S4R, SC8R, CSS8, and C3D8R [18]. The reason for using shell elements (S4R and SC8R) is because these elements are used to model structures that have a much smaller thickness compared to the other two dimensions. In the literature study it already became clear that these type of elements are typically used for the modelling of shells. These shell elements use first order shear deformation theory and are based on two dimensional plane stress constitutive behavior. Another element that was chosen was the solid continuum shell element (CSS8). The reason that this element was used is because of its improved behavior in bending compared to the S4R and SC8R elements. It has a three dimensional constitutive behavior, which is an improvement on the S4R and SC8R elements. This element was created to close the gap between the SC8R element and C3D8R element. The C3D8R element was not yet seen in literature for the analysis of shells, however, this element is able to give good results if large deformations are present. The SC8R, CSS8, and C3D8R elements can even be stacked on top of each other to get a better through thickness response.

For the linear analyses six models were created using different elements and meshes. The S4R, SC8R, and CSS8 element were modelled with one element through the thickness, see figure 4.1a. It should be noted that in figure 4.1a the S4R element could be replaced by the SC8R and CSS8 element. For the CSS8 element another model was made with three elements through the thickness (T-t-T), whereas the face sheets were represented by two elements and the core by one element. A visual representation of the mesh through the thickness can be seen in figure 4.1b. The same was done for the C3D8R element model, see figure 4.1c. A combination of SC8R elements for the face sheets and the CSS8 element for the core was created as well (SC8R + CSS8), see figure 4.1d. The reason for using a CSS8 element for the core is because the CSS8 element has a superior bending behavior, which can be beneficial for capturing the transverse shear of the core. The way in which the 3D element models were created was to use the orphan meshing option within Abaqus. When orphan meshing is used the S4R element model is extruded resulting in a 3D element model. This method ensures that a regular mesh is created.

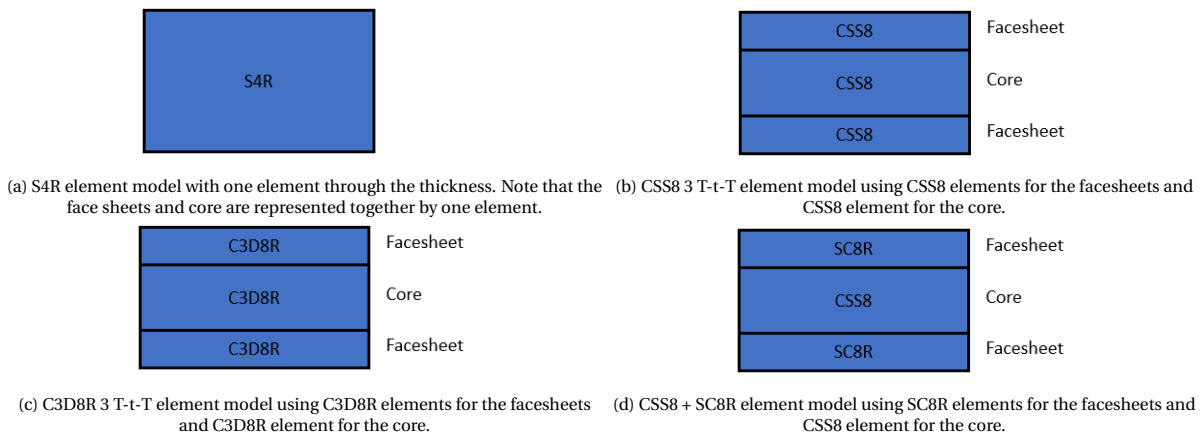


Figure 4.1: Through the thickness mesh of the different element models.

For all the elements the layup was defined using the composite layup option in Abaqus. The core was represented as a ply within the layup with its own material properties and thickness. It should be noted that each element has its own way in which the orientation of the composite plies are applied. For the S4R and the SC8R elements a cylindrical coordinate system had to be created and the normal direction had to be pointed in the direction of the radial axis. Moreover, the one direction of the coordinate system had to be aligned with the required zero degree ply direction. This method ensures that the stacking direction and rotation around the stacking direction is maintained for all elements. For the CSS8 and the C3D8R elements a different process had to be used. This is because these elements are 3D solids and define the coordinate system of the elements in a different way. For these elements the one direction of the element is always pointing in the radial direction of the cylinder. In order to correctly apply the coordinate system of these elements a discrete definition was used, which creates a local coordinate system for each element. For this method a surface of the cylindrical shell had to be defined in order to define the stacking direction. Moreover, a primary axis had to be assigned and had to be in the direction of the axial direction of the cylindrical shell.

The boundary conditions and forces were applied using reference points. These were tied to the edge nodes using a rigid body tie. A visual representation can be seen in figure 4.2. The reason for using reference points is due to easy post processing. For this model a clamped boundary condition was used for the bottom of the cylindrical shell (reference point 1) and the top of the cylindrical shell (reference point 2) was constrained in all directions except for the axial direction. The force was applied at the top of the cylindrical shell in axial direction.

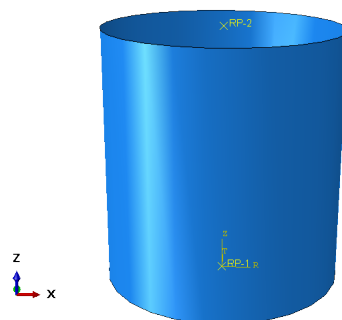


Figure 4.2: Finite element model of the sandwich composite cylindrical shell with reference points.

### 4.1.2. Mesh convergence study

In order to determine the mesh size a convergence study was performed. Eigenvalue analyses were executed for mesh sizes of 20 mm, 10 mm, 5 mm, 2.5 mm, and 1.25 mm using the S4R element model. A visual representation of a 20 mm mesh can be seen in figure 4.3. It should be noted that a regular mesh was used

since there are no places of interests such as cut outs or stress concentrations. The load applied was 1 N in the negative axial direction. After performing an eigenvalue analysis, the buckling load can be obtained by multiplying the eigenvalue with the load applied.

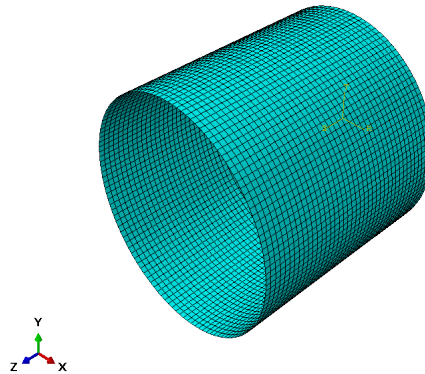


Figure 4.3: Regular mesh of the sandwich composite cylindrical shell using a mesh size of 20 mm.

The results of the eigenvalue analyses can be seen in table 4.4. It should be noted that the computational times that are shown in the tables within this chapter are determined by using the same office computer with one CPU. When looking at the results in the table it be seen that the computational time increases drastically when the mesh size is decreased. This is expected because when there are more elements in the model there are more degrees of freedom that need to be solved for, increasing the computational time. When looking at table 4.4 it can be seen that decreasing the mesh below 5 mm does not result in a big change of the buckling load. Since the increase of the computational time of the models using a mesh smaller than 5 mm are significant, a mesh size of 5 mm is preferred.

Table 4.4: First three force eigenvalues and CPU times of the sandwich composite cylindrical shell using different mesh sizes.

Mesh size [mm]	Force eigenvalue 1 [kN]	Force eigenvalue 2 [kN]	Force eigenvalue 3 [kN]	CPU time [s]
20	811.8	811.8	812.1	95
10	807.2	807.2	808.0	629
5	806.1	806.1	806.5	2622
2.5	805.8	805.8	806.1	12099
1.25	805.7	805.8	806.0	64572

Besides the force eigenvalues also the mode shapes were compared in order to check if a smaller mesh size gives a different mode shape. It is possible that some mode shapes cannot be simulated if the mesh is too coarse, resulting in a different mode shape than when a smaller mesh size is used. The mode shapes for the different mesh sizes can be seen in figure 4.4. It should be noted that in this figure only the first mode shapes are shown because the second and third mode shapes look similar. When looking at the figure it can be seen that for all the mesh sizes the mode shapes are the same. However, when looking at a mesh size of 20 mm and 10 mm the mode shapes give some irregularities due to the mesh size being too coarse. Since the mode shape is an important phenomenon to capture when looking at the buckling behavior of shells, a minimum mesh size of 5 mm has to be used for further analysis.



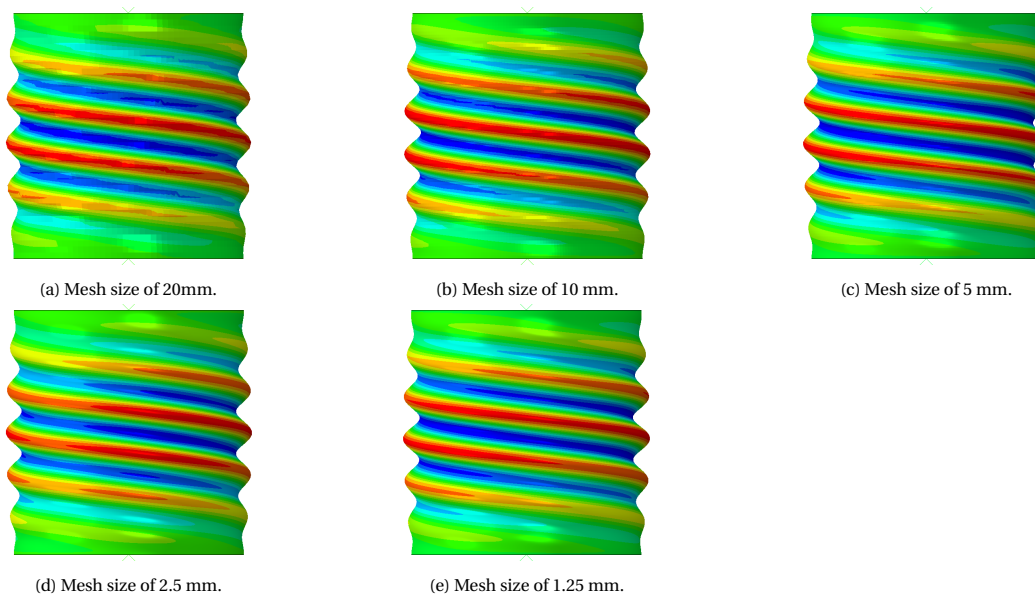


Figure 4.4: First buckling mode shapes of the sandwich composite cylindrical shell using different mesh sizes. For generating the figures a scaling factor of 30 was employed.

#### 4.1.3. Results of linear static analysis and eigenvalue analysis

Different element models were created to investigate the linear static analysis results and eigenvalue analysis results. In order to compare the results and verify the model of the linear eigenvalue analysis the analytical buckling load of the pristine sandwich composite cylindrical shell had to be determined. For this calculation two different methods were used: the SP-8007 guideline [42] and the method presented by Bert and Reese [44].

First thing to note is that the calculation proposed by the SP-8007 guideline is not meant for sandwich composite shells, but for composite shells. The equations were modified in order to still use the NASA guideline because this method is also able to predict the knockdown factor which can be of interest for further analyses. The way in which the SP8007 guideline calculates the buckling load is by using equation 4.1. Whereas,  $N_x$  is the buckling load per meter,  $l$  is the length of the cylindrical shell, and  $m$  is the number of half waves. The  $A$  terms can be calculated by using the stiffness terms of the laminate. The way in which the guideline was modified was to include the core in the calculation of the stiffness terms.

$$N_x = \left( \frac{l}{m\pi} \right)^2 \frac{\begin{vmatrix} A_{11} & A_{12} & A_{13} \\ A_{21} & A_{22} & A_{23} \\ A_{31} & A_{32} & A_{33} \end{vmatrix}}{\begin{vmatrix} A_{11} & A_{12} \\ A_{21} & A_{22} \end{vmatrix}} \quad (4.1)$$

The Bert and Reese method is applicable for sandwich composite shells and therefore, could directly be used to calculate the analytical buckling load. Since the method is quite extensive, the final equation is not given here. The way in which the analytical buckling load is calculated is by using stiffness terms of the facesheets and stiffness terms of the core.

Both of these methods use simply supported boundary conditions. This is important to note since the finite element models are created using clamped boundary conditions and thus, a difference can be present between the analytical solution and the finite element solution. The analytical buckling loads calculated by both methods can be seen in table 4.5. It can be seen that there is a difference of 10% between the analytical buckling loads.

Table 4.5: Analytical buckling loads calculated for the sandwich composite cylindrical shell using different methods.

Method	Analytical buckling load [kN]
SP-8007	873.0
Bert and Reese	792.8

Before performing an eigenvalue analysis, a linear static analysis was performed to get the linear stiffness of the cylindrical shell. For the linear static analysis, a load was used in the order of the analytical buckling load and had a value of 900 kN. This load was applied in the negative axial direction. The results of the analysis can be seen in table 4.6 for the models with different types of elements. What can be seen is that the displacements are all close to each other. This means that all element models give the same stiffness of the sandwich composite cylindrical shell. When looking at the CPU time it can be seen that the CSS8 element with three elements through the thickness takes the longest. This is due to the increase in number of elements. It can also be seen that for the models with one element through the thickness the CPU time of the S4R and the SC8R element models are similar and that the CPU time of the CSS8 element model takes more time to finish. This can be explained by the fact that the CSS8 element uses 3D constitutive relations and full integration, which takes more time.

Table 4.6: Displacement of the sandwich composite cylindrical shell due to a force of 900 kN in axial direction.

Element	Displacement [mm]	CPU time [s]
S4R	4.9	31
SC8R	4.9	35
CSS8	4.8	91
CSS8 3 T-t-T	4.9	207
C3D8R 3 T-t-T	4.9	105
SC8R + CSS8	4.9	129

Besides a linear static analysis also an eigenvalue analysis was performed. For performing an eigenvalue analysis, a load of -1 N in axial direction was applied at the top reference point. For the different element models the first three eigenvalues and CPU times are compared. The results can be seen in table 4.7. A difference of less than 9% is obtained for all element models when comparing the force eigenvalues to the analytical solution obtained by the SP-8007 guideline. The difference can be explained by the fact that this method is not meant for sandwich composite shells. The difference between the calculated Bert and Reese buckling load and the finite element results are below 2% for all element models except for the CSS8 element model. The reason for this can be that the CSS8 element is not able to represent a sandwich composite structure by one element through the thickness due to the difference in stiffness between the face sheets and the core. Therefore, another model was analysed with more elements through the thickness. Three elements through the thickness were used whereas two elements were used for the facesheets and one element was used for the core. When increasing the number of elements through the thickness it can be seen that the force eigenvalues are closer to the values of the other element models.

When looking at the CPU times it can be seen that for the models with one element through the thickness the CSS8 element model takes the longest and is not even able to give a similar buckling load when compared to the other element models. Furthermore, when the number of elements through the thickness is increased the computational time increases. This is due to the larger amount of elements used.

Table 4.7: First three force eigenvalues and CPU times for the sandwich composite cylindrical shell using different element models.

Element model	Force eigenvalue 1 [kN]	Force eigenvalue 2 [kN]	Force eigenvalue 3 [kN]	CPU time [s]
S4R	806.1	806.1	806.5	2622
SC8R	806.1	806.1	806.5	3493
CSS8	857.0	857.1	857.5	8938
CSS8 3 T-t-T	802.7	802.7	803.2	30696
C3D8R 3 T-t-T	808.6	808.6	809.8	4968
SC8R + CSS8	804.9	804.9	805.0	16134

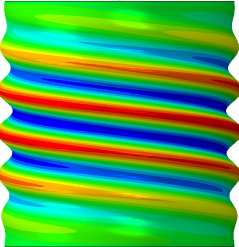
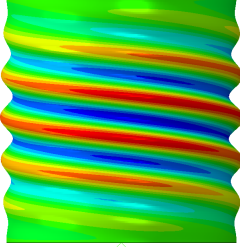
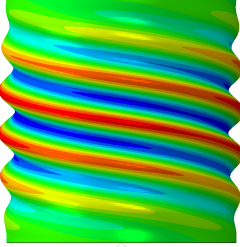
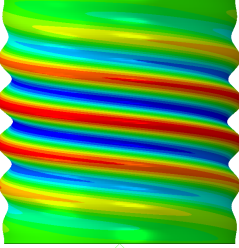
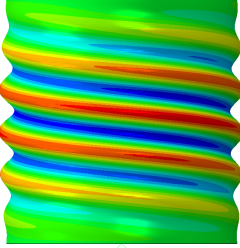
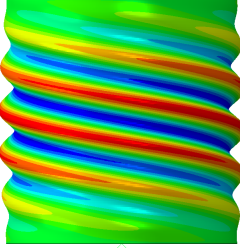
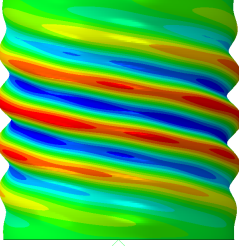
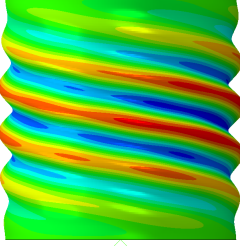
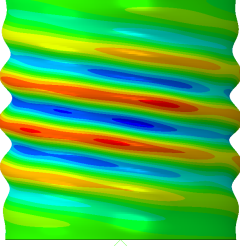
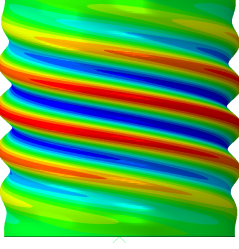
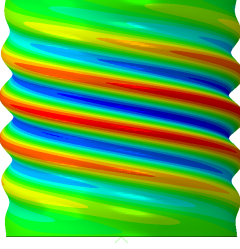
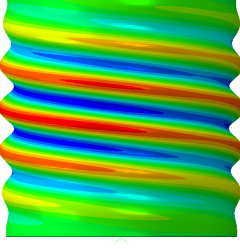
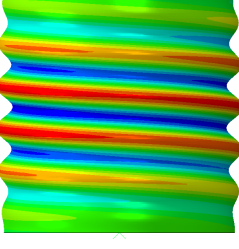
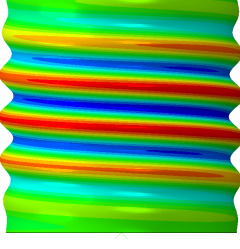
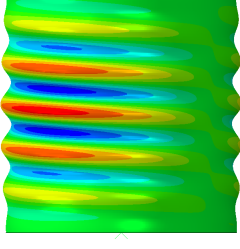
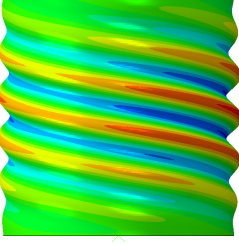
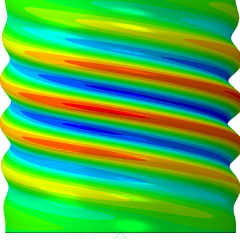
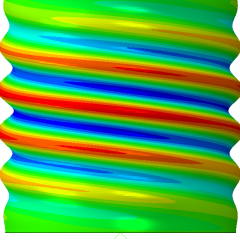
Besides a force based eigenvalue analysis also a displacement based eigenvalue analysis was performed. This was done in order to determine the displacement at which buckling happens. When the load and displacement at which buckling happens are known, a point can be constructed and it can be seen if the point is located somewhere along the line of the linear static analysis. This was an important step in the verification process since the point has to be located on the line of the linear static analysis. The displacement based eigenvalue analysis was done by applying a displacement of -1 mm in axial direction at the top reference point. The results can be seen in table 4.8. It can be observed that the results of the CSS8 element model gives higher displacement eigenvalues compared to the other element models. Because of the fact that the displacement determined using the linear static analysis is the same as for the other element models, the buckling of the CSS8 element model happens later compared to the other element models. Since all the other element models give a similar buckling load and displacement, the CSS8 element model is not able to predict the buckling behavior of a sandwich composite cylindrical shell. Moreover, the CPU times are comparable to the results obtained for the force based eigenvalue analysis. This is expected because the same analysis is performed.

Table 4.8: First three displacement eigenvalues and CPU times for the sandwich composite cylindrical shell using different element models.

Element	Displacement eigenvalue 1 [mm]	Displacement eigenvalue 2 [mm]	Displacement eigenvalue 3 [mm]	CPU time [s]
S4R	4.3	4.3	4.4	2607
SC8R	4.4	4.3	4.4	3463
CSS8	4.6	4.6	4.6	9132
CSS8 3 T-t-T	4.3	4.3	4.3	31175
C3D8R T-t-T	4.4	4.4	4.4	4639
SC8R + CSS8	4.3	4.3	4.3	16469

Next to the force eigenvalues also the buckling mode shapes are an output of the eigenvalue analysis. These are also compared to see if there are any differences between different element models. The first three buckling mode shapes of the different element models can be seen in table 4.9. What can be seen is that all element models give the same buckling shapes for the first two modes. There are five waves in axial direction and one wave in the circumferential direction. It should be noted that the first two mode shapes of the C3D8R 3 T-t-T element model is less rotated around the circumferential direction when compared to the other element models. The third mode shape does give a different mode shape, which means that the C3D8R 3 T-t-T element model is not able to predict the right the mode shapes. Besides the fact that the CSS8 element model has a buckling load much higher than the other buckling loads, the buckling mode shapes are close to the buckling mode shapes of the other element models.

Table 4.9: First three buckling mode shapes of the sandwich composite cylindrical shell using different element models. For generating the figures a scaling factor of 30 was employed.

	First mode	Second mode	Third mode
S4R			
SC8R			
CSS8			
CSS8 3 T-t-T			
C3D8R 3 T-t-T			
SC8R + CSS8			

## 4.2. Dynamic analysis of the sandwich composite cylindrical shell

For shell structures a dynamic analysis is also of interest. This is because by performing a dynamic analysis it is possible to capture the behavior after buckling and the final point of failure, and to capture geometric non-linearity of the structure. Due to the unstable postbuckling behavior of circular thin walled structures, the load drop after buckling is an important feature to capture. The dynamic analysis of the cylindrical shell were ran using the dynamic implicit solver in Abaqus. This solver was chosen due to the low computational time compared to the dynamic explicit solver. Since a lot of analyses had to be performed the computational time had to be as low as possible.

The dynamic implicit analysis was performed using an applied displacement. The reason for a displacement based analysis is because the actual tests of shells are also controlled using an applied displacement. Since the rate in which the displacement is applied can vary, the displacement rate is determined first. This displacement rate is then used for further analyses. After that, the results of the dynamic analysis is explained for the cylindrical shell.

### 4.2.1. Sensitivity to displacement rate

For a dynamic implicit analysis the displacement rate has to be determined. This was done by doing a convergence study using displacement rates of 10 mm/s, 5 mm/s, 2 mm/s, and 1 mm/s. Since the buckling of shells can be seen as a quasi-static problem, a low displacement rate is preferred. However, the lower the displacement rate the longer the analysis takes. This means that a trade-off should be made between the computational time and the quality of the results. The displacement rate that is chosen in this subsection is used for further analyses unless stated otherwise. Important to note is that the first analyses that are performed for the cylindrical, conical, and cylindrical-conical shell have to be accurate in terms of buckling load and deformation shape. This is because the buckling behavior of the cylindrical-conical shell is not yet fully understood. This means that the computational time is of less importance when compared to the accuracy of the results.

A dynamic implicit solver requires several inputs. For example, the time parameters. These parameters are an important factor in the dynamic implicit analysis; the lower the time parameters the higher the computational time. However, when using lower time parameters the accuracy of the results are increased. Therefore, an optimum has to be found such that the results are still accurate and that the computational time is reasonable. By determining the time parameters it is important that there are no negative eigenvalues prior to buckling. When this happens it means that the dynamic analysis overshoots the buckling load. Since an accurate prediction was needed, the time parameters were determined such that there were no negative eigenvalues prior to buckling. The time parameters that were used for the dynamic analysis were 0.001, 0.001, and 1e-5 for the initial increment size, maximum increment size, and the minimum increment size, respectively. Moreover, also the time period had to be specified. This parameter was determined by using the displacement rates of 10 mm/s, 5 mm/s, 2 mm/s, and 1 mm/s. The displacement applied was determined by using a value in the range of the first displacement eigenvalue obtained by the eigenvalue analysis. By using the total applied displacement and the displacement rate the time period could be calculated.

The model that was used for the analysis was the same as the one used for the linear analysis. The only difference is that a displacement is applied to the reference point located on the top of the cylindrical shell. For the dynamic analysis only the SC8R element model was used, this because of the results obtained by the eigenvalue analysis and the low computational time.

The force-displacement graph was obtained by extracting the reaction force and displacement in axial direction of the reference point located at the top of the shell at each moment in time. The force-displacement graphs by using a displacement rate of 10 mm/s, 5 mm/s, 2 mm/s, and 1 mm/s can be seen in figure 4.5. The linear static analysis line is included as a reference. From the graph it can be seen that the force-displacement curve converges with decreasing displacement rate. When looking at the post-buckling path of the different graphs it can be seen that by using a displacement rate of 10 mm/s and 2 mm/s the same post buckling path is followed. For a displacement rate of 5 mm/s a different post buckling path can be observed which diverges from the other post buckling paths. This means that a displacement rate of 5 mm/s will give a different post buckling behavior compared to the other three displacement rates.

The values of the buckling loads and CPU times can be seen in table 4.10. What can be observed is that when the displacement rate is decreased the computational time increases. Since for the first couple of analyses the computational time is of less importance the convergence of the buckling load will weigh more in choosing a displacement rate. When looking at the buckling load of the different displacement rates it can be observed that at a displacement rate of 2 mm/s the buckling load is converged. Therefore, there is no need

to use a displacement rate lower than this value. For further analysis a displacement rate of 2 mm/s is used. When a qualitative comparison is sufficient, a higher displacement rate can be used since the buckling load of all four displacement rates are relatively close to each other. This will save computational time.

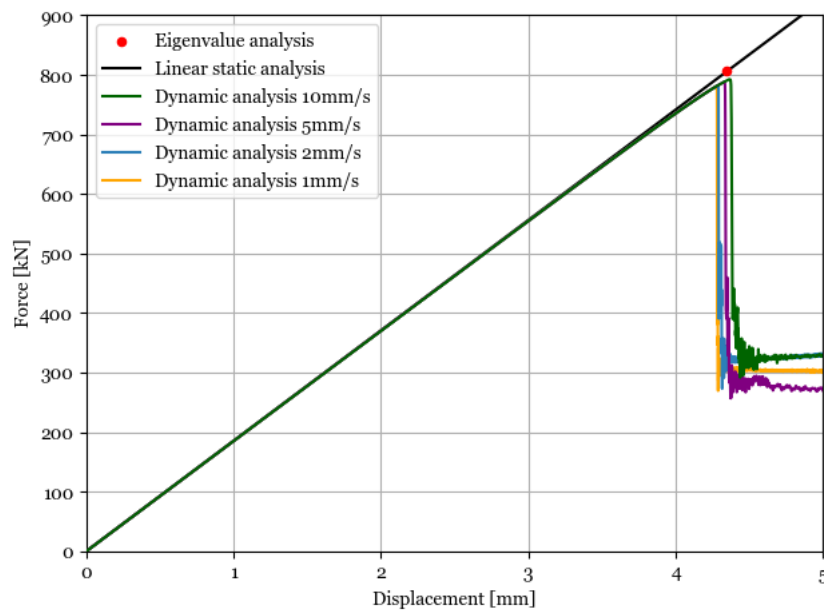


Figure 4.5: Force-displacement graphs of the sandwich composite cylindrical shell using a displacement rate of 10 mm/s, 5 mm/s, 2 mm/s, and 1 mm/s.

Table 4.10: Buckling loads, CPU times, and difference with respect to 1 mm/s for the sandwich composite cylindrical shell using different displacement rates.

Displacement rate [mm/s]	Buckling load [kN]	CPU time [s]	Difference in buckling load w.r.t. 1 mm/s [%]
10	792.7	49358	1.5
5	788.3	93112	0.9
2	782.4	173432	0.2
1	781.2	334931	

#### 4.2.2. Results of the dynamic implicit analysis

This subsection investigates the non-linear buckling behavior of the cylindrical shell by performing a dynamic implicit analysis. Moreover, a dynamic implicit analysis is able to capture the behavior of the shell right after buckling. In this subsection a comparison is made between the buckling load and mode shape determined by the eigenvalue analysis and the buckling load and deformation shape of the dynamic implicit analysis. For the dynamic analysis the same properties as described in the previous subsection were used. The force-displacement graph determined by the dynamic analysis can be seen in figure 4.6. The buckling load predicted by the dynamic analysis is 782.4 kN with a displacement of 4.3 mm. The difference between the buckling load determined by the eigenvalue analysis and the dynamic analysis is 2.9%. It can also be observed that the stiffness is the same as for the linear static analysis. This means that there is a good correlation between the results of linear analyses and the dynamic analysis.

The deformation shape of the cylindrical shell for each stage can be seen in figure 4.7. It should be noted that there are four different stages that can be distinguished: deformation shape before buckling, deformation shape at the buckling load, deformation shape right after buckling, and deformation shape in the post buckling regime. What can be seen is that the shape at the buckling load is not the same as predicted by the eigenvalue analysis, there are some waves present but are more located near the boundary conditions. After buckling the deformation shape changes from straight waves to a diamond pattern. In the post buckling

regime the deformation shape is more concentrated at the middle of the cylindrical shell.

The reason that there is a difference between the buckling shape of the eigenvalue and dynamic implicit analysis is due to the effect of the boundary condition in the dynamic analysis. This effect cannot be captured by an eigenvalue analysis because of the non-linearity. If the length of the cylindrical shell was longer, the effect of the boundary would be less and a better comparison between the mode shape determined by the eigenvalue analysis and dynamic analysis can be made.

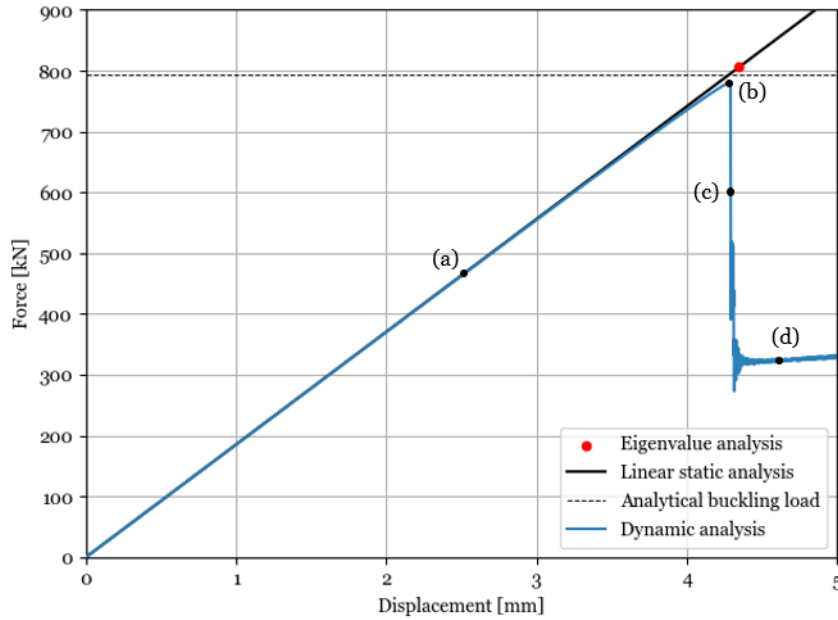
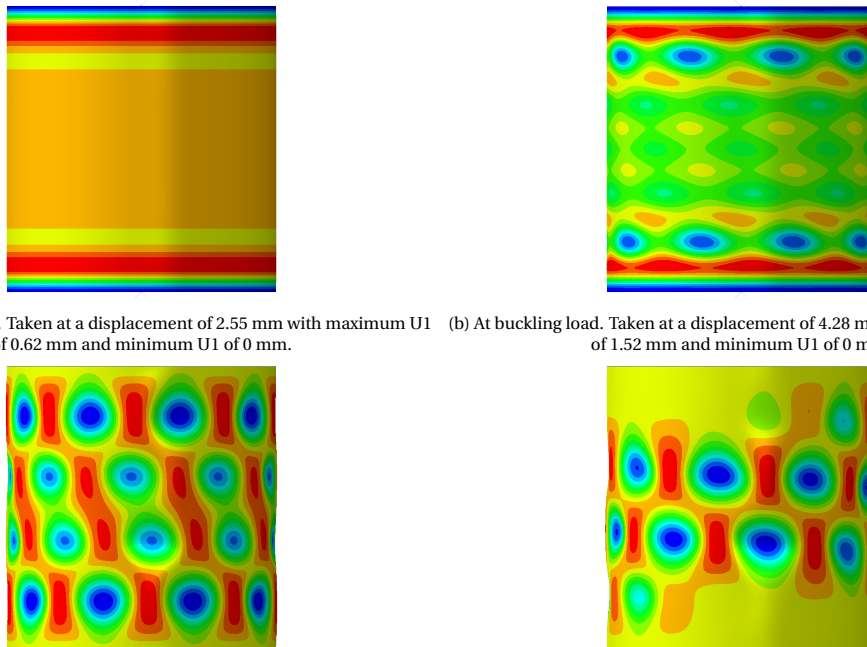


Figure 4.6: Force-displacement graph of the sandwich composite cylindrical shell. Whereas, (a), (b), (c), and (d) represent the different phases of deformation.



(a) Before buckling. Taken at a displacement of 2.55 mm with maximum U1 of 0.62 mm and minimum U1 of 0 mm. (b) At buckling load. Taken at a displacement of 4.28 mm with maximum U1 of 1.52 mm and minimum U1 of 0 mm.

(c) Right after buckling. Taken at a displacement of 4.29 mm with maximum U1 of 5.09 mm and minimum U1 of -11.2 mm. (d) Post-buckling regime. Taken at a displacement of 4.56 mm with maximum U1 of 10.2 mm and minimum U1 of -21.8 mm

Figure 4.7: Deformation shapes in radial direction of the sandwich composite cylindrical shell with a scaling factor of 1. Whereas, (a), (b), (c), and (d) represent the different phases of deformation and U1 denotes the out of plane deformation.

### 4.3. Linear analyses of the sandwich composite conical shell

For the sandwich composite conical shell the same linear analyses were performed as for the sandwich composite cylindrical shell in order to determine the stiffness of the shell and to determine the linear buckling load. The dimensions of the sandwich composite conical shell were based on the dimensions of the sandwich composite cylindrical shell as already explained above. The large diameter of the cone matches the diameter of the cylinder, and the height of the cone is the same as the cylinder. The semi-vertex angle of the cone is 15°. The dimensions of the shell can be seen in table 4.11. It can be seen that the same diameter and height were used as for the cylindrical shell. Moreover, the same materials were used as for the cylindrical shell and the material properties of the composite facesheets and foam core can be seen in tables 4.2 and 4.3, respectively.

This section is meant to get more insight into the behavior of conical shells compared to cylindrical shells. This includes the modelling techniques that have to be used for conical shells, the difference in buckling load and mode shape. In this section also a comparison between the different kind of elements is given.

Table 4.11: Geometrical properties of the sandwich composite conical shell.

Length [mm]	Large diameter [mm]	Lay-up [deg]	Core thickness [mm]	Semi-vertex angle [deg]
800	800	[56,0,-56]	1.9	15

#### 4.3.1. Modelling techniques

The modelling of the sandwich composite conical shell was done in the same way as for the sandwich composite cylindrical shell. This means that the same elements were used, the same methods of defining the orientation were employed, and the same techniques for applying the loads and boundary conditions were used. For the analysis of the conical shell also six models were created using the same type of elements as for the cylindrical shell. A visual representation of the conical shell model can be seen in figure 4.8.

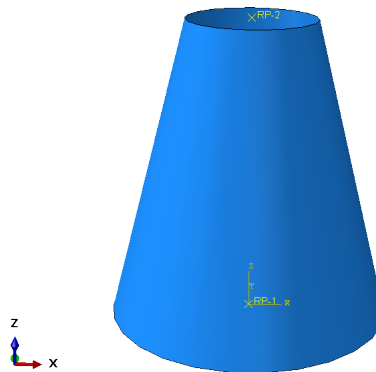


Figure 4.8: Finite element model of the sandwich composite conical shell with reference points.

When modelling a conical shell, attention has to be paid to the edges. When a S4R model is transformed into a 3D element model, the edges of the cone become perpendicular to the cone angle. When a cone is manufactured, the edges of the cone are trimmed at the end such that the edges are parallel to the loading surface. Since the model made in Abaqus should represent the manufactured specimen as accurate as possible, the Abaqus model had to be changed. This was done by perturbing the edge nodes by a certain amount such that the nodes along the lower edge had a z-coordinate of 0 and that the nodes along the upper edge had a z-coordinate of 800. It should be noted that when doing this also the thickness of the elements were changed such that a total thickness of 2.95 mm was maintained. A visual representation can be seen in figure 4.9.



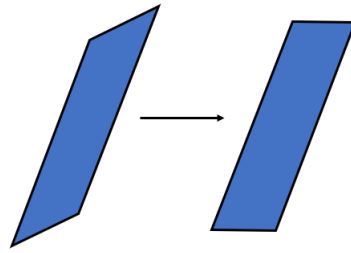


Figure 4.9: Problem with the cone edges when extruding the S4R model.

### 4.3.2. Mesh convergence study

In order to determine which mesh size to use for the sandwich composite conical shell, a mesh convergence study was performed. The way in which the mesh for the conical shell was created was by defining the number of elements in the circumferential direction according to the mesh size. Then Abaqus calculated the height needed for the elements by enforcing an aspect ratio of 1 in the middle of the conical shell. The same height is used for each element. Due to this, the number of elements in the conical shell is higher than the number of elements in the cylindrical shell when the same mesh size is used. For performing the mesh convergence study, the S4R element model was used. Mesh sizes of 20 mm, 10 mm, 5 mm, 2.5 mm, and 1.25 mm were tested. It should be noted that these mesh sizes are determined by using the large diameter of the conical shell. In figure 4.10 the mesh can be seen for a mesh size of 20 mm.

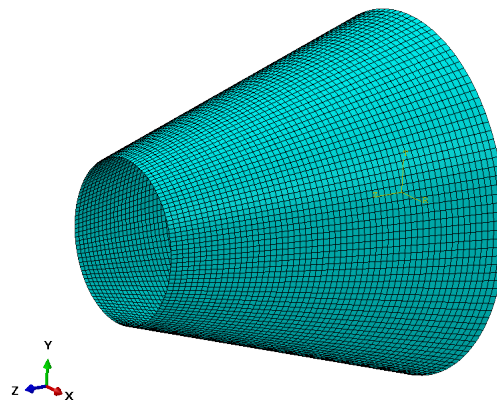


Figure 4.10: Regular mesh of the sandwich composite conical shell using a S4R element and a mesh size of 20 mm.

For each of the mesh sizes, an eigenvalue analysis was performed and the results can be seen in table 4.12.

Table 4.12: First three force eigenvalues and CPU times of the sandwich composite conical shell using different mesh sizes.

Mesh size [mm]	Number of elements [-]	Force eigenvalue 1 [kN]	Force eigenvalue 2 [kN]	Force eigenvalue 3 [kN]	CPU time [s]
20	126	717.9	718.0	718.6	157
10	251	713.8	713.9	713.9	578
5	500	712.5	712.6	712.7	4035
2.5	1005	712.2	712.2	712.5	17927
1.25	2011	712.1	712.2	712.4	89635

The first aspect to notice from the table is that the force eigenvalues converge when the mesh size is decreased. The same can be observed as what was observed in the mesh convergence study of the cylindrical

shell, the CPU time increases with decreasing mesh size. Moreover, at a mesh size of 5 mm the force eigenvalues are converged and the CPU time is still reasonable.

For the mesh convergence study also the mode shapes are compared. The first three mode shapes have a similar shape, so only the first mode shapes are shown here. In figure 4.11 the buckling mode shapes for the different mesh sizes are shown. It can be seen that for a mesh size of 20 mm the mode shape has some irregularities and that the shape is less twisted when compared to the mode shapes of the models using a 5 mm and 2.5 mm mesh. The 10 mm mode shape is giving a different mode shape, this can be explained by a numerical error. This is because the 20 mm mesh is able to give the right mode shape, so the difference cannot be explained by the mesh being too coarse. Since the mode shape of the 5 mm mesh is the same as the mode shape of the 2.5 mm mesh, the 5 mm mesh is used for further simulations.

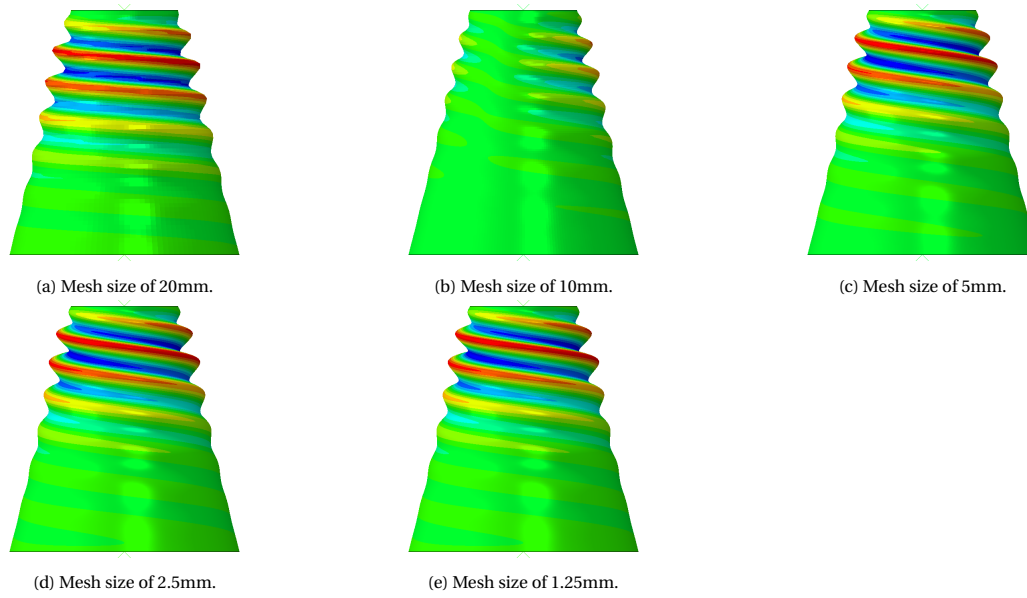


Figure 4.11: First buckling mode shapes of the sandwich composite conical shell using different mesh sizes. For generating the figures a scaling factor of 30 was employed.

### 4.3.3. Results of linear static analysis and eigenvalue analysis

Before executing the eigenvalue analysis of the different element models, first a linear static analysis was performed. For this analysis, a load of -900 kN was applied at the top reference point of the conical shell. This load was used in order to be able to compare the results with the results of the linear static analysis of the cylindrical shell. The results for the different element models can be seen in table 4.13. It can be seen that for all element models the displacements are similar. The same trend for the CPU time as described in subsection 4.1.3 can be observed here as well. It can also be seen that the displacements of the conical shell are higher compared to the displacement of the cylindrical shell. This is expected because of the semi-vertex angle of the conical shell.

Table 4.13: Displacements of the sandwich composite conical shell due to a force 900 kN in axial direction.

Element	Displacement [mm]	CPU time [s]
S4R	7.7	49
SC8R	7.7	51
CSS8	7.7	116
CSS8 3 T-t-T	7.7	239
C3D8R 3 T-t-T	7.7	146
SC8R + CSS8	7.7	176

For the conical shell also an eigenvalue analysis was performed. In order to verify the results of this analysis the analytical buckling load was calculated. The analytical buckling load was calculated using equation 4.2

[41], whereas  $P_{Cone}$  is the buckling load of the conical shell,  $P_{Cylinder}$  is the buckling load of the cylindrical shell with the same material properties, height, and diameter as the conical shell, and  $\alpha$  is the semi-vertex angle. Since the material properties and dimensions of the sandwich composite cylindrical shell are the same, the buckling load obtained by the Bert and Reese method was used to calculate the buckling load of the sandwich composite conical shell. The analytical buckling load of the sandwich composite conical shell is 739.7 kN.

$$P_{Cone} = P_{Cylinder} \cdot \cos^2 \alpha \quad (4.2)$$

The results of the eigenvalue analysis for the different element models can be seen in table 4.14. The difference with the analytical solution is less than 4.5% except for the CSS8 element model. The same trend as for the cylindrical shell eigenvalue analysis results can be observed for the conical shell as well. Only the CSS8 element model shows different results compared to the other element models. The computational time results are also similar to the results of the cylindrical shell eigenvalue results. It should be noted that the buckling load is about 10% lower than the buckling load of the cylindrical shell.

Table 4.14: First three force eigenvalues and CPU times for the sandwich composite conical shell using different element models.

Element	Force eigenvalue 1 [mm]	Force eigenvalue 2 [mm]	Force eigenvalue 3 [mm]	CPU time [s]
S4R	712.5	712.6	712.7	4035
SC8R	712.6	712.6	712.8	2755
CSS8	788.0	788.0	788.9	5691
CSS8 3 T-t-T	707.5	707.6	708.3	14152
C3D8R 3 T-t-T	714.9	714.9	716.0	4491
SC8R + CSS8	709.4	709.4	710.6	8620

Also a displacement based eigenvalue analysis was performed. This was done in order to verify the results given by the different analyses, as already described in subsection 4.1.3. The results of the eigenvalue analysis using an applied displacement can be seen in table 4.15. What can be observed is that the displacement eigenvalues are all within 1% except for the CSS8 element model. This element model gave higher displacement eigenvalues. Since the displacement of the linear static analysis is the same for all element models, it means that the buckling of the CSS8 element model is predicted later when compared to the other element models. This was also observed for the cylindrical shell. Moreover, the CPU times are comparable to the CPU times obtained for the force based eigenvalue analysis. This is expected because the same analysis was performed.

Table 4.15: First three displacement eigenvalues and CPU times for the sandwich composite conical shell using different element models.

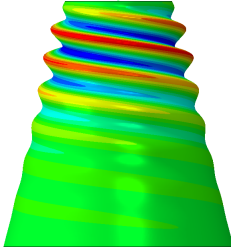
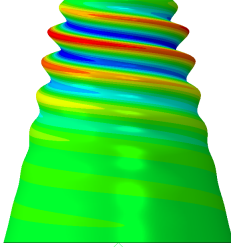
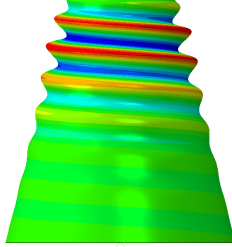
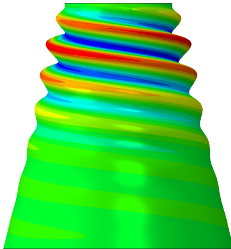
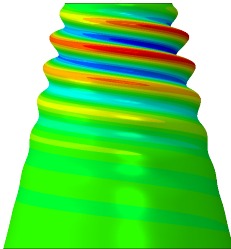
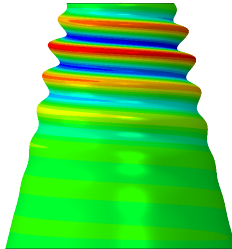
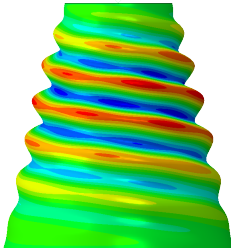
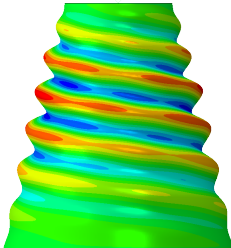
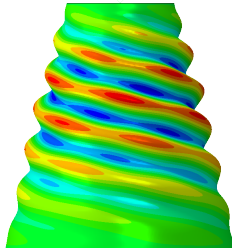
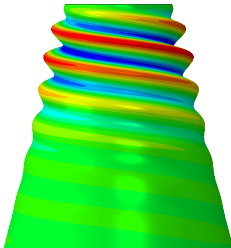
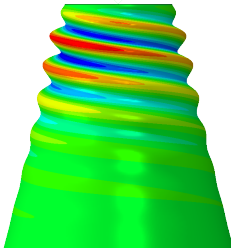
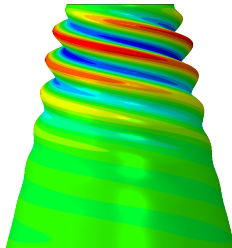
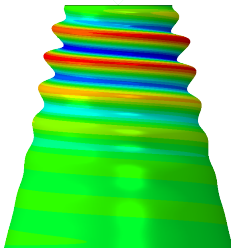
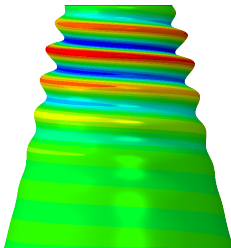
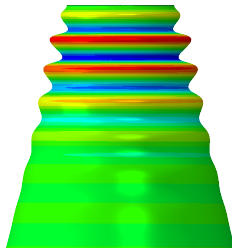
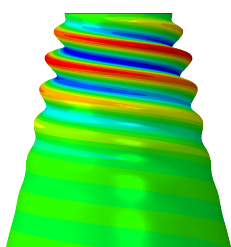
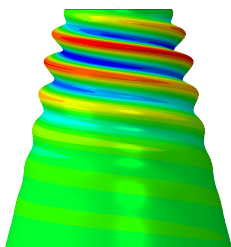
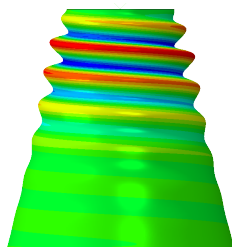
Element	Displacement eigenvalue 1 [mm]	Displacement eigenvalue 2 [mm]	Displacement eigenvalue 3 [mm]	CPU time [s]
S4R	6.1	6.1	6.1	3312
SC8R	6.1	6.1	6.1	2348
CSS8	6.8	6.8	6.8	5655
CSS8 3 T-t-T	6.1	6.1	6.1	14122
C3D8R 3 T-t-T	6.1	6.1	6.1	4482
SC8R + CSS8	6.1	6.1	6.1	8577

The first three buckling mode shapes of the conical shell of the different element models can be seen in figure 4.16. What can be seen is that for the S4R, SC8R, and CS8R+CSS8 element models the three mode shapes look similar. The CSS8 3 T-t-T element model shows similar mode shapes for the first two buckling mode shapes but for the third buckling mode shape the buckling waves are more twisted when compared to the other element models. The C3D8R 3 T-t-T element model shows a less twisted shape for the first two buckling mode shapes. Since for these two models the buckling mode shapes show buckling at the top, these

models are still considered accurate since the force eigenvalues are similar. The CSS8 element model shows different mode shapes for the first three buckling modes. Since the force eigenvalues of this model are different as well, the CSS8 element model is not able to give accurate results for this sandwich composite conical shell.

When comparing the mode shapes of the conical shell with the mode shapes of the cylindrical shell it can be seen that the deformation for the conical shell is present at the top of the shell whereas the deformation of the cylindrical shell is present along the whole length of the cylinder. This is expected because the cylindrical shell has a constant radius resulting in a mode shape covering the whole length of the shell. Whereas, a conical shell has a smaller radius at the top, which results in a smaller area to withstand the load and therefore, the top is the weakest section of the conical shell resulting in a deformation at the top.

Table 4.16: First three buckling mode shapes of the sandwich composite conical shell of different element models. For generating the figures a scaling factor of 30 was employed.

	First mode	Second mode	Third mode
S4R			
SC8R			
CSS8			
CSS8 3 T-t-T			
C3D8R 3 T-t-T			
SC8R + CSS8			

#### 4.4. Dynamic analysis of the sandwich composite conical shell

A dynamic analysis was performed for the conical shell to capture the behavior of the shell right after buckling and to investigate the effects of the geometric non-linearity prior to buckling. A dynamic implicit analysis was used for the dynamic analysis of the conical shell. In order to compare the dynamic analysis results throughout the thesis the same time parameters and displacement rate were used as discussed in section 4.2. The SC8R element model was employed for the analysis because of the good results for the linear analyses and a low CPU time. The force-displacement graph of the dynamic analysis can be seen in figure 4.12. The buckling load obtained using the dynamic analysis is 684.8 kN with a displacement of 5.9 mm. The difference between the buckling load obtained using the eigenvalue analysis and the dynamic analysis is 4.9%. It can also be seen that the stiffness prior to buckling is the same when compared to the linear static analysis. This means that there is a good correlation between the results of the linear analyses and the dynamic analysis.

The deformation shapes can be seen in figure 4.13. There are four stages in the force-displacement graph that are of interest as already explained in section 4.2. What can be seen is that the deformation shape at the buckling load has waves located mostly at the top of the conical shell. This was already predicted by the eigenvalue analysis. Moreover, right after buckling a diamond pattern appears at the top of the shell and travels down towards the bottom of the conical shell when in the post buckling regime.

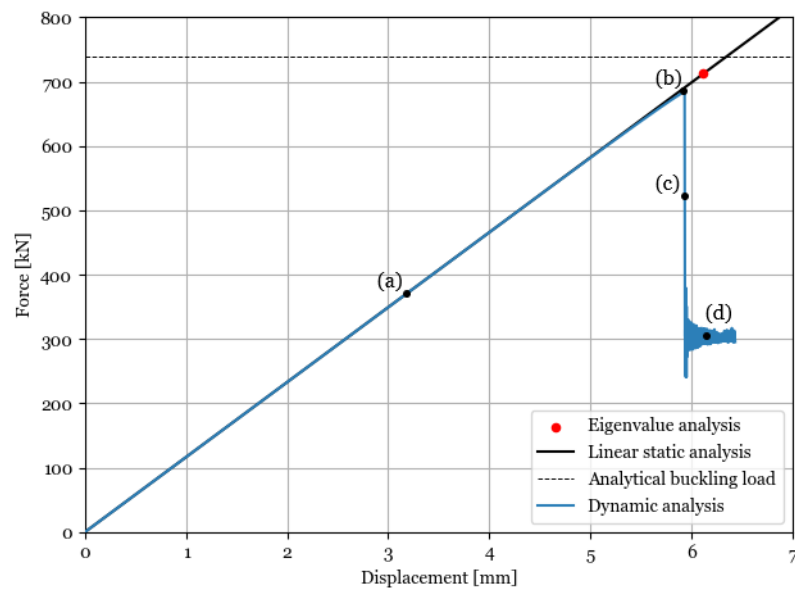


Figure 4.12: Force-displacement graph of the sandwich composite conical shell. Whereas, (a), (b), (c), and (d) represent the different phases of deformation.

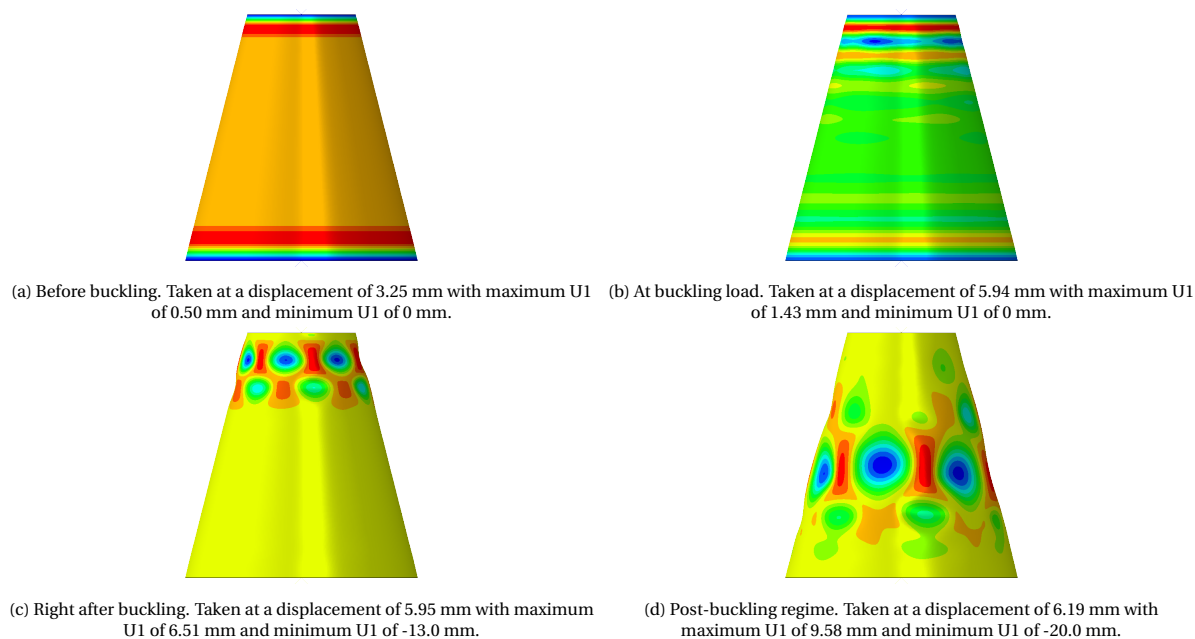


Figure 4.13: Deformation shapes in radial direction of the sandwich composite conical shell with a scaling factor of 1. Whereas, (a), (b), (c), and (d) represent the different phases of deformation and U1 denotes the out of plane deformation.

## 4.5. Sensitivity to conical height

This section investigates what happens to the buckling load and mode shape when the conical height is decreased. Since the mandrel dimensions were already known, the semi-vertex angle was kept the same and at a value of 15°. The conical heights that were analysed were 800mm, 600 mm, 400 mm, and 200 mm. First, an eigenvalue analysis was performed of each model to see the difference in buckling load. The SC8R element was used for the analyses. Only the first three eigenvalues were compared to limit the computational time. The first three force eigenvalues can be seen in table 4.17. What can be seen is that the first force eigenvalues of the 800 mm, 600 mm, and 400 mm conical height are close to each other (within 7%). This implies that the length of the conical shell does not influence the buckling load. This was already observed for cylindrical shells. It can be seen that when changing the cylindrical height, the buckling load calculated using the analytical method proposed by Bert and Reese does not change. The 200 mm conical height model has a higher force eigenvalue and is 19% higher compared to the 800 mm conical height model. The reason that the buckling load changes by a higher percentage for the 200 mm conical height model can be explained by the fact that at this height the shape of the conical shell looks more like a ring than a cone, resulting in a different structure and thus a different buckling behavior.

Table 4.17: First three force eigenvalues of the conical shell with different conical heights using the SC8R element model.

Height [mm]	Force eigenvalue 1 [kN]	Force eigenvalue 2 [kN]	Force eigenvalue 3 [kN]
800	712.6	712.6	712.8
600	736.2	736.3	737.2
400	761.1	761.2	761.7
200	844.1	844.1	846.1

The first buckling mode shapes can be seen in figure 4.14. Only the first buckling mode shapes are shown here because the second and third buckling mode shapes look similar. What can be observed is that for the models with a conical height of 800 mm, 600 mm, and 400 mm the buckling mode shape consist of waves while the 200 mm height model shows a more diamond shaped pattern. It can also be seen that when the conical height is decreased the buckling mode shape covers the full conical length instead of only the top of the shell as what can be observed for the 800 mm conical height model.

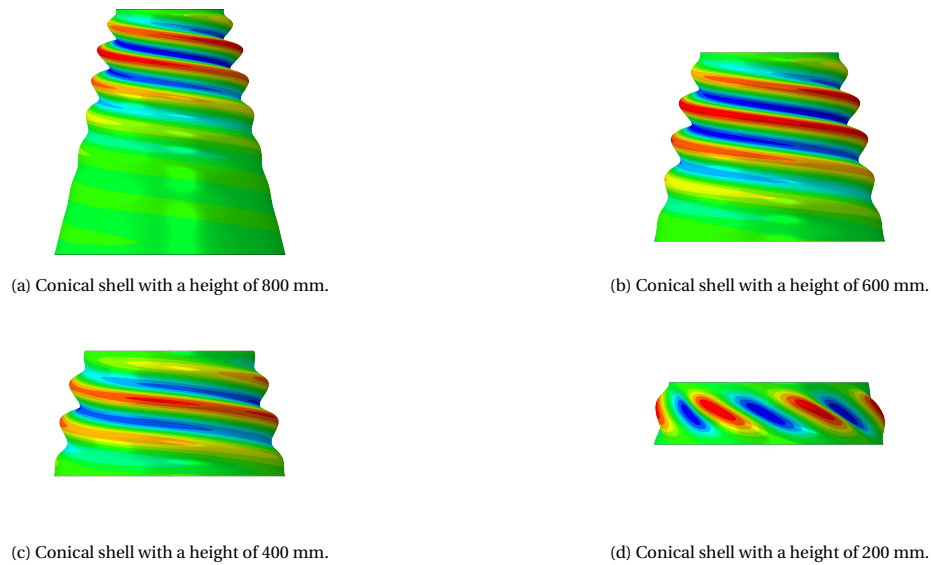


Figure 4.14: First buckling mode shape of the sandwich composite conical shells with different heights. For generating the figures a scaling factor of 30 was employed.

For the different conical height models a dynamic analysis was performed in order to see if there is a difference between the eigenvalue analysis and dynamic analysis results and to see if there is any non-linear behavior. The force-displacement graphs of the dynamic analysis can be seen in figure 4.15. What can be seen in the figure is that the stiffness of the conical shell increases if the length is decreased. The buckling loads determined by the dynamic analysis can be seen in table 4.18. What can be observed is that the buckling load does not change when decreasing the conical height except for low values of the height. This was also observed when looking at the eigenvalue analysis results. The difference between the eigenvalue analysis buckling loads and the dynamic buckling loads is less than 7% for all conical height models. This means that there is a good correlation between the results of the eigenvalue analysis and the dynamic implicit analysis.

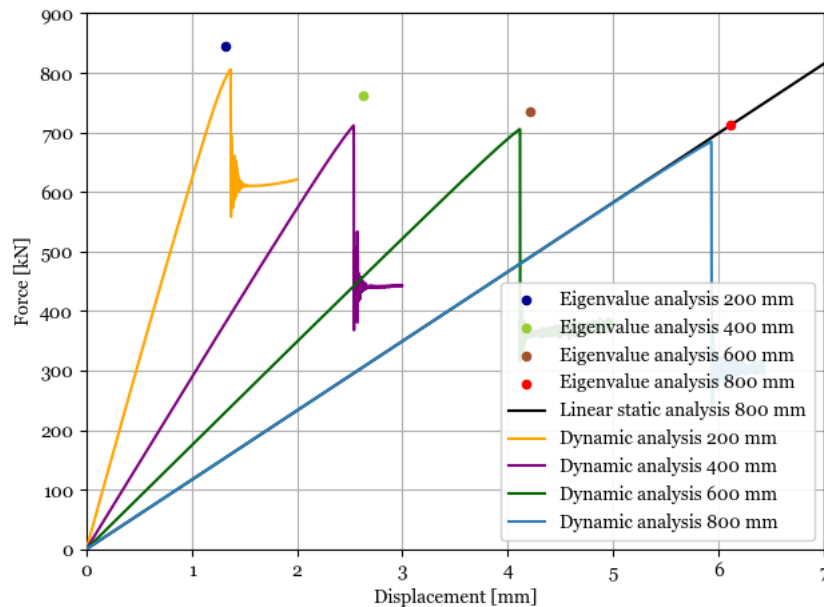


Figure 4.15: Force-displacement graphs of the sandwich composite conical shells with a height of 800 mm, 600 mm, 400 mm, and 200 mm using the SC8R element model.



Table 4.18: Buckling loads of the different height models determined by the dynamic analysis.

<b>Height [mm]</b>	<b>800</b>	<b>600</b>	<b>400</b>	<b>200</b>
Buckling load [kN]	684.8	705.3	711.6	806.0



# 5

## Sandwich composite cylindrical-conical shell

Since the buckling behavior of the sandwich composite cylindrical shell and conical shell are known, the next step is to analyse the buckling behavior of the cylindrical-conical shell. In order to be able to compare the results of chapter 4 with the results in this chapter, analyses were performed using the same geometry and material properties for the cylindrical part and conical part as described in chapter 4. The cylindrical-conical shell model was created by using the separate models of the cylindrical shell and conical shell. In order to further explore and understand the buckling behavior of cylindrical-conical shells, different models were created. The buckling behavior is investigated by doing both linear analyses and a non-linear analysis. Moreover, a mesh sensitivity study is performed in order to determine the right mesh for the cylindrical-conical shell. After that, the sensitivity to conical height and semi-vertex angle is investigated. Throughout the chapter comparisons are made between the cylindrical-conical shell and the separate shells.

### 5.1. Modelling techniques

For creating the cylindrical-conical shell the two separate models of the cylindrical shell and conical shell were used. These models were placed on top of each other and the nodes were merged along the boundary resulting in the complex shell structure. The lay-up, material properties, boundary conditions, and loading conditions were applied using the same methods as described in subsection 4.1.1. For the cylindrical-conical shell, the same mesh was used as for the separate models. However, when doing this it had to be checked if the number of elements of the cylindrical shell in circumferential direction was the same as for the conical shell. For the investigation of the cylindrical-conical shell two element models were created: one using S4R elements and one using SC8R elements. The reason for using these elements was because of the good results obtained for the separate shells and due to the low computational time.

It should be noted that for the analysis of the buckling behavior of the sandwich composite cylindrical-conical shell a lot of different models had to be created. For every case first the separate models of the cylindrical shell and conical shell had to be made and then the models had to be combined in order to create the cylindrical-conical shell. This takes a lot of time and the work is very repetitive. Therefore, for creating the cylindrical-conical shell models a Python code was created which was able to generate the input files that are needed for running a job in Abaqus. This input file contains the node locations, element definition, boundary conditions, forces, and type of analysis. It should be noted that the Python code was based on the model created in Abaqus. This means that the same modelling technique applies for the model generated by Python as described above. The input file of the Python code was identical to the input file generated by Abaqus. The only difference lies in the numerical errors when calculating the node locations. The input file was generated using the following main steps:

- Input parameters: mesh size, cylindrical height, diameter, conical height, semi-vertex angle, material properties, lay-up, and thickness.
- Step 1: Use the mesh size and geometrical properties to calculate the number of elements in circumferential and axial direction.

- Step 2: Create a list of radii for the conical shell part using the number of elements in axial direction and the geometrical properties.
- Step 3: Use the number of elements and geometrical properties to determine all the node locations. It should be noted that for the node locations of the cylindrical shell a constant radius was used and for the node locations of the conical shell the list with radii was used.
- Step 4: Define the elements by using the nodes.
- Step 5: Write the input file.

It should be noted that two Python codes were generated: one for the S4R element model and one for the SC8R element model.

## 5.2. Linear analyses

First a linear static analysis was performed in order to determine the stiffness of the cylindrical-conical shell. A load of 900 kN was applied in negative axial direction in order to compare the results with the results of the separate shells. The results for the linear static analysis can be seen in table 5.1. What can be observed is that the displacement is higher when compared to the displacements of the cylindrical and conical shell. This means that the stiffness of the cylindrical-conical shell is lower. The CPU time is higher when compared to the results of the separate shells. This is expected because there are more elements present.

Table 5.1: Displacement of the sandwich composite cylindrical-conical shell due to a force of 900 kN in axial direction.

Element	Displacement [mm]	CPU time [s]
S4R	14.6	90
SC8R	14.6	95

Also an eigenvalue analysis was performed. It should be noted that for the cylindrical-conical shell no analytical expression could be found for calculating the buckling load. The buckling loads of the cylindrical and conical shell that were obtained by the eigenvalue analyses were verified with the analytical solution. This implies that the same modelling approach should also be valid for the cylindrical-conical shell. The results of the eigenvalue analysis can be seen in table 5.2. It can be seen that the buckling load is the same as the buckling load for the conical shell. Moreover, it can be observed that there is no difference between the S4R and SC8R element models.

Table 5.2: First three force eigenvalues and CPU times of sandwich composite cylindrical-conical shell using a S4R element model and a SC8R element model.

Element	Force eigenvalue 1 [kN]	Force eigenvalue 2 [kN]	Force eigenvalue 3 [kN]	CPU time [s]
S4R	712.5	712.6	712.8	5517
SC8R	712.6	712.6	712.8	4399

The mode shapes were determined using the eigenvalue analysis. The mode shapes of the S4R and SC8R element models gave the same mode shapes and; therefore, only the mode shapes obtained using the S4R element model are shown here. The mode shapes of the first three force eigenvalues can be seen in figure 5.1. It can be seen that the deformation is located only at the top of the cylindrical-conical shell. It seems like the cylindrical shell acts as a boundary condition. When comparing the mode shape of the conical part of the cylindrical-conical shell to the mode shape of the conical shell alone it can be seen that the same mode shape is obtained. This is expected because the buckling load of the cylindrical-conical shell is the same as the buckling load of the conical shell.

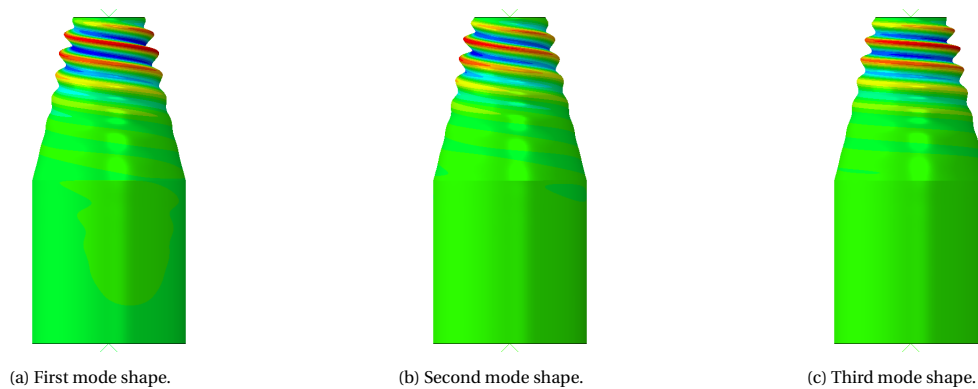


Figure 5.1: First three buckling mode shapes of sandwich composite cylindrical-conical shell using the S4R element model. For generating the figures a scaling factor of 30 was employed.

### 5.3. Dynamic analysis

A dynamic implicit analysis was performed in order to investigate if the buckling load and mode shape are the same as predicted by the eigenvalue analysis and to construct the force displacement graph of the cylindrical-conical shell. For the analysis, the SC8R element model was used. Before performing the dynamic implicit analysis, an eigenvalue analysis was performed which was done using an applied displacement. This was needed in order to determine the order of magnitude of the applied displacement for the dynamic implicit analysis. A displacement of -1 mm was added to the top reference point and results in a displacement eigenvalue of 11.5 mm. For the dynamic implicit analysis a displacement of 12 mm was applied over a time of 6 s. The same time parameters were employed as described in chapter 4.

The force-displacement graph determined by the dynamic implicit analysis can be seen in figure 5.2. A buckling load of 441.5 kN is obtained by the dynamic implicit analysis. Moreover, what can be seen is that the eigenvalue analysis gives a buckling load that is 38% higher than the buckling load obtained by the dynamic analysis. It can also be seen that the slope of the force displacement graph is non-linear, which was not observed in the dynamic analysis results of the cylindrical shell and conical shell. The deformation shapes of the cylindrical-conical shell can be seen in figure 5.3. In figure 5.3a and 5.3b it can be seen that the interface (region where the conical shell part and cylindrical shell part come together) plays a major role in the deformation of the shell. It was expected that the interface should have some impact on the buckling behavior of the shell because at the interface the shape of the shell changes. However, this was not yet seen in the results of the eigenvalue analysis. The mode shape obtained by the dynamic analysis is therefore, different compared to the mode shape of the eigenvalue analysis.

The difference between the results of the eigenvalue analysis and the dynamic implicit analysis can be explained by the non-linearity of the problem. It can be seen that in the stage prior to buckling there is already a large deformation at the interface. This creates a drop in stiffness of the cylindrical-conical shell. Due to this, the buckling of the structure happens earlier. These results imply that the interface is indeed the weakest point of the shell structure. The difference between the eigenvalue analysis and dynamic implicit analysis is further investigated in the next chapter.

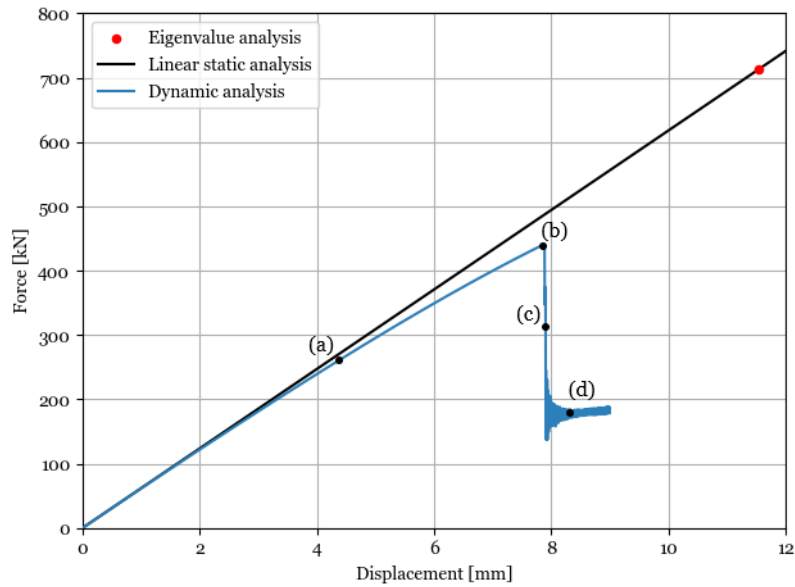


Figure 5.2: Force-displacement graph of sandwich composite cylindrical-conical shell. Whereas, (a), (b), (c), and (d) represent the different phases of deformation.



(a) Deformation shape prior to buckling. Taken at a displacement of 4.40 mm (b) Deformation shape at buckling load. Taken at a displacement of 3.95 mm with maximum U1 of 2.2 mm and minimum U1 of 0 mm.



(c) Deformation shape right after buckling. Taken at a displacement of 3.96 mm with maximum U1 of 6.9 mm and minimum U1 of -14.5 mm. (d) Deformation shape in post buckling regime. Taken at a displacement of 8.31 mm with maximum U1 of 16.6 mm and minimum U1 of -42.7 mm.

Figure 5.3: Deformation shapes in radial direction of the sandwich composite cylindrical-conical shell with a scaling factor of 1. Whereas, (a), (b), (c), and (d) represent the different phases of deformation and U1 denotes the out of plane deformation.

## 5.4. Mesh comparison

Since there is a difference between the eigenvalue analysis and dynamic implicit analysis, it is suspected that there is a mesh bias at the top of the conical shell part. This is because at the top of the cylindrical-conical shell the mesh size is smaller compared to the mesh size at the interface. Therefore, different meshes were generated in order to check if the buckling is always present at the top of the cylindrical-conical shell. The following meshes were created:

- Mesh 1: The mesh proposed in section 5.1. This mesh is used as reference mesh.
- Mesh 2: Bias of 5 towards the interface. The bias was applied only on the conical part of the shell. This mesh was created to decrease the mesh size of the elements towards the interface. Important to note is that the number of the elements is the same.
- Mesh 3: Bias of 5 towards the interface for the cylindrical shell part and conical shell part. This means that around the interface the mesh is much denser compared to the rest of the model. This mesh was created to see if there is any effect if the mesh size of the cylindrical shell towards the interface is smaller. It should be noted that the number of elements was kept constant.
- Mesh 4: Using the equal number of elements in the conical part and the cylindrical part. This means that height of the elements in the conical part is increased. This mesh was used in order to see the difference in CPU time.

For these four different meshes an eigenvalue analysis was performed. The results can be seen in table 5.3. The difference with respect to mesh model 1 is less than 0.2% for all mesh models. When looking at the CPU times it can be seen that mesh model 4 has the lowest CPU time, which is expected because of the number of elements being less compared to the other mesh models. Furthermore, the mode shapes were determined and the mode shapes of the different meshes are similar to the mode shapes shown in figure 5.1. This means that a bias towards the interface does not move the buckling shape towards the intersection. Since all models gave the same results it was chosen to use the mesh 1 configuration for further analysis. This is because the aspect ratio of the elements is also an important factor. For mesh 2, mesh 3, and mesh 4 the maximum aspect ratio of the elements is around 2.5. For mesh 1 the maximum aspect ratio is 1.5. For Abaqus models, an aspect ratio of 1 is striven for, which results in that the mesh 1 configuration is used for further analyses.

Table 5.3: First three force eigenvalues and CPU times of the sandwich composite cylindrical-conical shell using different meshes.

Mesh [-]	Force eigenvalue 1[kN]	Force eigenvalue 2[kN]	Force eigenvalue 3[kN]	CPU time [s]
Mesh 1	712.6	712.6	712.8	4399
Mesh 2	713.5	713.6	713.8	3493
Mesh 3	713.5	713.6	713.8	3793
Mesh 4	713.0	713.0	713.2	2606

## 5.5. Sensitivity to conical height

In this section the sensitivity to conical height is investigated. It is investigated if the difference between the eigenvalue analysis and dynamic analysis decreases when the conical height is decreased. For the analysis, the geometrical properties of the cylindrical part of the cylindrical-conical shell were kept constant. For the conical part the semi-vertex angle was kept constant and the height was changed. The heights that were analysed were 1600 mm, 1400 mm, 1200 mm, and 1000 mm whereas the 1600 mm cylindrical-conical shell is the reference case. It should be noted that this corresponds to conical heights of 800 mm, 600 mm, 400 mm, and 200 mm, respectively. First, an eigenvalue analysis was performed and the results can be seen in table 5.4. What can be seen is that the buckling loads of the cylindrical-conical shells are the same as the buckling loads determined by the eigenvalue analysis of the separate shells. This means that the buckling load determined by the eigenvalue analysis is the similar to the buckling loads of the separate shells, depending on which shell has a lower buckling load. For the 1600 mm, 1400 mm, and 1200 mm cylindrical-conical shell the buckling load is close to the buckling load of the conical shells with a height of 800 mm, 600 mm, and 400 mm, respectively. For the 1000 mm cylindrical-conical shell the buckling load is similar to the buckling load of the cylindrical shell.

Table 5.4: First three force eigenvalues of the sandwich composite cylindrical-conical shells with different conical heights.

Height [mm]	Force eigenvalue 1 [kN]	Force eigenvalue 2 [kN]	Force eigenvalue 3 [kN]
1600	712.6	712.6	712.8
1400	735.8	735.8	736.7
1200	756.0	756.0	756.9
1000	793.9	794.8	794.8

In figure 5.4 the first buckling mode shapes of the cylindrical-conical models with a different conical height can be seen. For the cylindrical-conical shells with a height of 1600 mm, 1400 mm, and 1200 mm it can be seen that the deformation is only present in the conical part of the shell. It looks like the cylindrical part of the shell does not participate in the analysis. For the 1000 mm shell the deformation is present in the cylindrical part and conical part of the shell. It seems like the eigenvalue analysis is not able to capture the behavior of both the cylindrical and conical shell and neglects the transition area.

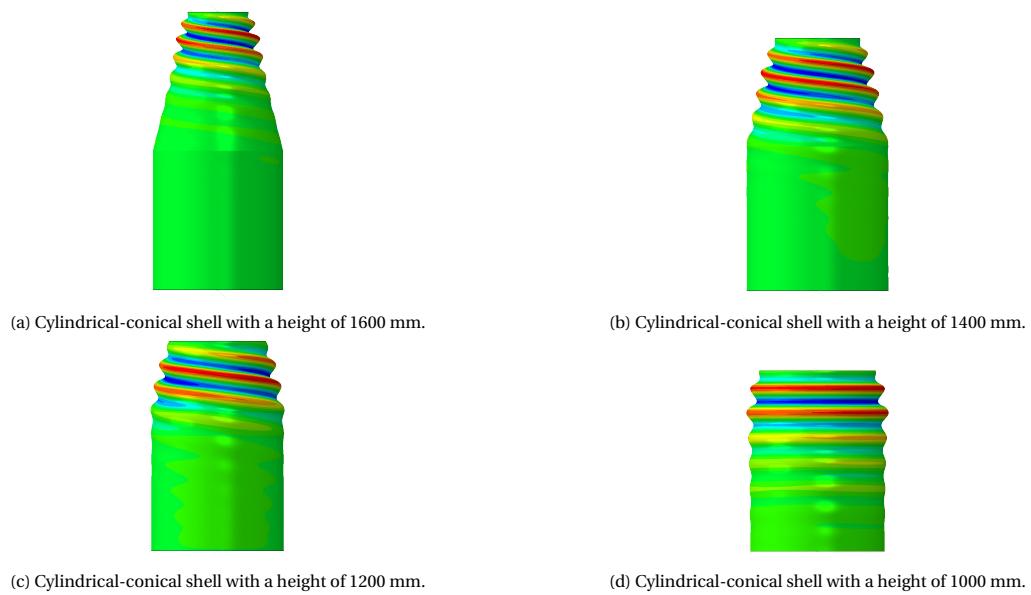


Figure 5.4: First buckling mode shapes of the sandwich composite cylindrical-conical shell with different conical heights. For generating the figures a scaling factor of 30 was employed.

Next to an eigenvalue analysis, a dynamic analysis was performed for the different height models. The results can be seen in figure 5.5. The buckling loads for each height model can be seen in table 5.5. What can be observed is that the buckling loads determined by the eigenvalue analysis are around 40% higher for all the height models. As already suggested, the eigenvalue analysis is not able to capture the right buckling behavior of cylindrical-conical shells. What also can be observed is that the buckling load almost does not change with decreasing conical height. This means that the buckling load of the cylindrical-conical shell is independent of the conical height. However, it can be observed that the stiffness does change when decreasing the conical height.

Moreover, the deformation shapes right before buckling were extracted from the dynamic analysis in order to make a comparison with the mode shapes obtained by the eigenvalue analysis. The deformation shapes just before buckling can be seen in figure 5.6. In the figures it can be seen that the deformation is mostly present around the interface and that the shapes are not similar to the mode shapes from the eigenvalue analysis. There is a very large deformation at the intersection which was also seen for the 1600 mm cylindrical-conical shell.



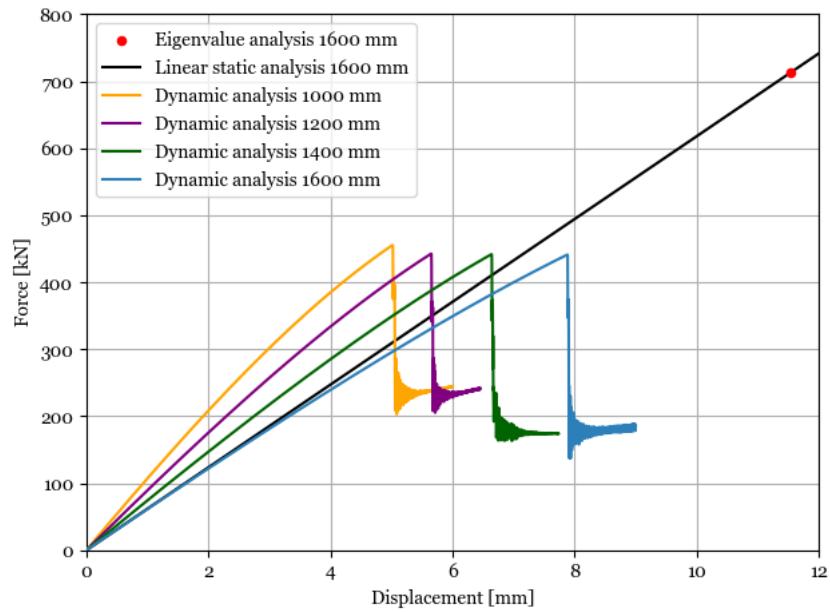
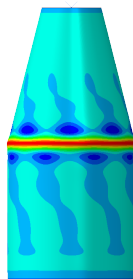


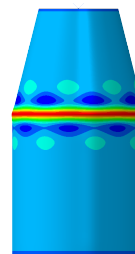
Figure 5.5: Force-displacement graphs of the sandwich composite cylindrical-conical shell with different conical heights.

Table 5.5: Buckling loads of the sandwich composite cylindrical-conical shell with different conical heights determined by the dynamic analysis.

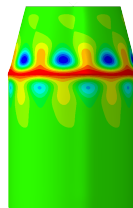
Height [mm]	1600	1400	1200	1000
Buckling load [kN]	441.5	441.8	442.6	455.5



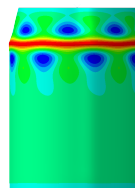
(a) Cylindrical-conical shell with a height of 1600 mm.



(b) Cylindrical-conical shell with a height of 1400 mm.



(c) Cylindrical-conical shell with a height of 1200 mm.



(d) Cylindrical-conical shell with a height of 1000 mm.

Figure 5.6: Deformation shapes right before buckling of the sandwich composite cylindrical-conical shell with different conical heights. For generating the figures a scaling factor of 1 was employed.

## 5.6. Sensitivity to semi-vertex angle

This section investigates the effect of the semi-vertex angle on the difference between the results obtained by the eigenvalue analysis and dynamic implicit analysis. Semi-vertex angles of  $0^\circ$ ,  $1^\circ$ ,  $2^\circ$ ,  $5^\circ$ ,  $10^\circ$ , and  $15^\circ$  were used in order to see at which semi-vertex angle the difference between both analyses starts. The cylindrical-conical shell used had the same lay-up and material properties as the other models proposed in this thesis. The length of the shell was 1200 mm, whereas the cylindrical part had a length of 800 mm and the conical part had a length of 400 mm. This in order to shorten the computational time and to make the results less dependent on the length of the conical shell.

The first step in analysing the effect of the semi-vertex angle was to do an eigenvalue analysis for the different cylindrical-conical shells. The first three force eigenvalues can be seen in table 5.6. What can be observed is that the buckling load decreases with increasing semi-vertex angle. The accompanying first mode shapes of the cylindrical-conical shells can be seen in figure 5.7. What can be seen is that for the models with a semi-vertex angle between  $0^\circ$  and  $5^\circ$  the deformation is located along the whole length of the cylindrical-conical shell and for the other models the deformation is present at the conical part of the cylindrical-conical shell. When looking at the force eigenvalues it can be seen that the cylindrical-conical shells with a semi-vertex angle of  $0^\circ$ ,  $1^\circ$ ,  $2^\circ$ , and  $5^\circ$  have the same buckling load, which is expected since the mode shapes look similar. It can be seen that when the semi-vertex angle increases the buckling load decreases, which can be explained by the fact that only the conical part buckles. The conical part has a lower buckling load compared to the cylindrical part.

Table 5.6: First three force eigenvalues of the 1200 mm cylindrical-conical shell with different semi-vertex angles.

Semi vertex angle [ $^\circ$ ]	Force eigenvalue 1 [kN]	Force eigenvalue 2 [kN]	Force eigenvalue 3 [kN]
0	801.1	801.1	801.6
1	801.1	801.1	801.8
2	801.0	801.1	801.9
5	800.0	800.0	800.9
10	787.3	787.3	788.1
15	756.0	756.0	756.9

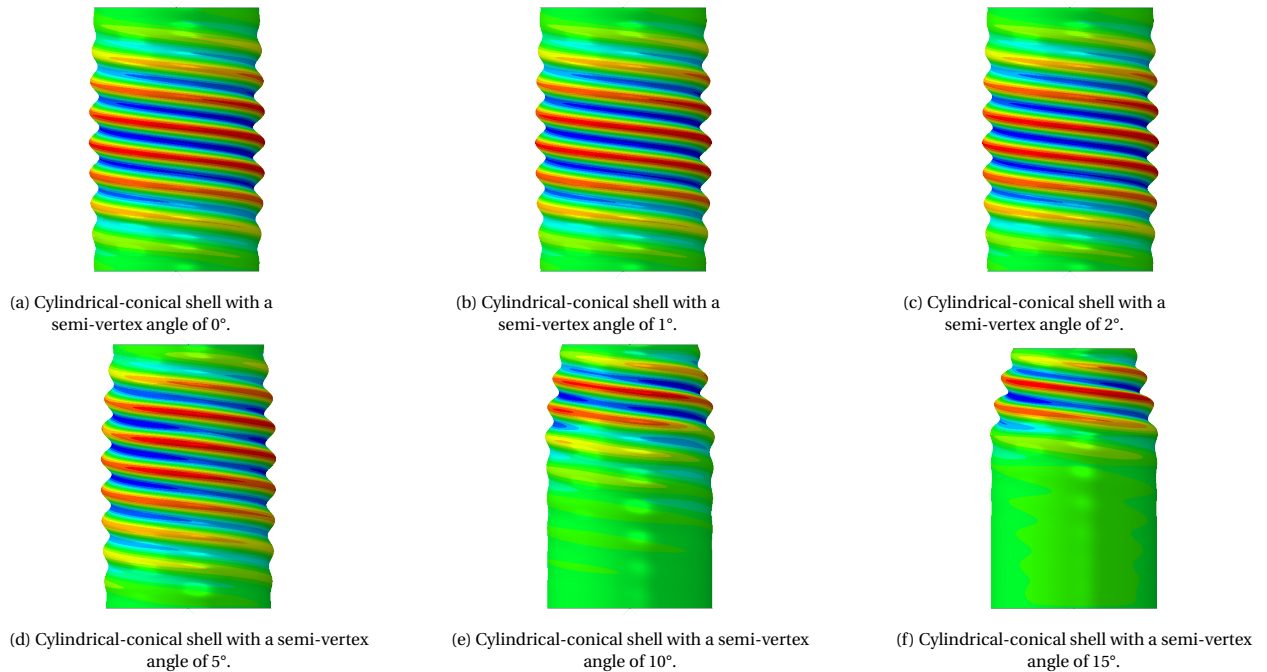


Figure 5.7: First buckling mode shapes of the 1200 mm sandwich composite cylindrical-conical shell with different semi-vertex angles. For generating the figures a scaling factor of 30 was employed.

A dynamic implicit analysis was also performed in order to see the differences with the eigenvalue analysis. It should be noted that the same dynamic properties were used as described in earlier sections. The force-displacement graphs can be seen in figure 5.8. What can be observed is that when using a semi-vertex angle of  $0^\circ$  the difference between the buckling loads of the eigenvalue analysis and dynamic analysis is 2.5%. At a semi-vertex angle of  $5^\circ$  the difference is already 30% and goes to 40% for a semi-vertex angle of  $15^\circ$ .

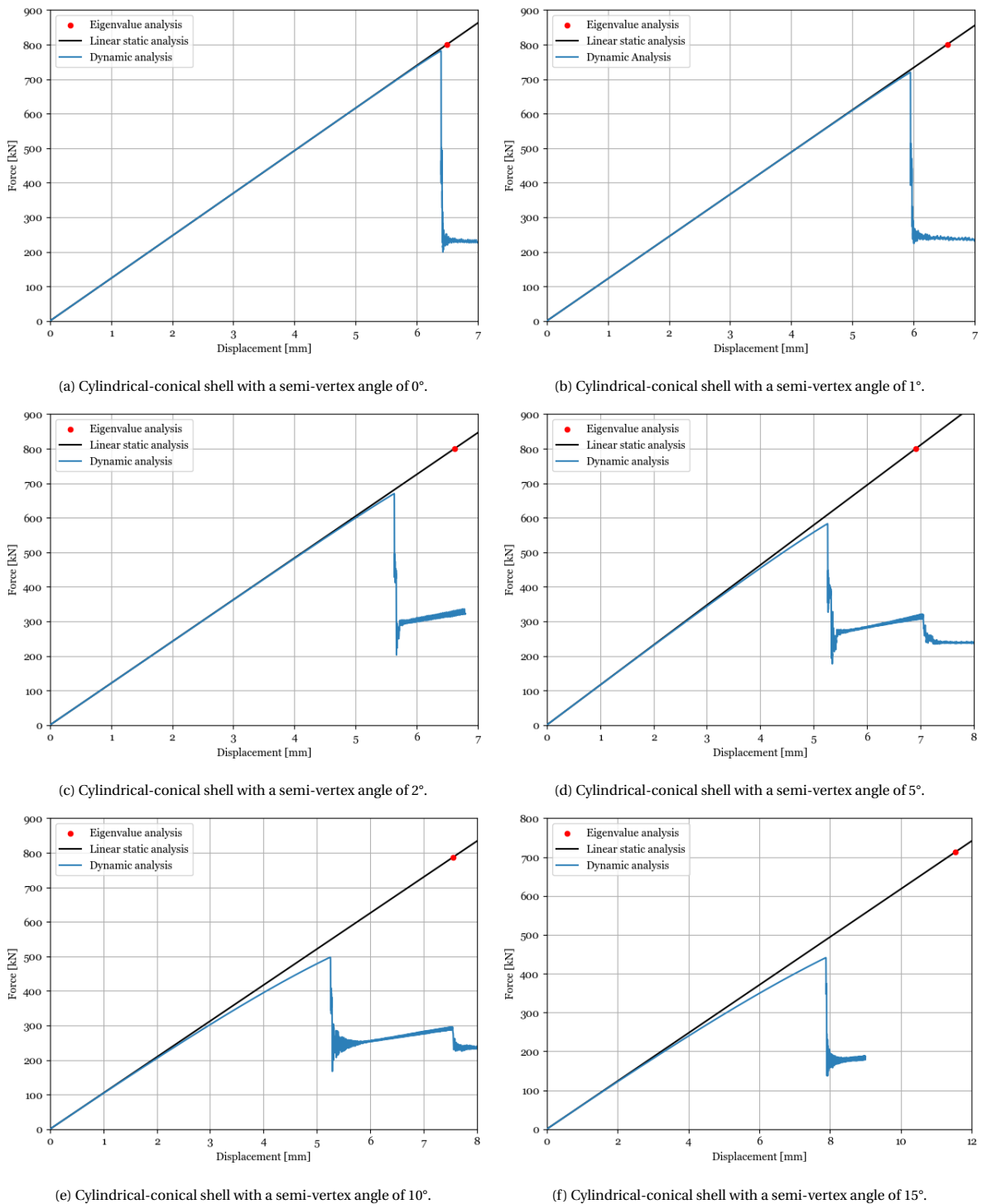


Figure 5.8: Force-displacement graphs of the 1200 mm sandwich composite cylindrical-conical shell with different semi-vertex angles.

To further investigate the difference also the deformation shapes just before buckling were extracted. The deformation shapes are shown in figure 5.9. What can be seen is that for semi-vertex angles higher than  $0^\circ$  the deformation is concentrated around the intersection. When comparing the deformation shapes with the mode shapes obtained by the eigenvalue analysis it can be seen that the eigenvalue analysis is not able to capture the behavior around the intersection. Interesting to note is that at a semi-vertex angle of  $1^\circ$  the behavior around the intersection is already dominating the buckling of the cylindrical-conical shell.

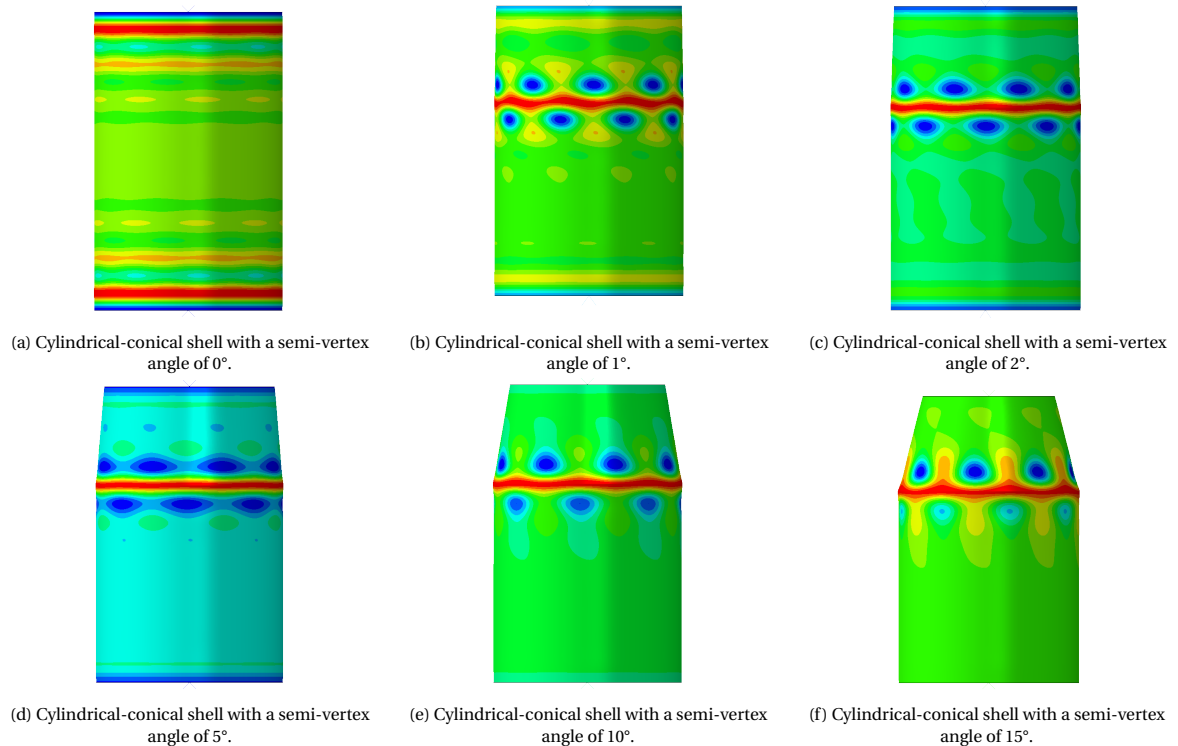


Figure 5.9: Deformation shapes right before buckling of the 1200 mm sandwich composite cylindrical-conical shell with different semi-vertex angles. For generating the figures a scaling factor of 1 was employed.

# 6

## Investigation of the non-linear behavior of the sandwich composite cylindrical-conical shell

Since there is a difference between the eigenvalue analysis and the dynamic implicit analysis, further investigation is needed. For the sandwich composite cylindrical shell and sandwich composite conical shell the eigenvalue analysis is able to capture the buckling load. However, for the sandwich composite cylindrical-conical shell the eigenvalue analysis is giving a buckling load which is 40% higher compared to the dynamic implicit analysis. Since for the eigenvalue analysis only deformation is present at the top of the conical part of the cylindrical-conical shell and nothing happens at the interface, it is further investigated if the eigenvalue analysis is not able to give accurate results for a sandwich composite cylindrical-conical shell structure. The reason for this is probably because of the non-linear behavior of the sandwich composite cylindrical-conical shell, which cannot be captured by the eigenvalue analysis.

This chapter further investigates the causes of the non-linear behavior and shows how the difference between the eigenvalue analysis and dynamic implicit analysis can be solved. First, the results given by the dynamic implicit analysis are verified. This is done by performing a non-linear Riks analysis, which is another solver within the Abaqus software that is able to capture non-linear effects. Moreover, a S4R element model was analysed to verify the results. After that, the radial deformation and strains are compared between the analyses. This in order to better understand the behavior of the transition area and to find out why this difference happens. In section 6.4, a preload is added before executing an eigenvalue analysis to see if including the non-linear behavior of the cylindrical-conical shell gives a better prediction for the eigenvalue analysis. Then the material properties are changed of the cylindrical part of the cylindrical-conical shell to see what happens if the cylindrical shell has a lower buckling load compared to the conical part of the shell. This is followed by the investigation of an aluminum cylindrical-conical shell to see if the eigenvalue analysis is able to give a buckling load closer to the dynamic implicit buckling load when an isotropic material is used. After that, a composite cylindrical-conical shell was analysed to see the difference between a composite cylindrical-conical shell and a sandwich composite cylindrical-conical shell. Finally, the effect of adding a radius of curvature at the transition and the effect of reinforcing the structure around the transition are investigated. It should be noted that for the analyses performed in this chapter the same modelling techniques are used as described in chapter 5 and the SC8R element model was employed unless stated otherwise.

### 6.1. Verification of the dynamic implicit analysis

For the verification of the results of the dynamic implicit analysis, two analyses were performed: the non-linear Riks analysis and a dynamic implicit analysis using the S4R element model. In order to verify the results the force-displacement graphs of the different analyses are compared. Both analyses are able to capture the non-linear effects of the shell.

The non-linear Riks solver was used in order to verify the force-displacement graph of the dynamic implicit analysis. The reason for choosing a non-linear Riks analysis is because of its ability to include non-linear effects. The non-linear Riks analysis is based on the arc-length method and generates the force-displacement

graph by using iterations. It solves simultaneously for loads and displacements and uses arcs to measure the progress of the solution. In the Abaqus manual [18] it is advised to use the non-linear Riks solver instead of using the eigenvalue analysis if there is any chance of material non-linearity or geometric non-linearity before buckling. In figure 5.2 it can be seen that there is non-linear behavior before buckling and therefore, this solver should be able to give a better prediction of the buckling load.

For the non-linear Riks solver, incremental parameters should be defined. The process of determining these parameters is the same as for the dynamic implicit analysis. For the non-linear Riks analysis the same incremental parameters were used. It should be noted that for the non-linear Riks solver to initiate buckling a small imperfection is needed. This is because it is a quasi-static analysis and for buckling to happen a trigger is needed. This section is meant to verify the result of the dynamic analysis so the non-linear Riks solver was used without adding any imperfection to the model and only the graphs prior to buckling are compared. The comparison between the non-linear Riks and dynamic implicit force-displacement graphs can be seen in figure 6.1. What can be seen is that the graphs are the same until buckling, which means that the graph obtained by the dynamic implicit analysis is verified.

It could be seen in the job diagnostics of the non-linear Riks analysis that negative eigenvalues start appearing after passing the buckling point determined by the dynamic implicit analysis. This means that the non-linear Riks analysis is following an unstable path after the buckling point. The result is that the non-linear Riks analysis overshoots the buckling load. This was expected as already explained above.

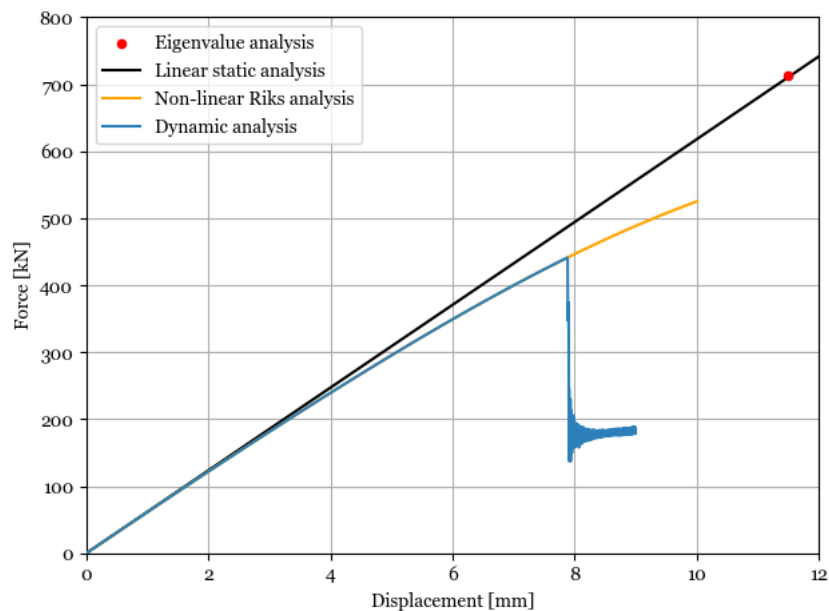


Figure 6.1: Force-displacement graphs obtained by the non-linear Riks analysis and dynamic implicit analysis of the sandwich composite cylindrical-conical shell.

Another way to verify the results given by the dynamic implicit analysis is to use another element model. The S4R element model was chosen because of the mesh being independent on the way in which the thickness is defined (2D element model) and because the mesh convergence studies in chapter 4 were done using S4R elements. A dynamic implicit analysis was performed to see the differences in the force-displacement graphs. The force displacement graphs of both element models can be seen in figure 6.2. It can be seen that both graphs are on top of each other. This means that the SC8R element model is build up correctly and that there is no difference between both element models.

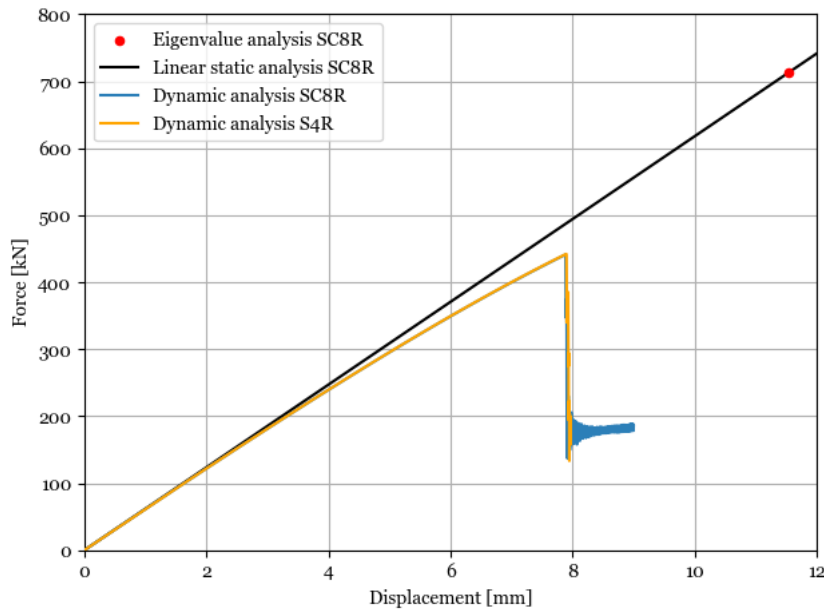


Figure 6.2: Force-displacement graphs obtained by the dynamic implicit analysis using the S4R element model and the SC8R element model of the sandwich composite cylindrical-conical shell.

## 6.2. Difference in radial deformation of linear analyses and non-linear analyses

To better understand the difference between the linear analyses and the non-linear analyses, a linear static analysis was performed. A load of -440 kN (just before buckling) was applied to the sandwich composite cylindrical-conical shell to be able to compare the deformation shapes of the linear static analysis, non-linear Riks analysis, and dynamic implicit analysis. When looking at the results of the dynamic implicit analysis it can be seen that there is a large radial deformation at the interface of the cylindrical-conical shell. In order to investigate if the linear static analysis is able to capture the same behavior as the non-linear analyses, the radial deformations are compared at the same displacement. At a load of -440 kN the displacement in axial direction of the linear static analysis is equal to -7.12 mm. To make the comparison, the radial deformation shapes of the non-linear analyses are also taken at an axial displacement of -7.12 mm. The maximum radial deformations and deformation shapes can be seen in table 6.1 and figure 6.3, respectively. It should be noted that a scaling factor of 20 is used for the representation of the deformation shapes. This is done in order to better visualize the difference.

When looking at table 6.1 it can be seen that the maximum radial displacements of the non-linear Riks and dynamic implicit analysis are the same. This is expected since the slope of the force-displacement graph of both analyses are similar. When looking at the difference between the linear static analysis and the non-linear analyses it can be seen that there is a difference of 23%. This means that the linear static analysis is not able to capture the large radial deformation at the interface. When looking at the deformation shapes it can be seen that the non-linear Riks analysis and the dynamic implicit analysis show a larger deformation at the interface. Moreover, when looking closely at the interface it can be seen that just before the structure bulges outward the structure is bulging inward. This is not seen for the linear static analysis. The deformation shape of the linear static analysis shows an increase in radial displacement until the maximum radial displacement is reached. Due to this difference the stiffness of the non-linear models are reduced, which results in a lower buckling load.

Table 6.1: Maximum radial displacement of the sandwich composite cylindrical-conical shell at a displacement of -7.12 mm in axial direction.

	<b>Max radial displacement [mm]</b>
Non-linear Riks	3.9
Dynamic implicit	3.9
Linear static	3.0
Difference [%]	-23

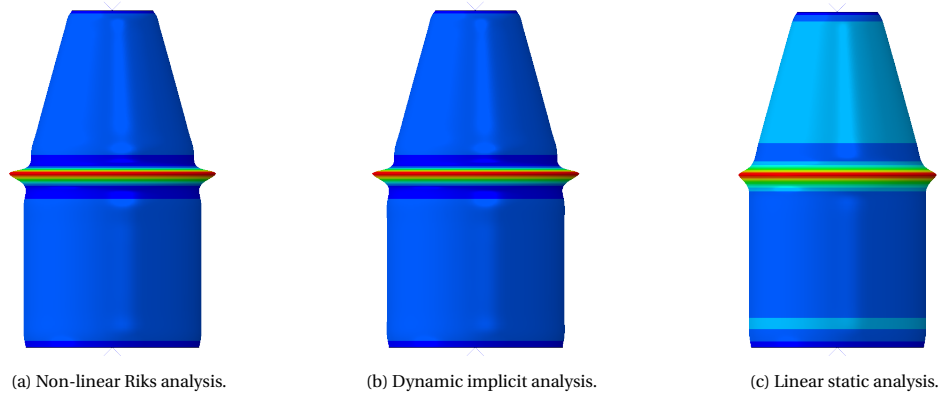


Figure 6.3: Radial deformation of the sandwich composite cylindrical-conical shell at a displacement of -7.12 mm in axial direction. For generating the figures a scaling factor of 20 was employed.

### 6.3. Difference in strains right before buckling of linear analyses and non-linear analyses

Looking at the strains of the cylindrical-conical shell can help in getting a better understanding of the non-linear behavior that is happening. The strain distribution can reveal why there is such a large deformation at the interface and why there is a difference between the linear and non-linear analyses. In this section the strains are compared on ply level for the non-linear Riks analysis, dynamic implicit analysis, and linear static analysis. The strains are compared at a load of -440 kN, which is just before the buckling happens for the dynamic implicit analysis.

First the strains are compared of the non-linear Riks analysis and the dynamic implicit analysis to verify that both analysis give the same results. The strains of the dynamic implicit analysis and non-linear Riks analysis can be seen in tables 6.2 and 6.3, respectively. It should be noted that the strains reported in the table are the maximum/minimum strains in each ply direction, whereas the positive strains stand for tension and the negative strains stand for compression. For the non-linear Riks analysis and dynamic implicit analysis the maximum and minimum strains are located at the exact same position for each ply. The maximum and minimum strains were located at the transition region. In the table Ply1 - Ply3 represent the strains of the inner face sheet and Ply4 - Ply6 represent the strains of the outer face sheet. The difference between the strains are presented in table 6.4. In the table it can be seen that the highest difference that can be observed is 0.3%. For almost all plies the same small difference occurs which can be explained by the fact that the strains extracted from both analyses were not exactly at a load of -440 kN due to the incremental solving technique. For both analysis an increment was chosen very close to a load of -440 kN. Since the difference between the strains is very small, the strains obtained by the dynamic implicit analysis are verified.



Table 6.2: Micro strains of the dynamic implicit analysis at a load of -440 kN. Ply1 - Ply3 are the strains of the inner face sheet. Ply4 - Ply6 are the strains of the outer face sheet.

	$\epsilon_{11}$	$\epsilon_{22}$	$\epsilon_{12}$
Ply1	3285	-6942	23700
Ply2	-13750	10843	264
Ply3	3681	-5214	-21890
Ply4	7535	-4990	-10990
Ply5	-7651	10854	-216
Ply6	8193	-5562	10042

Table 6.3: Micro strains of the non-linear Riks analysis at a load of -440 kN. Ply1 - Ply3 are the plies of the inner face sheet. Ply4 - Ply6 are the plies of the outer face sheet.

	$\epsilon_{11}$	$\epsilon_{22}$	$\epsilon_{12}$
Ply1	3288	-6947	23720
Ply2	-13770	10850	263
Ply3	3684	-5218	-21910
Ply4	7542	-4993	-11000
Ply5	-7655	10860	-216
Ply6	8201	-5565	10050

Table 6.4: Difference between the strains of the dynamic implicit analysis and non-linear Riks analysis in percentages. Ply1 - Ply3 are the plies of the inner face sheet. Ply4 - Ply6 are the plies of the outer face sheet.

	$\epsilon_{11}$	$\epsilon_{22}$	$\epsilon_{12}$
Ply1	0.1	0.1	0.1
Ply2	0.1	0.1	0.3
Ply3	0.1	0.1	0.1
Ply4	0.1	0.1	0.1
Ply5	0.1	0.1	0.0
Ply6	0.1	0.1	0.1

The strains of the dynamic implicit analysis and linear static analysis are also compared. The strains of the linear static analysis are presented in table 6.5. It should be noted that the strains are taken at the same element of the maximum/minimum strains of the dynamic implicit analysis. This in order to make a good comparison, however, it could be seen that the location of maximum/minimum strains of the dynamic implicit analysis coincided with the maximum/minimum strains obtained by the linear static analysis. When looking at the strains of the linear static analysis it can be seen that the strains are always less when compared to the strains of the dynamic implicit analysis. The difference in percentages between the strains of the dynamic implicit analysis and the linear static analysis can be seen in table 6.6. A maximum difference of 38% can be observed. For most of the plies the difference is around 30%. Since this difference is large, it can be concluded that there is a large deformation present at the transition region resulting in the non-linear behavior seen for the dynamic implicit analysis. This cannot be captured by the linear analyses.

Table 6.5: Micro strains of the linear static analysis at a load of -440 kN. Ply1 - Ply3 are the plies of the inner face sheet. Ply4 - Ply6 are the plies of the outer face sheet.

	$\epsilon_{11}$	$\epsilon_{22}$	$\epsilon_{12}$
Ply1	2326	-4716	16178
Ply2	-9480	7427	179
Ply3	2518	-3692	-15157
Ply4	4708	-4809	-9086
Ply5	-7340	7437	-150
Ply6	4969	-5213	8743

Table 6.6: Difference between the strains of the dynamic implicit analysis and linear static analysis in percentages. Ply1 - Ply3 are the plies of the inner face sheet. Ply4 - Ply6 are the plies of the outer face sheet.

	$\epsilon_{11}$	$\epsilon_{22}$	$\epsilon_{12}$
Ply1	-29.2	-32.1	-31.7
Ply2	-31.1	-31.5	-32.2
Ply3	-31.6	-29.2	-30.8
Ply4	-37.5	-3.6	-17.3
Ply5	-4.1	-31.5	-30.6
Ply6	-39.4	-6.3	-12.9

To further investigate the difference in strains of the dynamic implicit analysis and the linear static analysis the strain distributions are compared. The strain distributions for each ply are shown in figures 6.4, 6.5, and 6.6. It should be noted that the contours of the linear static analysis were changed to comply with the contours defined by the dynamic implicit analysis. The strain distributions of each ply and strain direction have its own contour. Moreover, the strain distributions are shown for the inner face sheet. This is because for the outer face sheet similar strain distributions were observed. When looking at the strain distributions it can be seen that for all the models the linear static analysis is able to capture the deformation at the interface. However, the strains at the interface are not that large as observed for the dynamic implicit analysis.

In figure 6.4 the strains of the  $+56^\circ$  ply (ply1) can be seen. When looking at figure 6.4a it can be seen that from top to the transition region first the strains are negative then close to the transition region the strains become even more negative and then at the transition region the strains become positive. For the linear static analysis the strains go from negative values to positive values. This means that not the same behavior is happening at the interface for the linear static analysis. In figures 6.4d and 6.4e it can be seen that the strains at the interface are more positive for the dynamic implicit than for the linear static analysis. For the strain in  $\epsilon_{22}$  direction it can be observed that the strains for the dynamic implicit analysis from top to the transition region go from negative to positive close to the transition region and then back to negative at the intersection. This is not seen for the linear static analysis, the strains are all negative.

Figure 6.5 shows the strains of the  $0^\circ$  ply (ply2). In figure 6.5a and figure 6.5b it can be seen that the dynamic implicit analysis and the linear static analysis are giving similar results. The difference lies in that the linear static analysis is not able to give as negative values as given for the dynamic implicit analysis. When looking at the figures of  $\epsilon_{22}$  it can be seen that the strains from top to the transition region for the dynamic implicit analysis go from positive values to negative values and back to positive values again at the transition. This is not seen for the linear static analysis, the strains are positive for the whole structure. Since this is the zero degree ply, the  $\epsilon_{22}$  are the hoop strains. It can be seen that just before the transition the hoop strains become negative, which can explain the buckling behavior of the dynamic implicit analysis of the cylindrical-conical shell. These negative hoop strains are not seen for the linear static analysis and therefore, a higher buckling load is obtained. Moreover, a comparison can be made between the strains of the perfect cylindrical-conical shell and perfect cylindrical and conical shells. For perfect cylindrical and conical shells the axial strains are negative and the hoop strains are positive. For the cylindrical-conical shell it can be seen that the axial strains are also negative, but that the hoop strains are both negative and positive. The negative hoop strains can explain the different behavior of the cylindrical-conical shell.

The strain distributions for the  $-56^\circ$  ply (ply3) can be seen in figure 6.6. The strain distributions of  $\epsilon_{11}$  for the dynamic implicit analysis and linear static analysis are similar to the behavior seen for the first ply. For  $\epsilon_{12}$  and  $\epsilon_{22}$  it can be seen that the dynamic implicit show more negative values compared to the linear static analysis.

The strain plots given here show that there is a major difference between the dynamic implicit analysis and the linear static analysis. The linear static analysis is not able to capture the same behavior around the interface as the dynamic implicit analysis. It can be seen that the strains of the dynamic implicit analysis sometimes change from positive to negative strains and from negative to positive strains right before the transition, which is not captured by the linear static analysis. Moreover, the linear static analysis is not able to give the same large magnitude of the strains at the interface as for the dynamic implicit analysis. This can be the reason why the linear static analysis is giving a higher buckling load compared to the dynamic implicit analysis.

Due to the behavior at the transition more research was performed on the behavior of the intersection of combined shell structures. It could be seen that for pressure vessels under internal pressure large nega-

tive strains appear at the transition area. In [63], [62], and [51] it is described that due to these large negative strains the structure fails at the interface. It should be noted that pressure vessels also consist out of a cylindrical-conical shell section. In [51] it is explained why these large strains appear and why the transition area is the weakest part of the combined shell. It is explained that when a vertical force is exerted on the conical part of the cylindrical-conical shell due to internal pressure, the conical part is pulled away from the cylindrical part. This force is taken up by the tension of the conical part in radial direction, which reaches its maximum at the intersection. At the intersection the vertical component of this tension is transferred to the cylindrical part. However, the radial component cannot be transferred to the cylindrical part and has to be taken up by the intersection. This radial component leads to compressive stresses and strains at the intersection which in most cases result in failure at the intersection. Since the loading condition for the sandwich composite cylindrical-conical shell in this research is axial compression the same explanation can be given as described for the pressure vessel under internal pressure. However, the cone is pushed away from the cylinder. This means that at the transition area large positive hoop stresses and strains appear, which can also be seen in the results.

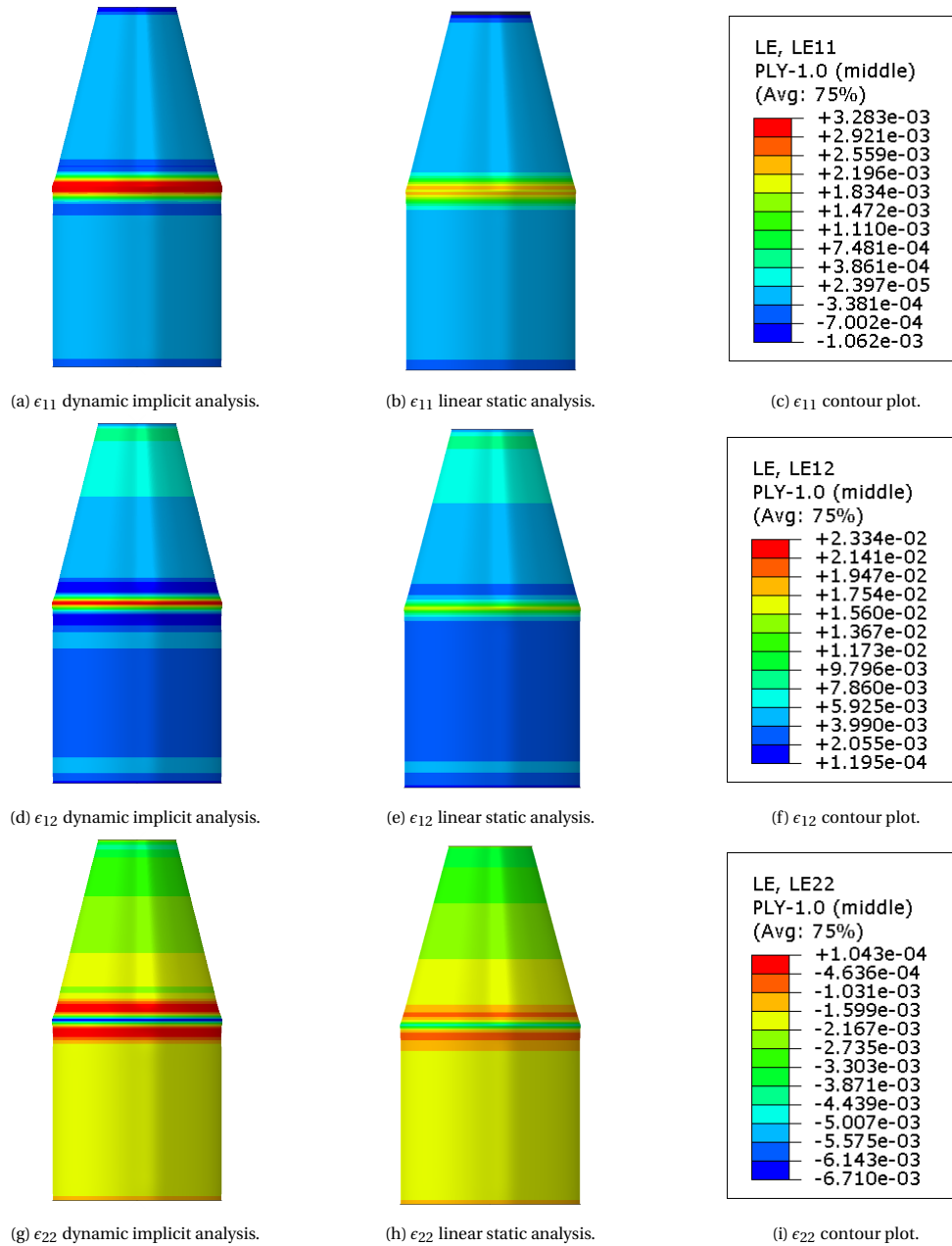


Figure 6.4: Strain distribution of the first ply in different directions of the dynamic implicit analysis and linear static analysis.

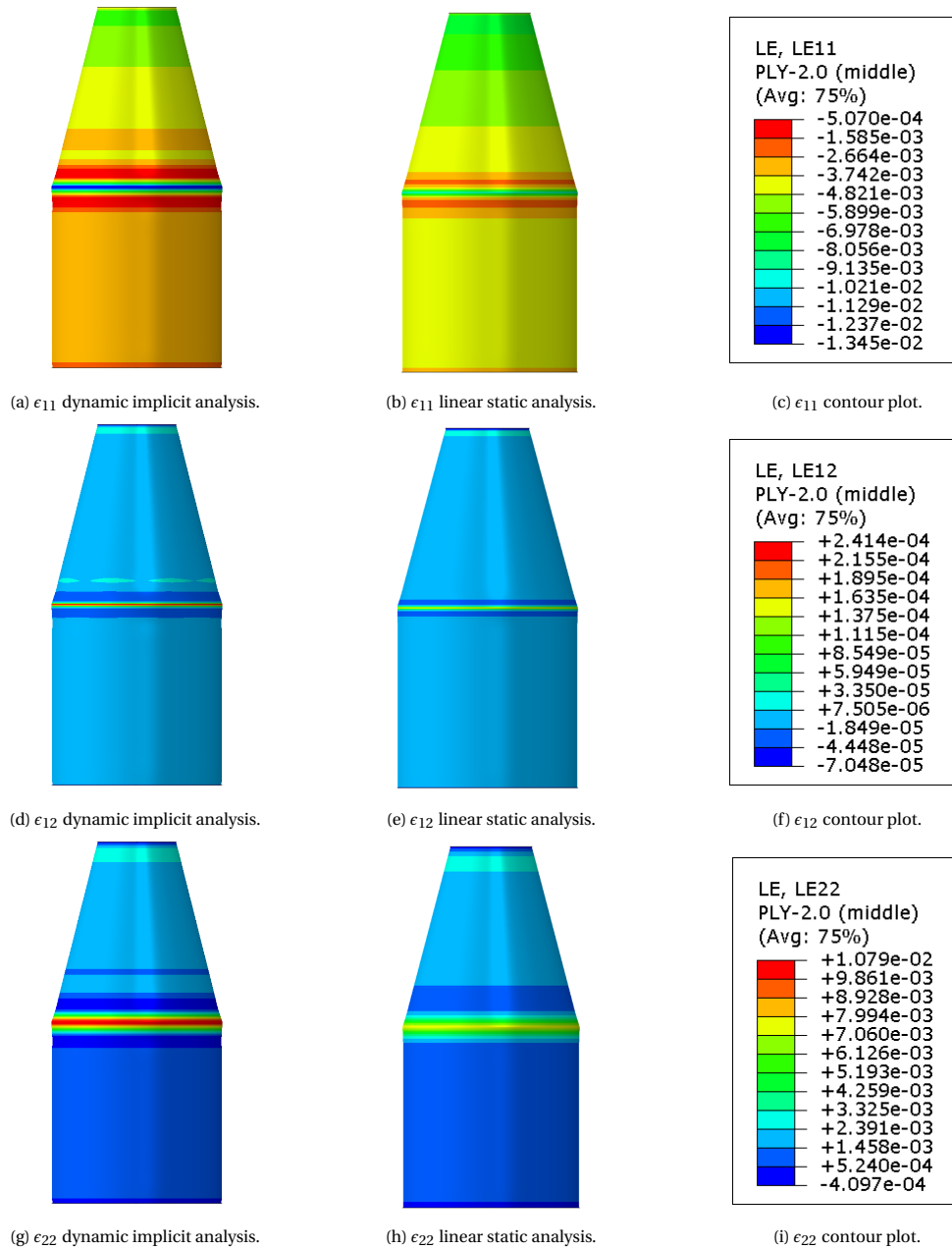


Figure 6.5: Strain distribution of the second ply in different directions of the dynamic implicit analysis and linear static analysis.

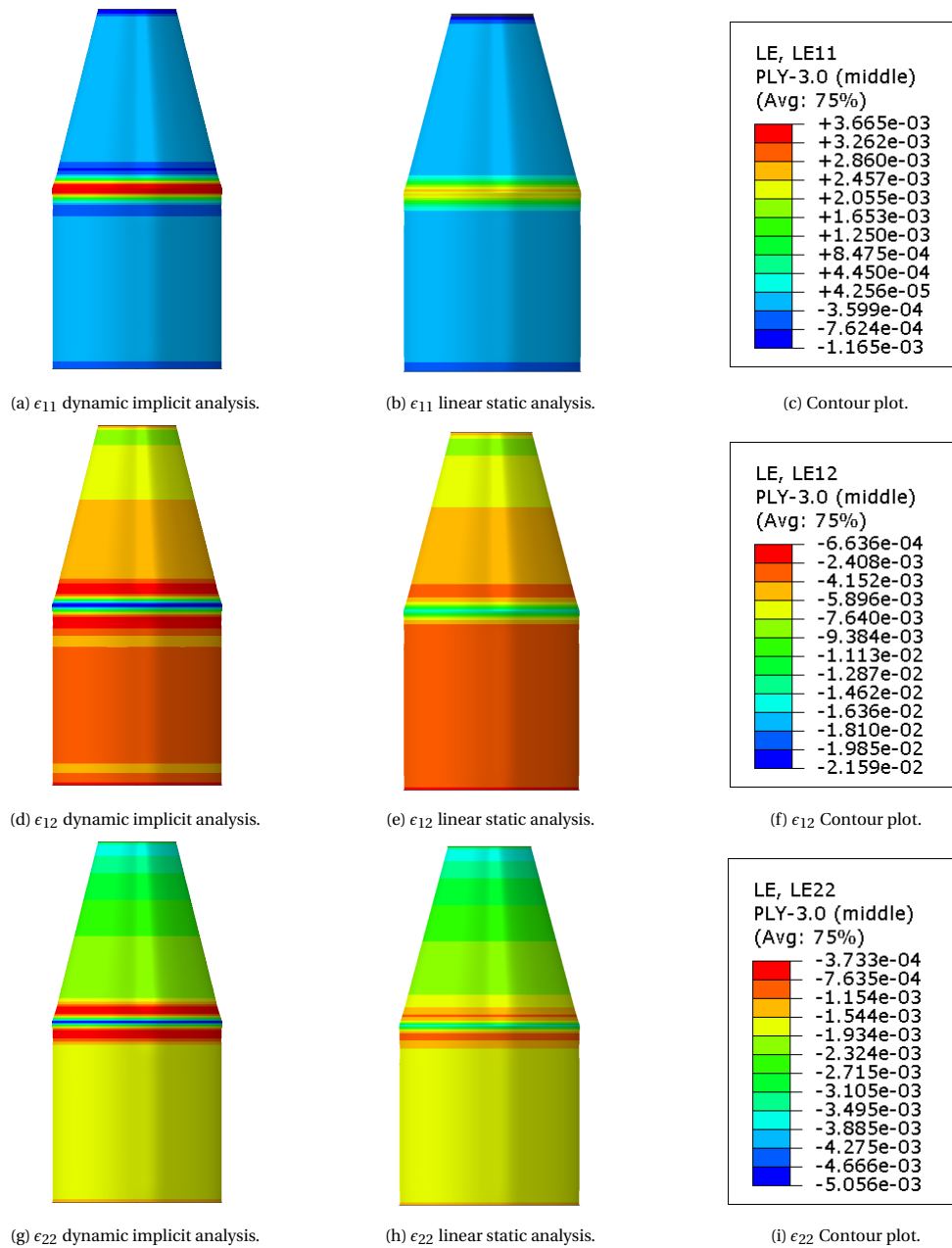


Figure 6.6: Strain distribution of the third ply in different directions of the dynamic implicit analysis and linear static analysis.

Launch vehicle structures are not meant to fail prior to buckling. Therefore, for the sandwich composite cylindrical-conical shell it is investigated if this does not happen. The failure strains of the IM7/8552 can be seen in table 6.7.

Table 6.7: Failure strains of the composite IM7/8552 material in micro strain [16].

$\epsilon_{11}^t$	$\epsilon_{11}^c$	$\epsilon_{22}^t$	$\epsilon_{22}^c$	$\epsilon_{12}$
15969	12280	6584	29400	11520

When comparing the failure strains with the strains obtained by the dynamic implicit analysis (see table 6.2) it can be concluded that the cylindrical-conical shell would fail before buckling. It can be seen that the +56°, 0°, and -56° ply of the inner face sheet and the 0° ply of the outer face sheet are the most critical plies. It can be seen that the structure fails prior to buckling due to these four plies. This means that for this structure a new design should be proposed because the cylindrical-conical shell proposed in this study is not able to withstand the load. For the thesis it does not matter that the cylindrical-conical shell would fail since the purpose of the thesis is to better understand the buckling behavior of cylindrical-conical shells. The thesis focuses more on analysing the behavior from a numerical point of view than from a design perspective.

## 6.4. Preloading structure before eigenvalue analysis

From section 6.2 it is known that large deformations are present at the interface and, therefore, the results of the eigenvalue analysis can be inaccurate. This is because these large deformations are non-linear effects which cannot be captured by the eigenvalue analysis alone. By preloading the structure before executing an eigenvalue analysis a buckling load can be obtained that includes the non-linear effects. Since the deformation pattern as can be seen in figure 5.3a is showing large deformation around the interface, this deformation shape should be included when performing an eigenvalue analysis. Therefore, before performing the eigenvalue analysis, a static general non-linear analysis step was performed. This analysis method is a static method which is able to capture non-linear effects. It uses the Newton Raphson iterative method to find a solution. It was decided to load the structure before performing the eigenvalue analysis by using a preload of -200, -300, and -400 kN. The force-displacement graph including the eigenvalue buckling points with a preload can be seen in figure 6.7. What can be seen is that the buckling load decreases with increasing preload. The values of the buckling loads using different preloads can be seen in table 6.8. By using a preload of -400 kN the difference between the buckling load predicted by the eigenvalue analysis and the dynamic analysis is less than 5%. From the table it can be concluded that the prediction given by the eigenvalue analysis is more accurate when a preload of below -300 kN is applied.

Table 6.8: Buckling loads obtained by the eigenvalue analysis after performing a preload of the sandwich cylindrical-conical shell and difference with respect to the dynamic buckling load.

Preload [kN]	Force eigenvalue1 [kN]	Difference w.r.t. dynamic analysis [%]
0 kN	712.6	38
-200 kN	666.9	34
-300 kN	558.8	21
-400 kN	463.6	5

The first mode shapes determined by the eigenvalue analysis performed after a preload can be seen in figure 6.8. The first mode shape of the model with a preload of 0 kN can be seen in figure 5.1a. What can be observed is that when adding a preload the eigenvalue analysis is giving a mode shape with a diamond deformation pattern around the interface. These mode shapes look similar to the mode shape obtained from the dynamic implicit analysis. This means that by adding a preload before performing an eigenvalue analysis can give a better prediction.

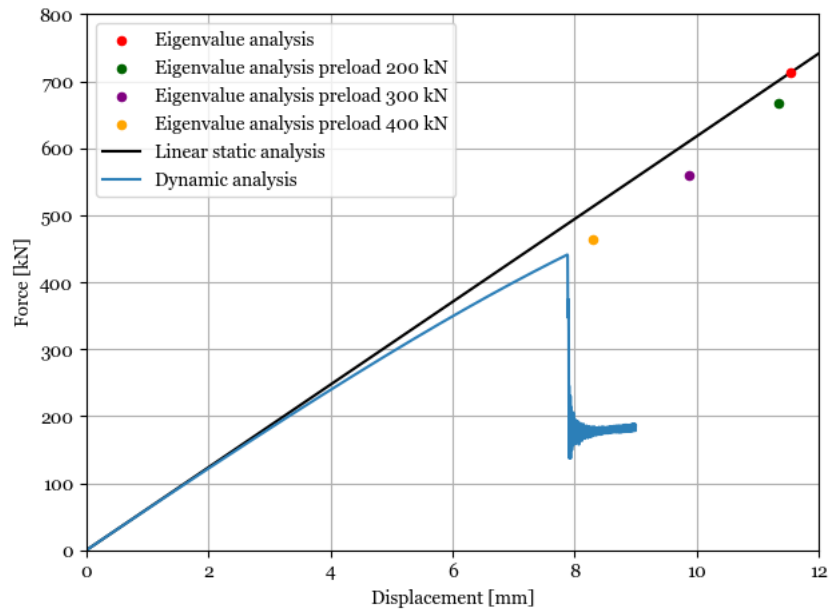


Figure 6.7: Force-displacement graph of the sandwich composite cylindrical-conical shell including the eigenvalue analysis points obtained after adding a preload.

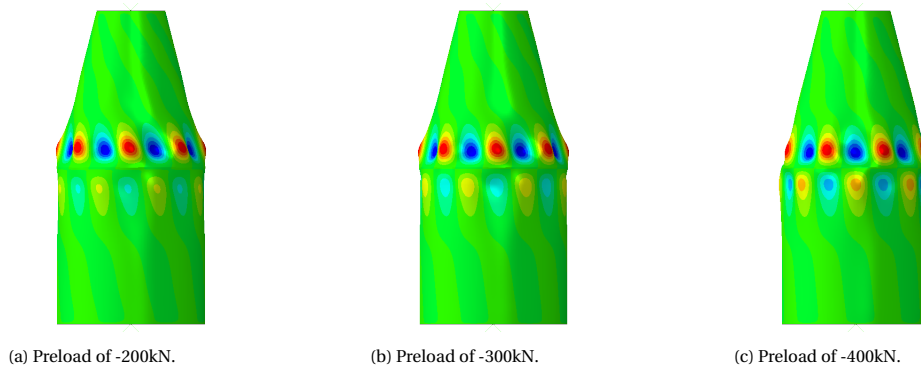


Figure 6.8: First buckling mode shape of the sandwich composite cylindrical-conical shell determined after adding a preload. For generating the figures a scaling factor of 30 was used.

What can be concluded from this section is that when adding a preload the prediction given by the eigenvalue analysis is able to give a buckling load and mode shape closer to the buckling load and deformation shape of the dynamic implicit analysis. An explanation for this is that around the intersection of the cylindrical-conical shell a large deformation is present. This is due to the interface being unconstrained. When a force is pushing down from the top at the interface the structure wants to bulge outwards, which is also known as the elephant foot effect [12]. This effect is also present around clamped boundaries as already seen in the chapter about the cylindrical shell. Due to this deformation, an axisymmetric imperfection is added to the structure around the interface. Since this imperfection is included in the dynamic implicit analysis the buckling load of the dynamic implicit analysis is much lower compared to the eigenvalue analysis. The reason that the eigenvalue analysis is not able to capture this is because the elephant foot effect is a geometrical non-linear problem which cannot be captured by linear analyses. This is the reason why adding a preload and thus, adding a deformation to the structure before executing an eigenvalue analysis gives a buckling load closer to the dynamic implicit buckling load.



## 6.5. Buckling load of cylindrical part same as conical part

When looking at the buckling loads obtained by the eigenvalue analysis of the separate cylindrical and conical shell, it can be seen that the buckling load of the conical shell is lower compared to the buckling load of the cylindrical shell. Since the value and mode shape obtained by the eigenvalue analysis of the sandwich composite cylindrical-conical shell is the same as the buckling load and mode shape of the conical shell alone, it is hypothesized that the result of the eigenvalue analysis is similar to that of the cylindrical or conical shell alone depending on which buckling load is lower. In order to verify this hypothesis, the material properties of the cylindrical shell were changed such that the buckling load of the cylindrical shell is much lower compared to the buckling load of the conical shell, which is equal to 712.6 kN. The reason for using the material properties as variables is because the result should be independent on geometry. The material properties were chosen such that the analytical buckling load of the cylindrical shell was around 500 kN. This value was chosen randomly and could have been any number well below 712.6 kN. The material properties used can be seen in table 6.9. By using the analytical expression for calculating the buckling load of the cylindrical shell using the material properties given in table 6.9 a buckling load of 545 kN is obtained.

Table 6.9: Material properties set 1 of sandwich composite cylindrical shell [50].

$E_{11}$ [MPa]	$E_{22}$ [MPa]	$\nu$ [-]	$G_{12}$ [MPa]
94800	7100	0.3	2900

The material properties of the conical part were kept the same. Within the Abaqus model this was achieved by creating two sets of elements, one for the conical shell part and one for the cylindrical shell part. Then the material properties were assigned using the two element sets resulting in two parts with different material properties. After the material properties were changed, an eigenvalue analysis and dynamic implicit analysis were performed.

The buckling load obtained by the eigenvalue analysis is equal to 559.2 kN. This value is close to the buckling load of the cylindrical shell alone as expected. The first buckling mode shape of the cylindrical-conical shell can be seen in figure 6.9. What can be seen is that only the cylindrical part of the cylindrical-conical shell is showing out of plane deformation and the conical shell part is not showing any deformation. It looks like that the conical shell is not taking part in the eigenvalue analysis. This suggests that the eigenvalue analysis is giving the buckling load and mode shape of either the cylindrical or conical shell alone depending on which buckling load is lower.

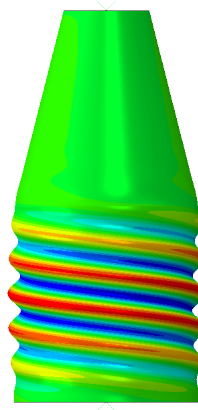


Figure 6.9: First buckling mode shape of sandwich composite cylindrical-conical shell using modified material properties. For generating this figure a scaling factor of 30 was employed.

A dynamic implicit analysis was performed to investigate if there is still a difference between the buckling load and mode shape obtained by the eigenvalue analysis and dynamic analysis. The force-displacement graphs can be seen in figure 6.10. It should be noted that in the graph the modified results represent the sandwich composite cylindrical-conical shell using material properties set 1 and the original result represents the sandwich composite cylindrical-conical shell as defined in previous analyses. The results of the original

sandwich composite cylindrical-conical shell are added as a reference. From the graph it can be seen that the buckling load obtained by the dynamic analysis is 351 kN. This value is again around 40% lower than the value given by the eigenvalue analysis. The deformation shape before buckling is presented in figure 6.11. When comparing the shape in figure 6.11 with the mode shape given in figure 6.9 it can be observed that the dynamic implicit analysis gives a shape that is more around the interface and that the eigenvalue analysis is giving a shape showing deformation only at the cylindrical shell. The eigenvalue analysis is not able to show the interaction between the two shells.

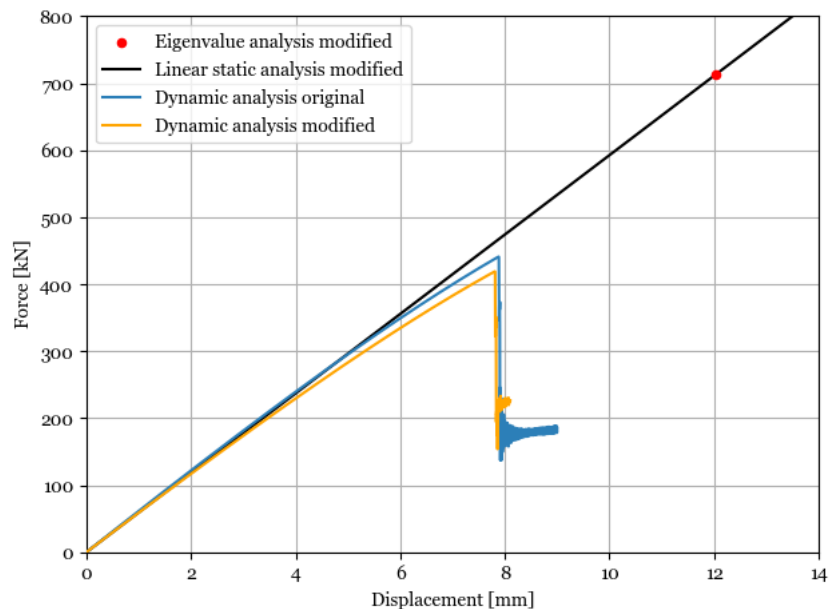


Figure 6.10: Force-displacement graphs of the sandwich composite cylindrical-conical shell using the modified material properties and using the original material properties for the cylindrical shell.

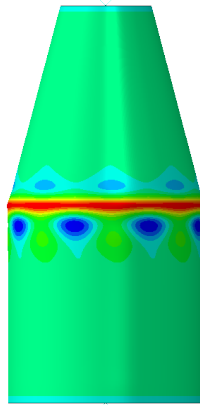


Figure 6.11: Radial deformation shape right before buckling of the sandwich composite cylindrical-conical shell using modified material properties. For generating this figure a scaling factor of 1 was employed.

By knowing this, it is investigated what happens when the buckling load of the cylindrical shell and conical shell are the same and equal to 712.6 kN. It is hypothesized that the buckling mode shape obtained by the eigenvalue analysis should be giving a mode shape that covers the whole shell and not only at the conical shell or cylindrical shell part. For this investigation again the material properties of the cylindrical shell part were changed. Since there were no actual material properties found that gave an analytical buckling load of 712.6 kN, the cylindrical shell material properties were made up such that an analytical buckling load of 712.6 kN could be achieved. The material properties used for the cylindrical shell can be seen in table 6.10.

Table 6.10: Material properties set 2 of sandwich composite cylindrical shell.

$E_{11}$ [MPa]	$E_{22}$ [MPa]	$\nu$ [-]	$G_{12}$ [MPa]
120000	9800	0.3	5950

The same method of implementing the different material properties for the cylindrical part and conical part was used as described above. First an eigenvalue analysis was performed. The buckling load obtained is equal to 712.6 kN as expected since the buckling load of the cylindrical shell and conical shell are both equal to 712.6 kN. However, the mode shape obtained can be seen in figure 6.13 and is the same as the mode shape given in figure 5.1a. This means that the eigenvalue analysis is not able to capture the interaction between the cylindrical and conical shell.

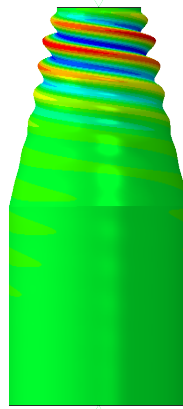


Figure 6.12: First buckling mode shape of sandwich composite cylindrical-conical shell using modified material properties. For generating this figure a scaling factor of 30 was employed.

Also a dynamic analysis was performed to see what happens if the cylindrical shell and conical shell part have the same buckling load. The force-displacement graphs can be seen in figure 6.13. It should be noted that in the graph the modified results represent the sandwich composite cylindrical-conical shell using material properties set 2 and the original result represents the sandwich composite cylindrical-conical shell as defined in previous analyses. The buckling load of the dynamic analysis is equal to 419.2 kN, which is again around 40% lower than the eigenvalue analysis result. The shape obtained by the dynamic implicit analysis is similar to the shape given in figure 6.11.

From this investigation it can be said that the eigenvalue analysis is not able to capture the behavior of the cylindrical and conical shell together, the transition is completely ignored. The buckling load and mode shape that are obtained by performing an eigenvalue analysis are similar to the buckling load and mode shapes of the separate shells. To conclude, the eigenvalue analysis is not able to capture the buckling behavior of sandwich composite cylindrical-conical shells.

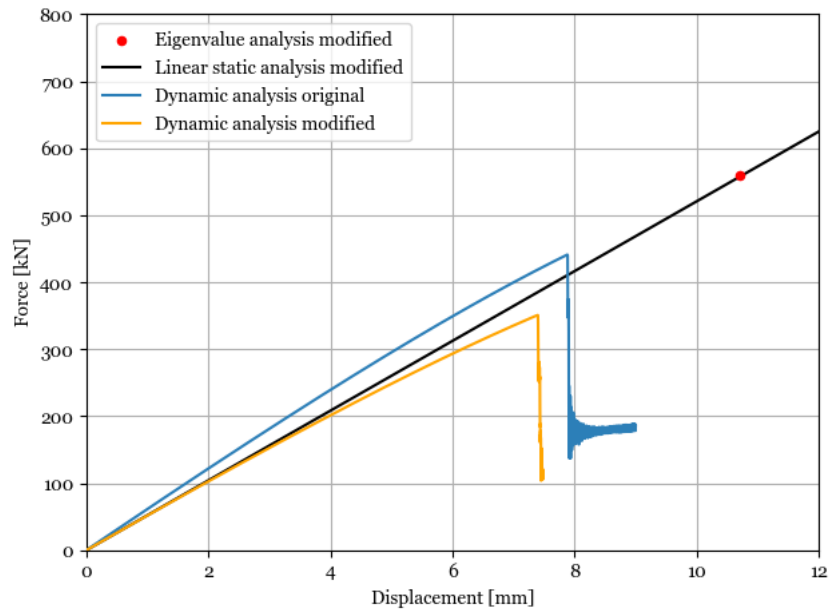


Figure 6.13: Force-displacement graphs of the sandwich composite cylindrical-conical shell using the modified material properties and using the original material properties for the cylindrical shell.

## 6.6. Aluminum cylindrical-conical shell

An aluminum cylindrical-conical shell was analysed in order to investigate if the difference between the eigenvalue analysis and dynamic implicit analysis is because of the sandwich composite material used. It might be that the difference is caused by the lay-up. Therefore, an eigenvalue and dynamic implicit analysis was performed using an aluminum cylindrical-conical shell. The dimensions of the cylindrical-conical shell were kept the same. This means that the thickness of the shell was equal to the total thickness of the sandwich composite shell which was equal to 2.95 mm. The material properties of the aluminum used can be seen in table 6.11.

Table 6.11: Material properties of aluminum 2024-T4 [49].

E [MPa]	$\nu$ [-]
73100	0.3

Firstly, an eigenvalue analysis was performed for the separate cylindrical and conical shell. This in order to be able to compare the eigenvalue analysis results of the shells alone and the combined cylindrical-conical shell. The buckling loads obtained can be seen in table 6.12.

Table 6.12: Buckling loads of the cylindrical shell and conical shell using eigenvalue analysis.

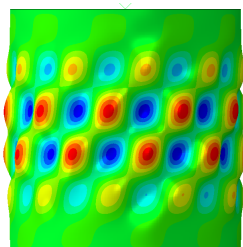
	Buckling load [kN]
Cylindrical shell	2437.7
Conical shell	2256.7

What can be seen is that the buckling load for the cylindrical shell is higher than the buckling load of the conical shell, as expected due to the semi-vertex angle. The buckling loads are verified by using equation 6.1 [42] for the cylindrical shell and equation 6.2 [41] for the conical shell. The buckling loads obtained are 2444.7 kN and 2280.9 kN, respectively.

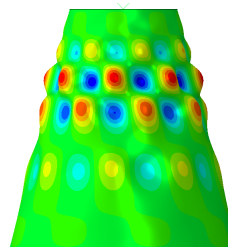
$$P_{cr} = \frac{2\pi Et^2}{\sqrt{3(1-\mu^2)}} \quad (6.1)$$

$$P_{cr} = \frac{2\pi Et^2 \cos\alpha^2}{\sqrt{3(1-\mu^2)}} \quad (6.2)$$

A difference of 0.3% is obtained for the cylindrical shell and a difference of 1.1% for the conical shell. The first mode shape of the cylindrical shell and conical shell can be seen in figure 6.14a and 6.14b, respectively. What can be seen is that for both models the mode shape shows a diamond pattern. For the conical shell the deformation is more located towards the top, which is expected because of the top of the shell being weaker as already explained.



(a) First mode shape of aluminum cylindrical shell.



(b) First mode shape of aluminum conical shell.

Figure 6.14: First mode shapes of aluminum cylindrical and conical shell. For generating this figure a scaling factor of 30 was employed.

A finite element model was also created for the cylindrical-conical shell model. This was done by using the same model as for the sandwich composite cylindrical-conical shell and by changing the sandwich lay-up to an isotropic material. For this model an eigenvalue analysis and a dynamic implicit analysis were performed. The buckling loads determined by the eigenvalue analysis and dynamic analysis can be seen in table 6.13. The force-displacement graph obtained by the dynamic implicit analysis is presented in figure 6.15. The difference between the buckling loads is 44%, which is again a large difference. It can also be seen that the buckling load obtained by the eigenvalue analysis is close to the buckling load of the conical shell alone. This means that the same behavior happens for an isotropic material.

The buckling shapes can be seen in figure 6.16. What can be seen is that for the isotropic cylindrical-conical shell the eigenvalue analysis is able to give a buckling mode shape that is located around the interface. It can be seen that the mode shape obtained is different compared to the mode shape determined by the eigenvalue analysis of the conical shell alone. The eigenvalue analysis is able to give a mode shape that looks similar to the dynamic implicit deformation shape right before buckling. The difference is that for the eigenvalue analysis the interface is not taken into account and the deformation is only located in the conical part of the shell and nothing happens in the cylindrical shell part. This is not the case for the deformation shape of the dynamic implicit analysis.

What can be concluded is that the eigenvalue analysis is not able to give accurate results for the isotropic cylindrical-conical shell model. The difference between the buckling load of the eigenvalue analysis and dynamic implicit analysis is 44%. However, the mode shape obtained is closer to the deformation shape determined by the dynamic implicit analysis, which was not seen for the sandwich composite cylindrical-conical shell model. Since the difference in buckling load is still big it can be said that the difference between both analyses is not because of the material used.

Table 6.13: Buckling loads of the eigenvalue analysis and dynamic implicit analysis.

	<b>Buckling load [kN]</b>
Eigenvalue analysis	2207.3
Dynamic implicit analysis	1226.7

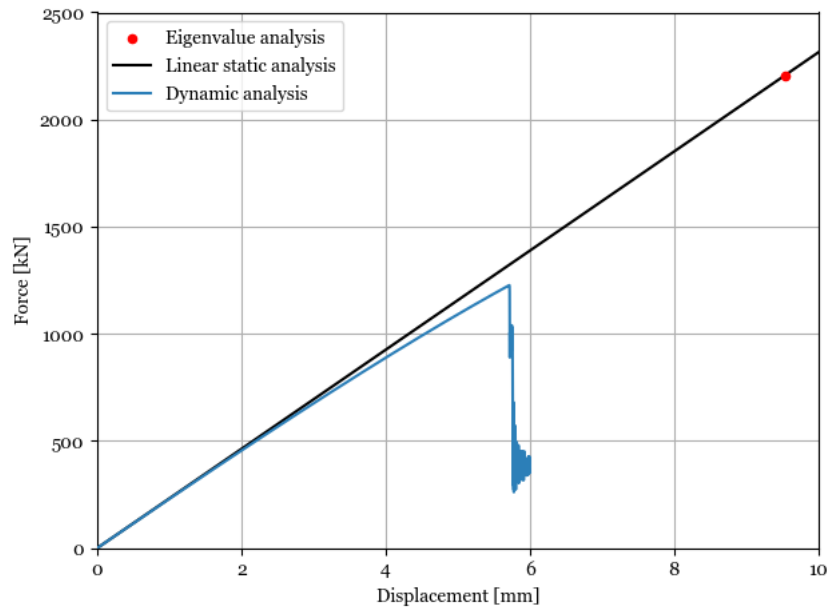
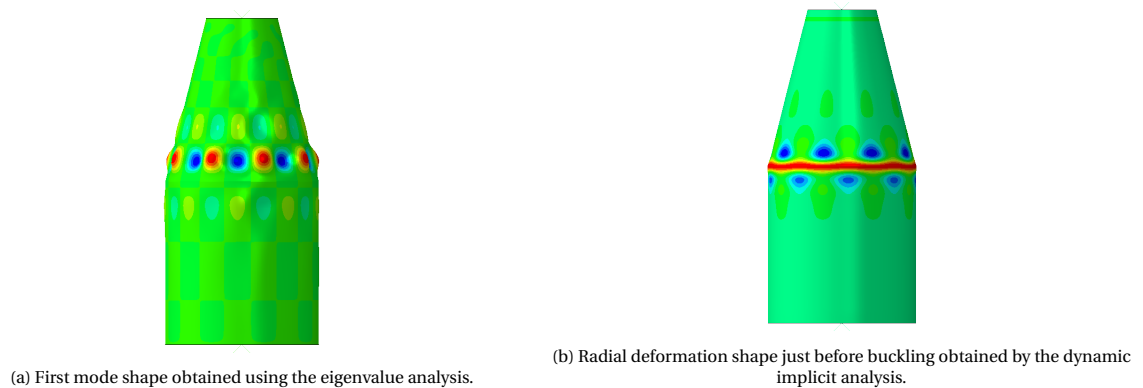


Figure 6.15: Force-displacement graph of aluminum cylindrical-conical shell.



(a) First mode shape obtained using the eigenvalue analysis.

(b) Radial deformation shape just before buckling obtained by the dynamic implicit analysis.

Figure 6.16: Deformation shapes obtained by the eigenvalue analysis and dynamic implicit analysis of the aluminum cylindrical-conical shell.

## 6.7. Composite cylindrical-conical shell

Most of the research done until now focused on the analysis of a sandwich composite material. Since the lay-up used for the sandwich composite shell has a nonconventional lay-up, this section focuses on a composite cylindrical-conical shell with a conventional lay-up. In this section it is investigated how the difference between the eigenvalue analysis and dynamic implicit analysis changes when a more conventional laminate is used. For the composite cylindrical-conical shell a quasi-isotropic lay-up was chosen. A quasi-isotropic lay-up was chosen because it has similar stiffness in all directions and has no coupling effects. Moreover, since a lot of studies have been performed on quasi-isotropic laminates the behavior of these laminates are better understood. A cylindrical-conical shell of 1600 mm with a semi-vertex angle of 15 degrees and a shell with a height of 1200 mm and a semi-vertex angle of 5 degrees were used. The 1600 mm shell was chosen because most of the analyses performed in this report had this configuration. The 1200 mm shell was used because for the sandwich composite cylindrical-conical shell with a height of 1200 mm and a semi-vertex angle of 5 degrees the difference between the eigenvalue analysis and dynamic implicit analysis was still large. Therefore, it was investigated if this difference decreases when a different material is used. The material properties used were the same as for the sandwich composite shell. Moreover, the lay-up used was as follows:  $[0, 45, 90, -45]_s$ . For these models a linear static analysis, an eigenvalue analysis, and a dynamic implicit analysis were per-

formed. It should be noted that the same modelling techniques were used as described in previous sections.

It is known that the eigenvalue analysis gives a buckling load close to either the buckling load of cylindrical or conical shell alone depending on which part has a lower buckling load. To be able to verify the results given by the eigenvalue analysis of the composite cylindrical-conical shell, first the analytical buckling loads of the cylindrical and conical shell were calculated. The analytical buckling loads were calculated using the SP-8007 guideline for composite cylindrical shells and the buckling load equation can be seen in equation 6.3 [42]. Whereas,  $N_x$  is the buckling load per meter,  $l$  is the length of the cylindrical shell, and  $m$  is the number of half waves. The  $A$  terms can be calculated by using the stiffness terms of the laminate. The buckling load of a composite conical shell was calculated using equation 6.4 [41]. Whereas,  $P_{Cone}$  is the buckling load of the conical shell,  $P_{Cylinder}$  is the buckling load of the cylindrical shell with the same material properties, height, and diameter as the conical shell, and  $\alpha$  is the semi-vertex angle.

$$N_x = \left( \frac{l}{m\pi} \right)^2 \frac{\begin{vmatrix} A_{11} & A_{12} & A_{13} \\ A_{21} & A_{22} & A_{23} \\ A_{31} & A_{32} & A_{33} \end{vmatrix}}{\begin{vmatrix} A_{11} & A_{12} \\ A_{21} & A_{22} \end{vmatrix}} \quad (6.3)$$

$$P_{Cone} = P_{Cylinder} \cdot \cos^2 \alpha \quad (6.4)$$

The buckling loads were calculated for a cylindrical shell of 800 mm, a conical shell of 800 mm with a semi-vertex angle of 15°, and a conical shell of 400 mm with a semi-vertex angle of 5°. The analytical buckling loads can be seen in table 6.14.

Table 6.14: Buckling loads of the composite cylindrical shell and conical shells calculated using the SP-8007 and SP-8019 guidelines.

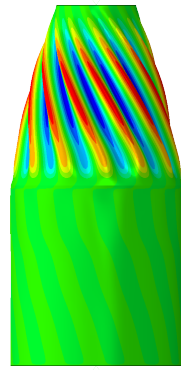
	SP-8007/SP-8019 buckling load [kN]
Cylindrical shell 800 mm	315.6
Conical shell 800 mm	294.5
Conical shell 400 mm	314.8

An eigenvalue analysis was performed using the composite cylindrical-conical shell of 1600 mm and the composite cylindrical-conical shell of 1200 mm. The buckling loads are reported in table 6.15. It can be seen that the buckling load of the 1600 mm is close to the analytical buckling load of the 800 mm conical shell. For the 1200 mm shell the buckling load is close to the analytical buckling load of both the cylindrical shell and conical shell since the buckling loads of the separate shells are similar. It should be noted that a difference between the buckling loads determined by the eigenvalue analysis and analytical method is around 15%. This difference can be explained by the fact that the analytical buckling loads represent the buckling of a cylindrical or conical shell alone and not a cylindrical-conical shell. However, the buckling loads obtained by the eigenvalue analyses are of the same order of magnitude as the values determined by the analytical method.

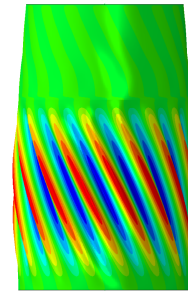
Table 6.15: Buckling loads of a quasi-isotropic cylindrical-conical shell with a length of 1600 mm and 1400 mm.

	Force eigenvalue 1 [kN]	Force eigenvalue 2 [kN]	Force eigenvalue 3 [kN]
1600 mm shell	249.8	249.8	250.2
1200 mm shell	271.1	271.1	272.1

The first mode shapes are shown in figure 6.17. What can be seen is that for the 1600 mm cylindrical-conical shell only the conical part is showing deformation and for the 1200 mm cylindrical-conical shell only the cylindrical shell is showing deformation. This can also be explained by the reason that the buckling load of the conical shell alone has a lower buckling load than the cylindrical shell alone. For the 1200 mm cylindrical-conical shell the analytical buckling loads are close to each other which means that either the cylindrical or conical part buckles. This was also already seen in an earlier section where the buckling load of the cylindrical shell is the same as the buckling load of the conical shell.



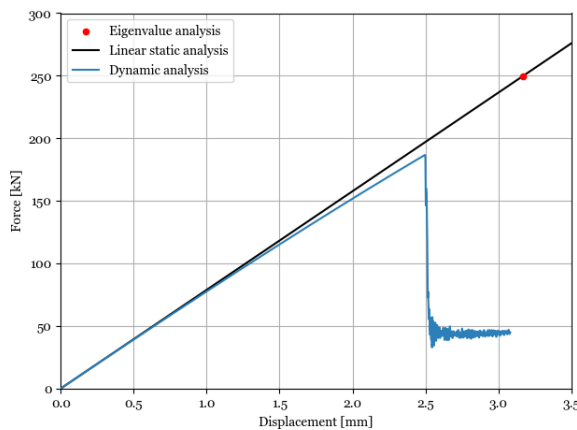
(a) 1600 mm cylindrical-conical shell.



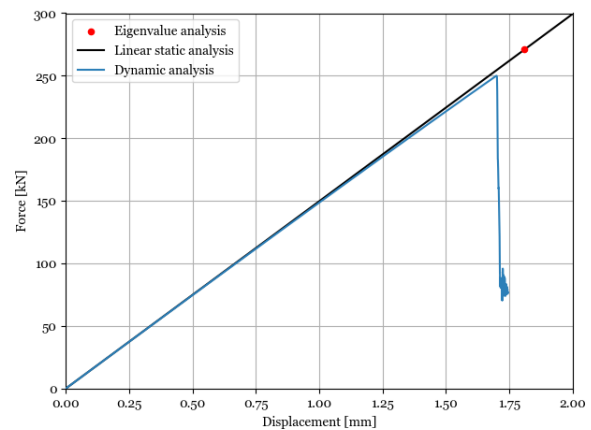
(b) 1200 mm cylindrical-conical shell.

Figure 6.17: First mode shapes of the 1600 mm and 1200 mm composite cylindrical-conical shell. For generating this figure a scaling factor of 30 was employed.

Moreover, dynamic implicit analyses were performed using both models. The force-displacement graphs can be seen in figure 6.18. The buckling loads obtained by the dynamic implicit analyses can be seen in table 6.16. It can be seen that for the 1600 mm composite cylindrical-conical shell the difference is bigger than for the 1200 mm composite cylindrical-conical shell. It can also be observed that the difference between the eigenvalue analysis and dynamic implicit analysis with respect to the difference observed for the sandwich composite cylindrical-conical shell is less. This means that the sandwich composite cylindrical shell is more sensitive to the non-linear behavior happening at the transition region. In figure 6.19 the radial deformation shapes right before buckling can be seen. When comparing these deformation shapes with the mode shapes obtained by the eigenvalue analysis it can again be seen that the eigenvalue analysis is not able to capture the interface.



(a) 1600 mm cylindrical-conical shell.



(b) 1200 mm cylindrical-conical shell.

Figure 6.18: Force-displacement graphs of the composite cylindrical-conical shells.

Table 6.16: Buckling loads of the composite cylindrical-conical shells with a height of 1600 mm and 1200 mm obtained by the dynamic implicit analysis and difference w.r.t. the eigenvalue analysis buckling load.

	<b>Buckling load [kN]</b>	<b>Difference w.r.t. eigenvalue analysis [%]</b>
1600 mm shell	186.6	25
1200 mm shell	249.9	8



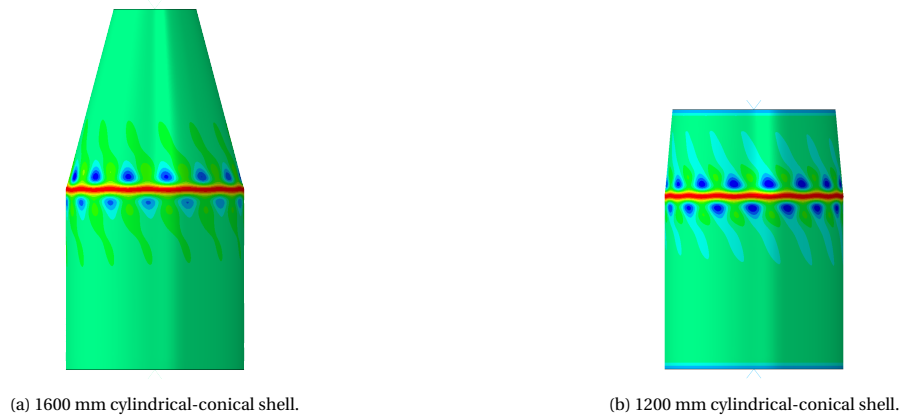


Figure 6.19: Radial deformation shapes right before buckling of the 1600 mm and 1200 mm cylindrical-conical shell. For generating this figure a scaling factor of 1 was employed.

### 6.8. Effect of radius of curvature at the interface

Until now the model of the sandwich composite cylindrical-conical shell was made by placing the models of the sandwich composite cylindrical shell and sandwich composite conical shell on top of each other and by merging the nodes along the boundary. This results in that at the interface there is a sharp transition between the cylindrical shell part and the conical shell part. However, when a cylindrical-conical shell is manufactured the interface will not have such a sharp transition. The transition will be more smooth. Therefore, this section investigates the effect of the buckling behavior when a smooth transition is incorporated in the model. The smooth transition between the two parts was created by adding a radius of curvature at the interface. The radius of curvature was equal to 380 mm and is used as preliminary estimate.

For investigating the effect of the radius of curvature at the transition two linear analyses were performed and one dynamic analysis. First, a linear static analysis was performed in order to see the difference of the stiffness between the model with radius of curvature and the model without radius of curvature. The load applied was -900 kN. The axial displacement obtained is 13.9 mm which is a bit less compared to the model without the radius of curvature. This means that the model is a bit more stiff. Moreover, an eigenvalue analysis was performed. This was done in order to investigate if the mode shape and buckling load change when the transition is more smooth. The buckling load obtained is 712.6 kN and the buckling mode shape of the first buckling mode can be seen in figure 6.20. When comparing the buckling load and mode shape with the model without the radius of curvature it can be seen that the results are the same.



Figure 6.20: First buckling mode shape of the model including a radius of curvature of 380mm. Scaling factor is equal to 30.

Next to two linear analyses also a dynamic analysis was performed. The force-displacement graphs of the model with radius of curvature and without radius of curvature can be seen in figure 6.21. The buckling loads are reported in table 6.17. What can be seen is that the buckling load is increased by 20%. This means that by adding a radius of curvature at the intersection the difference between the eigenvalue analysis and the dynamic analysis is decreased. However, still a difference of 26% can be observed. Furthermore, the stiffness of the model with radius of curvature is increased compared to the model without radius of curvature.

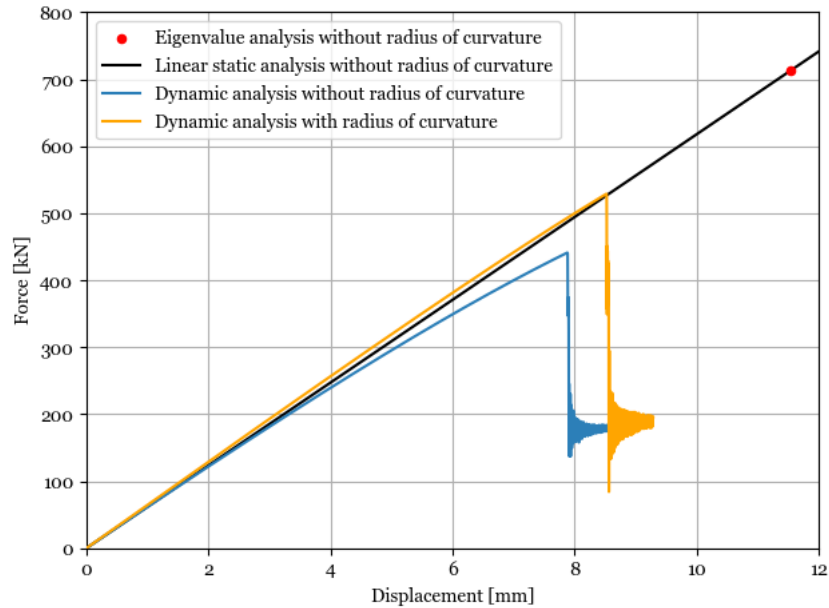


Figure 6.21: Force-displacement graphs of the sandwich composite cylindrical-conical shell model with and without radius of curvature.

Table 6.17: Buckling loads obtained by the dynamic analyses of the models with and without radius of curvature.

Model	Without radius of curvature	With radius of curvature
Buckling load [kN]	441.5	529.0

For the 1200 mm sandwich composite cylindrical-conical shell with a semi-vertex angle of  $5^\circ$  it could be seen that the difference between the eigenvalue analysis and dynamic implicit analysis is large (as discussed in section 5.6). However, it is expected that when a small semi-vertex angle is used the difference between both analyses should be small. This is because when a semi-vertex angle of  $5^\circ$  is used the angle is small enough that the cylindrical-conical shell looks more like a cylindrical shell. For cylindrical shells the difference between the eigenvalue analysis and dynamic implicit analysis is negligible; however, this small difference was not observed for the cylindrical-conical shell with a semi-vertex angle of  $5^\circ$ . Therefore, the effect of the radius of curvature was also investigated for this sandwich composite cylindrical-conical shell to see if the difference could be decreased. For this investigation two radii of curvature were used: 380 mm as used for the previous analysis and 1500 mm to see the effect of using a larger transition region. In order to see the difference between both models the meshes used can be seen in figure 6.22.



(a) Radius of curvature of 380 mm.



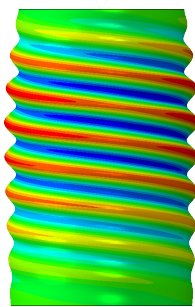
(b) Radius of curvature of 1500 mm.

Figure 6.22: Mesh of the 1200 mm shell including different radii of curvature.

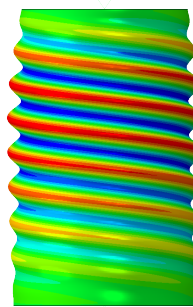
The buckling loads obtained by the eigenvalue analysis can be seen in table 6.18. All models have the same force eigenvalue. The eigenmode shapes of the models have a similar shape and can be seen in figure 6.23. What can be concluded is that by adding a radius of curvature to the structure the results of the eigenvalue analysis do not change.

Table 6.18: Force eigenvalues of the 1200 mm cylindrical conical shell with a semi-vertex angle of  $5^\circ$  using different radii of curvature at the transition.

Radius of curvature [mm]	Force eigenvalue 1 [kN]	Force eigenvalue 2 [kN]	Force eigenvalue 3 [kN]
-	800.0	800.0	800.9
380	799.9	799.9	800.8
1500	799.4	799.5	800.1



(a) Radius of curvature of 380 mm.



(b) Radius of curvature of 1500 mm.

Figure 6.23: First mode shape of the cylindrical-conical shell using different radii of curvature. A scaling factor of 30 was used.

Next to an eigenvalue analysis also a dynamic implicit analysis was performed to see the difference in results. The force-displacement graphs of the models with and without radius of curvature can be seen in figure 6.24. It can be observed that a radius of curvature of 380 mm only increases the buckling load by 2%. This can be explained by the fact that for the 1200 mm shell with a semi-vertex angle of  $5^\circ$  a radius of curvature of 380 mm results in a small transition. Therefore, also a larger transition area was investigated and it can be seen that it improves the results. The difference in buckling load of the eigenvalue analysis and dynamic implicit analysis for the 1500 mm radius of curvature is 10.6%. This means that by adding a large enough radius of curvature, the behavior at the transition area can be mitigated and a buckling load close to the eigenvalue analysis buckling load can be obtained.

The radial deformation shapes right before buckling of the models including a radius of curvature can be seen in figure 6.25. It can be seen that for the model with a radius of curvature of 380 mm the deformation is mostly located around the intersection. For the model with a radius of curvature of 1500 mm the axisymmetric behavior that was also seen for the eigenvalue analysis mode shape can be observed as well. However, still a lot of deformation is present at the transition. It can also be seen that the deformation is less concentrated at the intersection than for the model with a radius of curvature of 380 mm. This due to the longer transition area.

It can be concluded that the eigenvalue analysis is able to predict the behavior of the cylindrical-conical shell if a large radius of curvature is present, however, the effect at the transition area will not be mitigated by adding a large radius of curvature. This is due to the radial component which will always be present if there is a difference in slope in the geometry.

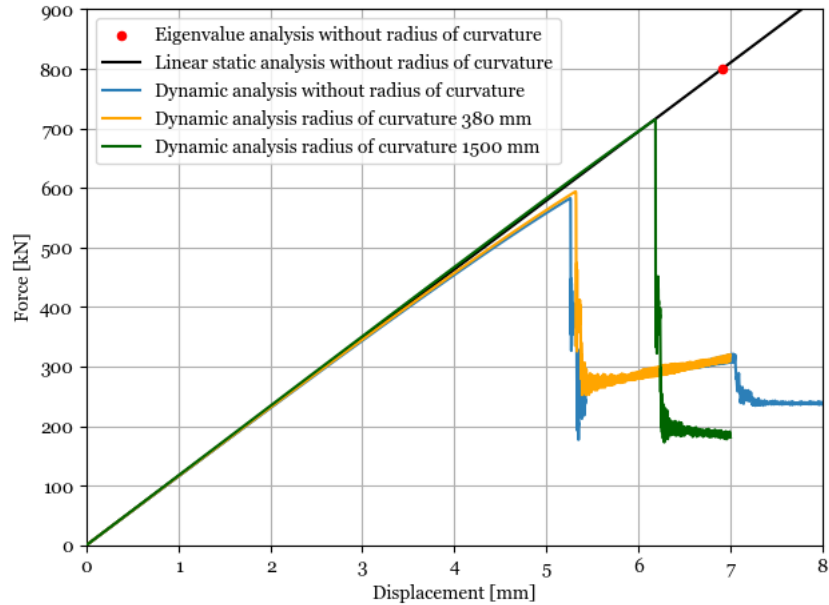
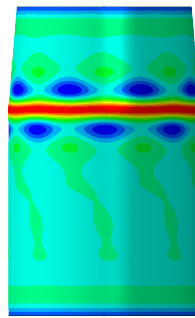
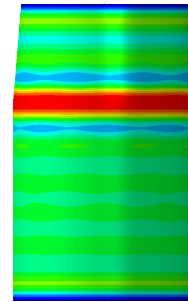


Figure 6.24: Force-displacement graphs of the 1200 mm sandwich composite cylindrical-conical shell model with and without radius of curvature with different values.



(a) Radius of curvature of 380 mm.



(b) Radius of curvature of 1500 mm.

Figure 6.25: Radial deformation shapes right before buckling for the 1200 mm shell including different radii of curvature. For generating this figure a scaling factor of 1 was employed.

## 6.9. Reinforcing the sandwich composite cylindrical-conical shell by using extra plies at the interface

In previous analyses it became clear that the interface is the weakest link of the structure. Therefore, in this section a reinforcement is added at the interface to stiffen the structure. It is investigated to what extent the non-linear behavior at the interface can be decreased by adding a reinforcement at the interface. In this section, first the design process of the reinforcement is explained. After that, the modelling technique used is elaborated on and the results are given.

It was chosen to reinforce the structure using extra plies around the transition area. The reinforcement consists of  $0^\circ$  plies since these lie in the same direction as the axial load. It was chosen to add 4-  $0^\circ$  plies to make sure the reinforcement is sufficient and that not too many plies are added. This means that around the transition area the cylindrical-conical shell is 0.7 mm thicker. It should be noted that the thickness is increased at both sides of the shell. For the design of the lay-up the design rules given in the book written by Kassapoglou [29] were used. In the book it is stated that the plies that lay in the same direction should not be next to each other. Moreover, the laminate should be symmetric in order to avoid coupling effects. By using

these rules the following lay-up was determined for the face sheets:  $[0, 56, 0, -56, 0]$ . The length in which the transition area had to be reinforced was determined by looking at the out of plane displacement results of the sandwich composite cylindrical-conical shell. The length that was chosen was equal to the length of the large out of plane displacements shown in figure 5.3a. This length was equal to 200 mm and was applied at a height of 700 mm. This length was chosen as a preliminary estimate.

The way in which the reinforcement was added to the model was done by increasing the thickness of the elements. This modelling technique was chosen because no additional elements were needed. It should be noted that for adding the reinforcement a Python code was created. First it had to be determined which elements needed a different thickness. This was done by using the reinforcement length of 200 mm. It should be noted that the reinforcement was located on the cylindrical part and conical part meaning that the elements that represent the nodes with a height higher than 700 mm and lower than 900 mm needed a thickness increase. These elements were put in a set to be able to easily change the lay-up of the elements located at the reinforcement area.

After the reinforcement was added to the model, the linear analyses were performed. A linear static analysis and eigenvalue analysis were performed. For the linear static analysis a load of -900 kN was applied and a displacement of 12.9 mm was obtained. This means that the model is more stiff compared to the cylindrical-conical shell model. This can be explained by the added  $0^\circ$  plies which should increase the stiffness of the model. The eigenvalue extracted from the eigenvalue analysis is equal to 712.6 kN. This is expected since the reinforcement is placed at the interface and the eigenmode shape obtained for the sandwich composite cylindrical-conical shell without reinforcement shows deformation at the top of the conical part, where no reinforcement is located. The mode shape for the cylindrical-conical with reinforcement can be seen in figure 6.26 and has a similar shape as the mode shape of the sandwich composite cylindrical-conical shell without reinforcement.



Figure 6.26: First mode shape of the reinforced cylindrical-conical shell. For generating this figure a scaling factor of 30 was employed.

A dynamic implicit analysis was also performed in order to see if the difference between the eigenvalue analysis and dynamic implicit analysis decreases when a reinforcement is added to the structure. The force-displacement graph can be seen in figure 6.27. The buckling loads of the model without reinforcement and with reinforcement can be seen in table 6.19. By adding a reinforcement the buckling load is increased by 42%. This results in a difference between the eigenvalue analysis and dynamic implicit analysis of 12.1%. This means that by adding a reinforcement to the structure a higher buckling load can be obtained and a smaller difference between the eigenvalue analysis and dynamic implicit analysis can be achieved. The reason that this happens is that when adding a reinforcement to the structure the amount of radial displacement at the interface decreases, which reduces the non-linear behavior of the structure.

Table 6.19: Buckling loads obtained by the dynamic analyses of the models with and without a reinforcement.

<b>Model</b>	<b>Without reinforcement</b>	<b>With reinforcement</b>
Buckling load [kN]	441.5	626.1

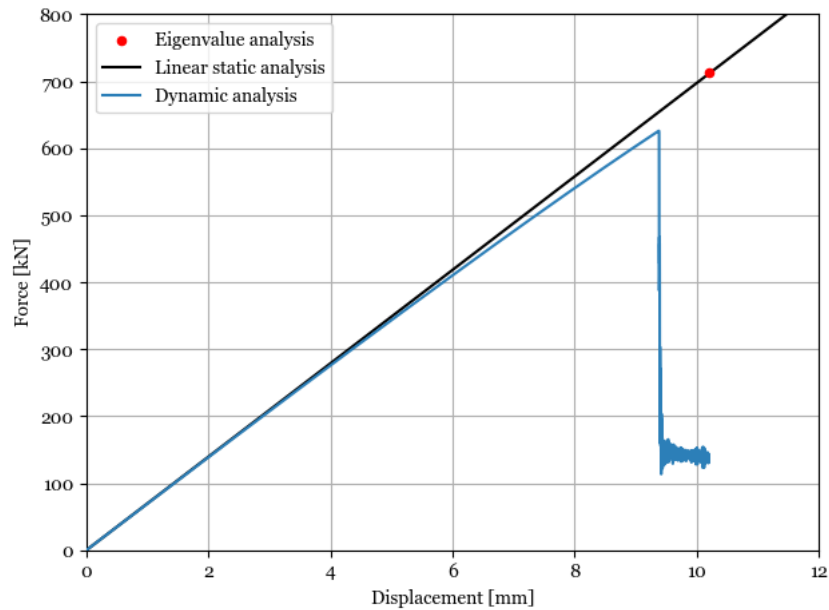


Figure 6.27: Force-displacement graph of the reinforced cylindrical-conical shell. The linear static and eigenvalue buckling point are included in the model.

The radial deformation shape right before buckling can be seen in figure 6.28. What can be seen is that the deformation is again mostly located around the transition between the cylindrical part and conical part. The deformation shape looks similar to the one obtained for the cylindrical-conical shell without radius of curvature. This means that the eigenvalue analysis is able to predict the buckling load of this shell but not able to give the right mode shape.

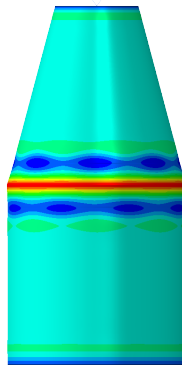


Figure 6.28: Radial deformation right before buckling of cylindrical-conical shell with a reinforcement of 200 mm. A scaling factor of 1 was used.

There is still a difference observed between the eigenvalue analysis and the dynamic implicit analysis when a reinforcement is included in the model. Therefore, the reinforcement length was increased to see if the difference can be mitigated. A reinforcement length of 300 mm was chosen, which means that an extra 50 mm on the cylindrical shell part and conical shell part was added. The same lay-up was used as described in the beginning of this section. First linear analyses were performed. For a linear static analysis a displacement of 12.5 mm was observed when a load of -900 kN was applied. This means that the model is more stiff than the model with a reinforcement length of 200 mm, which is expected since more material is added. The force eigenvalue obtained by the eigenvalue analysis is the same as for the model with a reinforcement length of 200 mm and the same mode shape is obtained, see figure 6.26.

After the linear analyses, also a dynamic implicit analysis was performed. The force-displacement graph can be seen in figure 6.29. It can be seen that the buckling loads of the eigenvalue analysis and dynamic im-

PLICIT analysis are close to each other. The buckling load obtained has a value of 683 kN, which is an increase of 9% with respect to the model with a reinforcement of 200 mm. The difference between the force eigenvalue and the buckling load of the dynamic implicit analysis is 4.1 %, which means that by adding a reinforcement of 300 mm the difference between the eigenvalue analysis and dynamic analysis is small. This also means that the behavior at the transition is mitigated.

The radial deformation shape right before buckling can be seen in figure 6.30. What can be seen is that the radial deformation is similar to that of the eigenvalue analysis. It can be seen that only in the conical part there is radial deformation. This means that by adding a reinforcement to the structure the response is able to separate the behavior of the cylindrical part and the conical part. It should be noted that the behavior around the intersection is still present however it is not fully dominating the buckling behavior of the cylindrical-conical shell anymore. The reason why the deformation around the transition is still present is due to the non-linearity of the problem which is always present even if a reinforcement is added. What can be concluded is that when the radial deformation at the transition area is reduced, the eigenvalue analysis is able to predict the buckling behavior of a cylindrical-conical shell.

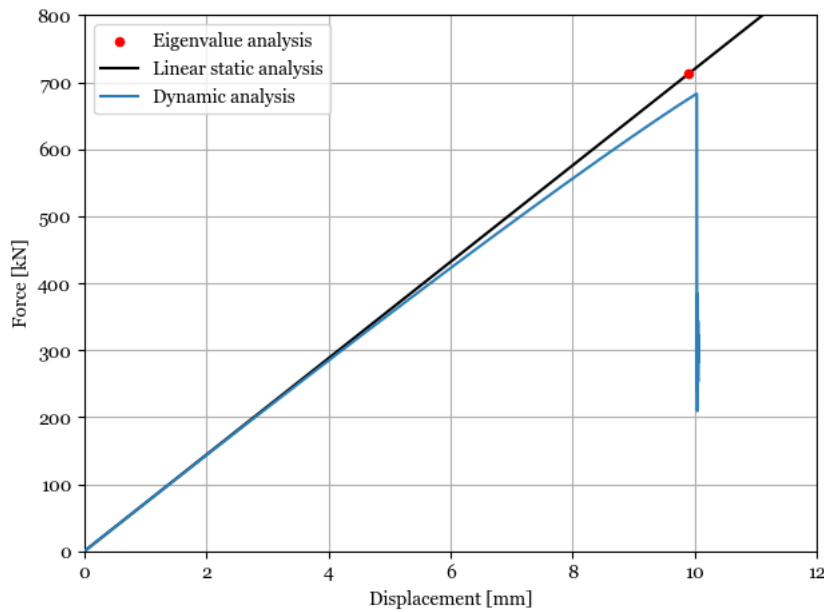


Figure 6.29: Force-displacement graph of the cylindrical-conical shell including a reinforcement of 300 mm.

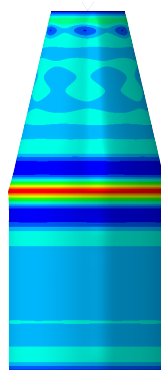


Figure 6.30: Radial deformation right before buckling of cylindrical-conical shell with a reinforcement of 300 mm. A scaling factor of 1 was used.





# 7

## Sensitivity to geometrical imperfections

When a cylindrical or conical shell is manufactured, the structure will never be perfectly circular. This is due to manufacturing processes and the limitations of the accuracy of the machines used during manufacturing. This means that imperfections are introduced into the shell and will have an effect on the buckling behavior. The reason that the imperfection sensitivity has to be investigated is due to the fact that a shell structure has a large radius/thickness ratio. From the literature study it is known that the buckling load can be reduced to almost half of the buckling load of a pristine structure if imperfections are present. Since this is such a large reduction it is important that imperfections are included in the analyses in order to give a better prediction of the buckling behavior of shells.

Imperfection analyses are performed on the sandwich composite cylindrical, conical, and cylindrical-conical shell models. It should be noted that the cylindrical-conical shell analysed in this chapter is the one as presented in chapter 5. The reason for investigating these shells is in order to see the difference in imperfection sensitivity and to be able to compare the different structures. There are five models analysed: a cylindrical shell of 800 mm, a conical shell of 800 mm and 400 mm, and a cylindrical-conical shell of 1600 mm and 1200 mm. Before looking at the imperfection sensitivities of these shells, a computational time study was performed. The reason for this is that the computational time of a dynamic implicit analysis of the cylindrical-conical shell model was about two days when using the dynamic implicit parameters determined in section 4.2.1. It should be noted that at the university a calculation cluster is available with 20 CPUs. Since this is a long time and a lot of analyses had to be performed in this chapter a computational time study was done first in order to decrease the computational time of further analysis. After that, geometrical imperfections are introduced into the models and a comparison is made between the imperfection sensitivity of the different shells. It should be noted that this chapter focuses on the geometrical imperfections since this was proven to give a large reduction in buckling load as stated in the literature study. The reason that no other imperfections were implemented in the analyses is because this section is meant to compare the imperfection sensitivities of the different shells and is not meant to compare the effect of different imperfections.

### 7.1. Computational time study

The computational time of a dynamic implicit analysis of the sandwich composite cylindrical-conical shell is about two days when using the TU Delft facilities. Since this is a lot of time and a lot of analyses had to be performed in this chapter, a decrease of computational time was needed. For analysing the imperfection sensitivity of a shell the buckling load is of interest. This is because it is important to know to which extent the buckling load is reduced when introducing imperfections into the structure. Since it is of interest to qualitatively compare the buckling response, the parameters of the dynamic implicit analysis were changed to more efficiently run the analyses. A computational time study was performed and the parameters of the model were changed in order to see the effect on the buckling load. The parameters that were changed were the mesh size, loading rate, and increment size. There were five different cases created and are shown in table 7.1. Case 1 is the case that was used for previous analyses and the results of this case are used as the reference case. It can be seen that for each of the different cases only 1 parameter was changed except for case 5. The reason for changing one parameter at the time was in order to investigate the effect of a parameter alone on the buckling behavior of the cylindrical-conical shell.

Table 7.1: The dynamic implicit parameters used for the 5 cases analysed for the computational time study of the sandwich composite cylindrical-conical shell.

	Case1	Case2	Case3	Case4	Case5
Mesh size [mm]	5	10	5	5	10
Max number of increments	10000	10000	10000	10000	10000
Increment size initial	0.001	0.001	0.01	0.001	0.001
Increment size maximum	0.001	0.001	0.01	0.001	0.001
Increment size minimum	1.00E-05	1.00E-05	1.00E-05	1.00E-05	1.00E-05
Time period [s]	4.5	4.5	4.5	1.8	1.8
Loading applied [mm]	9	9	9	9	9
Loading rate [mm/s]	2	2	2	5	5

For each of these cases a dynamic implicit analysis was performed and the load-displacement graphs, buckling loads, and computational times are compared. The load-displacement graphs of each case are shown in figure 7.1. What can be seen is that cases 1,2,4, and 5 show a force-displacement graph that are very similar to each other. Only case 3 shows a buckling load which is higher compared to the other cases. Moreover, the post buckling paths of all cases are similar. When looking at table 7.2 it can be seen that the buckling loads of cases 2,4, and 5 give a buckling load with a difference of less than 0.5% percent compared to the reference case. Since the difference in buckling load of case 3 is 3.2% and the computational time is not decreased that much compared to the other cases, this case will not be used for further analysis. The buckling loads of cases 2,4, and 5 are close to the buckling load of case 1 and, therefore, each of these cases can be used for further analyses. Since case 5 shows the biggest decrease in computational time (89.7%) this case is used for further analyses in this chapter.

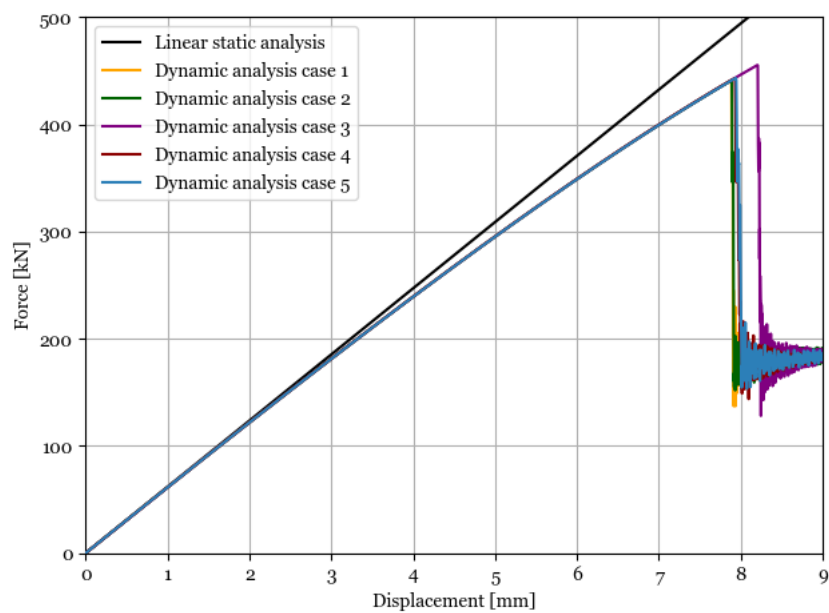


Figure 7.1: Force-displacement graphs of the sandwich composite cylindrical-conical shell using 5 cases with different dynamic implicit parameters.

Table 7.2: Buckling loads, CPU times, and difference with respect to the reference case of the sandwich composite cylindrical conical shells using different dynamic implicit parameters.

	Buckling load [kN]	CPU time [s]	Difference w.r.t. buckling load case1 [%]	Difference CPU time w.r.t case1 [%]
Case1	441.5	925700		
Case2	441.1	227987	-0.1	-75.4
Case3	455.5	370917	3.2	-59.9
Case4	443.0	441380	0.3	-52.3
Case5	443.3	95458	0.4	-89.7

## 7.2. Axisymmetric imperfection

The first imperfection analysed is an axisymmetric imperfection, which is a geometrical imperfection. This type of imperfection is based on an analytical expression. The reason for using this type of imperfection is because it is independent on the results of any analysis.

The equation for implementing an axisymmetric imperfection into a model is given in equation 7.1. Where  $\xi$  is the imperfection amplitude,  $m$  is the number of half waves,  $L$  is the length of the shell, and  $x$  is the axial position. This imperfection was implemented in the model by giving the nodes a perturbation in the radius for each height step.

$$\Delta R = \xi * \cos\left(\frac{m * \pi * x}{L}\right) \quad (7.1)$$

Amplitudes of 10%, 20%, 50%, and 100% were used to investigate the imperfection sensitivity. The amplitude is defined as a percentage of the thickness, which means that an amplitude of 10% results in an imperfection of 0.295 mm. The number of half-waves of the axisymmetric imperfection were determined by using the analytical buckling load calculation method proposed by Bert and Reese. It should be noted that for the conical shell no analytical expression for the buckling mode was found. Therefore, the number of half waves calculated for the cylindrical shell were also used for the conical shell. The number of half waves used for the cylindrical-conical shell was determined by adding the number of half waves of the cylindrical and conical shell. In figure 7.2 a visual representation can be seen of a cylindrical shell and conical shell with an axisymmetric imperfection. Note that this model uses a very high amplitude (300%) to better visualize the imperfection added.

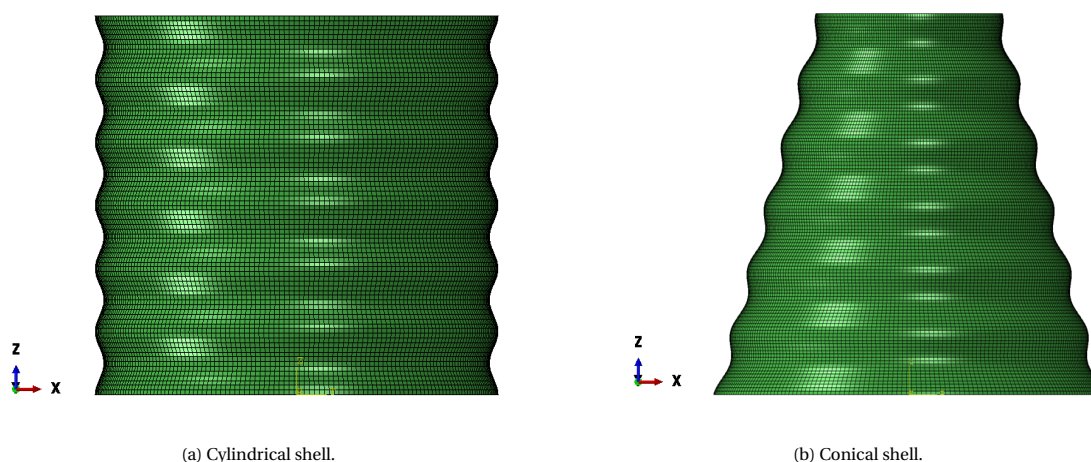


Figure 7.2: Shells including an axisymmetric imperfection with an amplitude of 300% and 12 half waves.

### 7.2.1. Cylindrical shell

The axisymmetric imperfection implemented in the model had 12 half waves. The buckling loads obtained for each imperfection amplitude can be seen in table 7.3. In the table also the KDF values can be seen, which is a measure that is commonly used when imperfections are added to shell structures. This factor shows the amount in which the buckling load is decreased when adding an imperfection with respect to the buckling

load determined by the eigenvalue analysis of the model without imperfection. The KDF value is determined by dividing the buckling load with imperfection by the buckling load without imperfection. It should be noted that the KDF accounts for both non-linearity and imperfections. What can be seen in the table is that the buckling load decreases significantly with increasing amplitude. At an amplitude of 10% the KDF is 0.69, which is equal to a decrease of the buckling load with respect to the buckling load of the model without imperfection of 30%. These results show the importance of including imperfections into the model. An amplitude of 10% is equal to an imperfection of 0.295 mm which is an imperfection that is not considerably large and possible to be introduced during the manufacturing process. If this happens the buckling load of the structure would be significantly lower than predicted.

Moreover, a comparison is made between the KDF value predicted by the SP-8007 guideline and the KDF values obtained by adding an axisymmetric imperfection. In the literature review it is stated that the SP-8007 guideline is outdated and result in parts that are over-designed. The KDF value determined using the SP-8007 guideline is equal to 0.59. In table 7.3 it can be seen that at an imperfection amplitude of 20% this value is reached. At an amplitude of 20% the imperfection is equal to 0.59 mm which is quite large and will not happen during the manufacturing process due to tolerances and regulations. This means that the KDF value determined by the SP-8007 guideline is overly conservative.

The force-displacement graphs of the cylindrical shell including the axisymmetric imperfections can be seen in figure 7.3. It can be seen that adding an axisymmetric imperfection has a significant effect on both the stiffness and buckling load of the cylindrical shell. It can also be seen that the drop after buckling decreases with increasing imperfection amplitude. It can even be observed that with an amplitude of 100% no sudden drop in load occurs. This is due to the fact that with an amplitude of 100% the cylindrical shell acts more like a spring resulting in no buckling of the structure. The structure will just deform in axial direction but will not show sudden changes in out of plane displacement. Furthermore, the post buckling paths of the models with an amplitude of 10% and 20% show similar paths. For all the other models a different post buckling path is followed.

Table 7.3: Buckling loads of the sandwich composite cylindrical shell including axisymmetric imperfection.

Imperfection	0%	10%	20%	50%	100%
Buckling load [kN]	782.4	556.3	458.7	316.9	/
KDF [-]		0.69	0.57	0.39	/

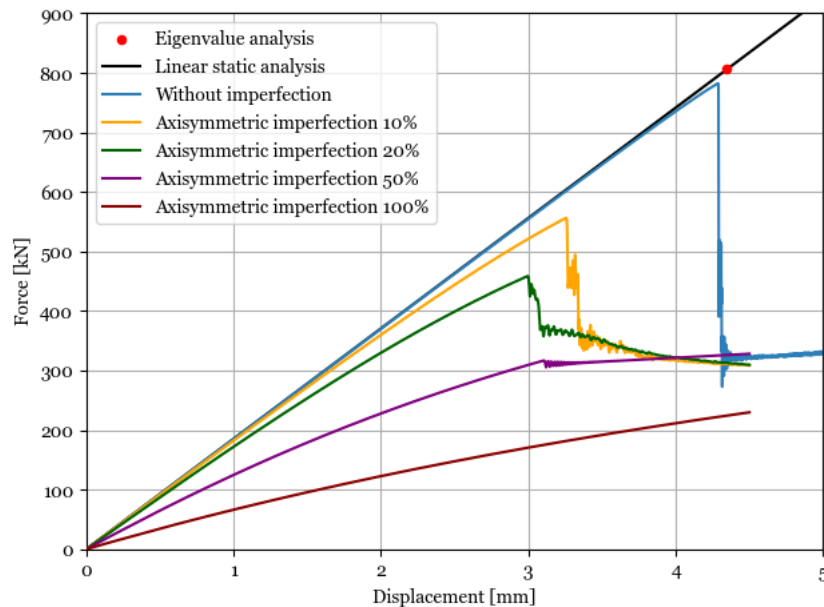


Figure 7.3: Force-displacement graphs of the sandwich composite cylindrical shell with axisymmetric imperfection.

### 7.2.2. Conical shell

For the conical shell two models were analysed including an axisymmetric imperfection, one with a height of 800 mm and one with a height of 400 mm. For the 800 mm and 400 mm height models 12 and 6 halve waves were added to the model, respectively.

The buckling loads of the conical shell with a height of 800 mm including an axisymmetric imperfection using different amplitudes can be seen in table 7.4. It can be seen that the buckling load decreases significantly with increasing amplitude. At an imperfection amplitude of 10% the KDF is equal to 0.71. What also can be observed is that the values of the KDFs are similar to that of the cylindrical shell model with an axisymmetric imperfection. This was expected because in literature it was said that conical shells have a similar sensitivity to imperfections as cylindrical shells when small semi-vertex angles are employed [45]. Moreover, also for the conical shell a guideline was established for determining the buckling load and KDFs named the SP-8019. However, in this guideline there is no particular section assigned to composite cones. In the guideline it is stated that the KDF is not dependent on geometry and, therefore, an universal KDF was assumed for all types of conical shells. The value of the KDF specified by the SP-8019 guideline is equal to 0.33. When looking at table 7.4 it can be seen that only when adding an axisymmetric imperfection with an amplitude of 100% the KDF is lower than 0.33, which is not a realistic imperfection. The KDF for an imperfection amplitude of 10% is more than 2 times higher than the KDF predicted by the SP-8019 guideline. This means that the SP-8019 is very conservative when it comes to the design of sandwich composite conical shells.

The force-displacement graphs of the models including axisymmetric imperfection can be seen in figure 7.5. The same trend can be observed as for the cylindrical shell, when the amplitude increases the drop after buckling decreases. Moreover, it can be seen that the models without imperfection, axisymmetric imperfection of 10%, and 20% converge in the post buckling region. It can also be seen that with an axisymmetric imperfection of 50% an extra load drop is present at a higher displacement, which is not seen for the other models.

Table 7.4: Buckling loads of the sandwich composite conical shell with a height of 800 mm including axisymmetric imperfection.

Imperfection	0%	10%	20%	50%	100%
Buckling load [kN]	684.8	504.1	407.3	267.2	179.3
KDF [-]		0.71	0.57	0.38	0.25

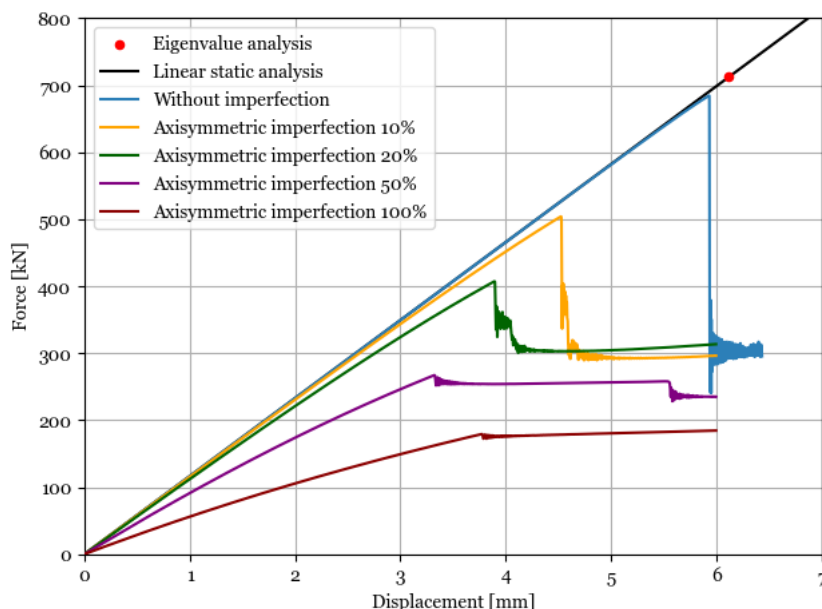


Figure 7.4: Force-displacement graphs of the sandwich composite conical shell with a height of 800 mm including axisymmetric imperfection.

The buckling loads of the conical shell with a height of 400 mm can be seen in table 7.5. It can be seen

that the buckling load decreases with increasing imperfection amplitude in the same way as the conical shell with a height of 800 mm. At an imperfection amplitude of 10% the KDF is equal to 0.71. This means that the model has a similar sensitivity to an axisymmetric imperfection as the the 800 mm height model. The force displacement graphs can be seen in figure 7.5. Similar results can be observed as for the force-displacement graphs of the 800 mm height model. The difference is that the post buckling paths of all models are different and do not converge. Moreover, the model with an imperfection amplitude of 100% is not showing any buckling as was seen for the cylindrical shell model with an imperfection amplitude of 100%. For this shell the same explanation can be used as given in the cylindrical shell section.

Table 7.5: Buckling loads of the sandwich composite conical shell with a height of 400 mm including axisymmetric imperfection.

Imperfection	0%	10%	20%	50%	100%
Buckling load [kN]	711.6	540.8	446.5	313.7	/
KDF [-]		0.71	0.59	0.41	/

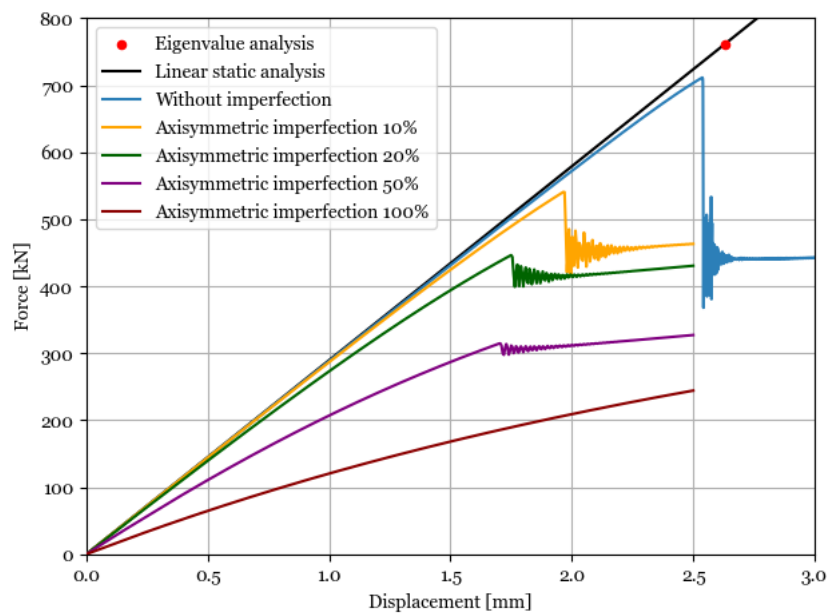


Figure 7.5: Force-displacement graphs of the sandwich composite conical shell with a height of 400 mm including axisymmetric imperfection.

### 7.2.3. Cylindrical-conical shell

For the cylindrical-conical shell two height models were analysed including an axisymmetric imperfection, one with a conical height of 400 mm and one with a conical height of 800 mm. The cylindrical shell part was kept the same and its height was equal to 800 mm. For the 1600 mm cylindrical-conical shell model 24 half waves were added and for the 1200 mm cylindrical-conical shell 18 half waves were added.

It should be noted that for cylindrical and conical shells the reduction in buckling load due to imperfections is a well studied aspect. However, for cylindrical-conical shells the behavior is not yet fully understood and the imperfection sensitivity is not fully known. There are also no design guidelines for these structures in which the KDFs are determined. Therefore, the KDFs that are presented in this thesis are not meant for design purposes. These were calculated to make a comparison with the KDFs of the cylindrical shell and cylindrical shells and to keep the consistency within this thesis.

From chapter 5 it is known that the difference between the eigenvalue analysis and dynamic implicit analysis is large due to the non-linear behavior. It should be noted that the KDF value determined for the separate shells is calculated by dividing the buckling load of the eigenvalue analysis by the buckling load of the dynamic implicit analysis including imperfections. This would mean that when calculating the KDF for the sandwich composite cylindrical-conical shells the value would be low due to the large difference between the eigenvalue analysis buckling load and dynamic implicit analysis buckling load. Therefore, for analysing

the imperfection sensitivity of the sandwich composite cylindrical-conical shells, two KDF factors were used: the KDF as defined for the separate shells and a KDF that only takes into account the reduction in buckling load due to imperfections ( $KDF_i$ ). This was done in order to isolate the effect of the reduction of the buckling load due to the non-linearity and imperfections. The  $KDF_i$  is a normalized buckling load that represents the reduction in buckling load due to imperfections only. This factor is calculated by dividing the buckling load determined by the model with imperfection by the buckling load determined by the model without imperfection (using the dynamic implicit buckling loads).

As already said above for these type of shells there are no guidelines or analytical expressions available to determine the KDF. This means that the KDFs can only be compared directly to the KDFs of the cylindrical shell and conical shells including an axisymmetric imperfection. The buckling loads of the 1600 mm sandwich composite cylindrical-conical shell including axisymmetric imperfection can be seen in table 7.6. The first thing to notice from the table is that the KDF at an imperfection amplitude of 10% has a value of 0.57. This means that there is a large reduction of the buckling load. However, when looking at the higher imperfection amplitudes it can be seen that the value does not decrease that much. This can be explained by the fact that the KDF also accounts for non-linearity as already explained. For the cylindrical-conical shell it is known that the non-linearity plays a big role when comparing the buckling loads of the eigenvalue analysis and dynamic implicit analysis. This means that it is logical that the KDF at an imperfection amplitude of 10% already shows a low KDF. Interesting to note is that the buckling load does not decrease that much when looking at higher imperfection amplitudes. In order to investigate the effect due to imperfections only the  $KDF_i$  values are used. What can be seen is that the  $KDF_i$  is 0.91 for a 10% imperfection amplitude, which means that the cylindrical-conical shell is not that sensitive to the axisymmetric imperfection shape.

For the comparison between the separate shells and the combined shell, the KDF values are compared in order to see the difference. What can be seen in table 7.6 is that the KDF value for the cylindrical-conical shell with imperfection amplitude of 10% is 0.57, which is lower compared to the KDFs of the separate models, see table 7.3 and table 7.4. However, it should be noted that the effect of the non-linearity is small for the separate shells (difference between eigenvalue analysis and dynamic implicit analysis of maximum 4.9%). For the sandwich composite cylindrical-conical shell this difference is 38%. This means that the cylindrical-conical shell has a smaller KDF compared to the separate shell models because of the non-linearity and not because of a higher imperfection sensitivity. When looking at the difference between the KDFs with imperfection amplitude of 10% and 20% of the separate shells and cylindrical-conical shell it can be seen that the cylindrical-conical shell shows a smaller decrease in KDF value than the separate shells. Moreover, when looking at the prebuckled shapes it could be seen that the cylindrical shell and conical shell were influenced by the axisymmetric imperfection while the cylindrical-conical shell was not. Due to these differences it can be concluded that the cylindrical-conical shell is much less sensitive to an axisymmetric imperfection when compared to the cylindrical shell and conical shell. This can be explained by the fact that the deformation shape right before buckling is around the interface and has more of a diamond pattern, see figure 5.3b. Since this is a completely different shape compared to an axisymmetric imperfection shape the cylindrical-conical shell is not very sensitive to an axisymmetric imperfection. It might be that an imperfection shape that more closely matches the deformed shape prior to buckling would have more of an impact on the buckling load.

The force-displacement graphs of the cylindrical-conical shell including axisymmetric imperfection can be seen in figure 7.6. What can be seen is that the buckling load decreases by a less extent when compared to the separate shell models, see figures 7.3 and 7.4. Moreover, the post buckling paths of the model without imperfection and axisymmetric amplitude of 10%, 20%, and 100% converge to the same value.

Table 7.6: Buckling loads of cylindrical-conical shell with a height of 1600 mm including axisymmetric imperfections.

<b>Imperfection</b>	<b>0%</b>	<b>10%</b>	<b>20%</b>	<b>50%</b>	<b>100%</b>
Buckling load [kN]	441.5	402.7	363.5	261.2	/
KDF [-]		0.57	0.51	0.37	/
$KDF_i$ [-]		0.91	0.82	0.59	/

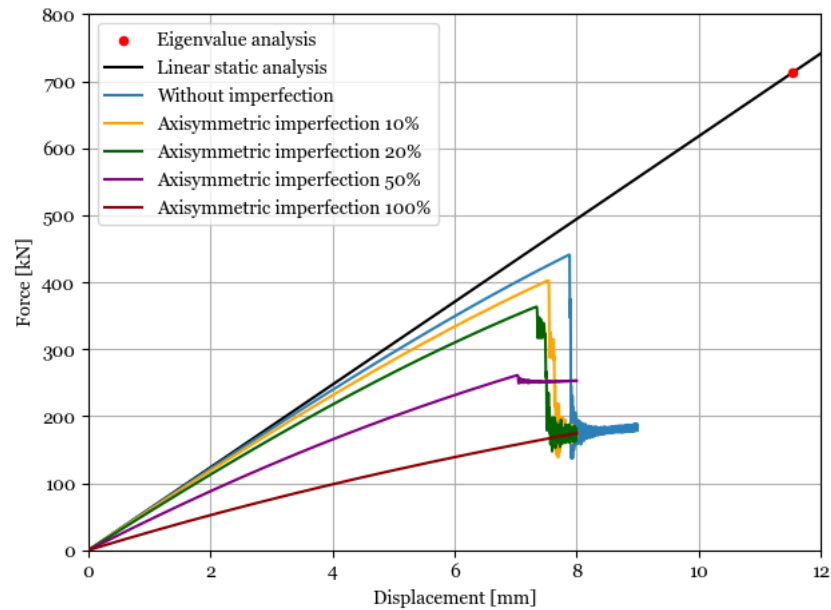


Figure 7.6: Force-displacement graphs of cylindrical-conical shell with a height of 1600mm including axisymmetric imperfection.

The buckling loads,  $KDF$ , and  $KDF_i$  of the cylindrical-conical shell with a height of 1200 mm can be seen in table 7.7. What can be seen is that this shell has a similar sensitivity to an axisymmetric imperfection as the 1600 mm shell. This means that the height of the conical shell does not influence the imperfection sensitivity of the cylindrical-conical shell. This was also observed for the conical shell. The force-displacement graphs can be seen in figure 7.7. The same trend can be observed as for the 1600 mm model. However, the post buckling paths of all models are different except for the model without imperfection and the model with an axisymmetric imperfection of 10%.

Table 7.7: Buckling loads of the sandwich composite cylindrical-conical shell with a height of 1200mm including axisymmetric imperfection.

<b>Imperfection</b>	<b>0%</b>	<b>10%</b>	<b>20%</b>	<b>50%</b>	<b>100%</b>
Buckling load [kN]	442.6	406.8	369.7	284.9	/
$KDF$ [-]		0.54	0.49	0.38	/
$KDF_i$ [-]		0.92	0.84	0.64	/



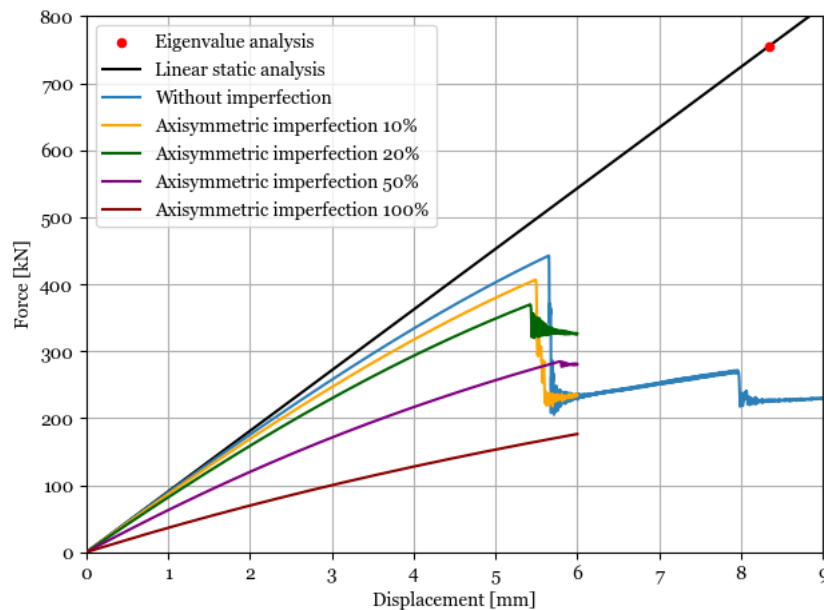


Figure 7.7: Force-displacement graphs of the sandwich composite cylindrical-conical shell with a height of 1200mm including axisymmetric imperfection.

### 7.3. Eigenmode imperfection

Another way to investigate the imperfection sensitivity of a shell is to use the eigenmodes extracted from the eigenvalue analysis. This method is used in many papers since it is an easy way to investigate the geometrical imperfection sensitivity of a shell in the early stages of the design process. In [28] a study is presented where a cylinder-cone-cylinder structure is analysed using the eigenmodes as an imperfection type. The results showed that the lowest KDF was obtained for the eigenmode imperfection when compared to the SPLA method and an axisymmetric imperfection. Due to these results, this section focuses on analysing the imperfection sensitivity using eigenmode imperfections. This in order to see if an eigenmode imperfection has greater effect on the buckling load than an axisymmetric imperfection. In this section two eigenmode imperfections were used to study the imperfection sensitivity, the eigenmode shape determined by the eigenvalue analysis and the eigenmode shape determined by the eigenvalue analysis after performing a preload. For this imperfection analysis only the model of the sandwich composite cylindrical-conical shell was used to investigate if this shell is not sensitive to other geometrical imperfections.

To implement the mode shape obtained by the eigenvalue analysis first the eigenvalue analysis had to be ran again in order to get a file with all the node locations of the mode shape. After that, the mode shape was added as an imperfection for the dynamic analysis by using the keyword \*IMPERFECTION. This keyword defines the mode shape that should be added and includes the amplitude. The amplitudes that were used for the analyses were 10%, 20%, 50%, and 100%. For this imperfection study the cylindrical-conical shell with a height of 1600 mm and 1200 mm were used. It should be noted that for the visualization of the imperfection sensitivity again two KDF factors were used: the KDF as defined for the separate shells and the  $KDF_i$  as described in the previous section.

#### 7.3.1. Eigenmode imperfection without preload

In this thesis the mode shape obtained by the eigenvalue analysis does not coincide with the deformation shapes from the dynamic implicit analysis. Since for the mode shape of the eigenvalue analysis nothing happens at the interface, the shape obtained by the eigenvalue analysis does not represent the buckling behavior of the sandwich composite cylindrical-conical shell. However, it is interesting to see if the structure is really not sensitive to this imperfection shape and, therefore, this mode shape was used as an imperfection for the cylindrical-conical shell. A visual representation of the mode shape can be seen in figure 5.1a.

The buckling loads, KDF, and  $KDF_i$  of the cylindrical-conical shell with a height of 1600 mm including the mode 1 imperfection can be seen in table 7.8. Again it can be seen that the KDF values are low, which can be explained due to the non-linear behavior of the cylindrical-conical shell. When looking at the  $KDF_i$

values it can be seen that the cylindrical-conical shell with a height of 1600 mm is not sensitive to the mode 1 imperfection. Only at an imperfection amplitude of 50% a reduction is seen, but this imperfection amplitude is not a realistic case. This is because an imperfection amplitude of 50% is equal to 1.475 mm, which does not happen due to manufacturing tolerances and due to regulations. Since there is almost no reduction in buckling load for the models with an imperfection amplitude of 10% and 20% it can be said that the shape obtained by the eigenvalue analysis is not a good representation of the imperfection sensitivity of the cylindrical-conical shell. The force-displacement graphs are shown in figure 7.8. What can be seen is that the graph of the model without imperfection and the graph of the models with an imperfection amplitude of 10% and 20% coincide with each other. The post-buckling path is also the same. This suggests that the post buckling shape is the same for each of the models. What can be concluded is that by adding the mode 1 as an imperfection it does not influence the buckling behavior of the cylindrical-conical shell. For the models with an imperfection amplitude of 50% and 100% the buckling behavior is different. This can be explained by the fact that these imperfections are an exaggeration of the reality.

When looking at the graph with an imperfection amplitude of 50% it can be seen that the solution stays constant after buckling. This is called a loading plateau. This phenomena is not meant to happen and is present here due to a numerical error. When this happens the solver is able to find a solution; however, this solution is not realistic. This problem can be solved by using smaller incremental parameters or a smaller displacement rate. The buckling load of this model was determined by using the highest point in the graph. It can also be seen that after the drop in the force-displacement graph the post-buckling path is the same as for the other models. When looking at the deformation shapes in the post-buckling regime of the different models it could be seen that the shapes were similar. This means that even when the behavior before collapse is different still the same post-buckling path can be obtained.

Table 7.8: Buckling loads of the sandwich composite cylindrical-conical shell with a height of 1600 mm including mode 1 imperfection shape.

Imperfection	0%	10%	20%	50%	100%
Buckling load [kN]	441.5	442.2	428.4	323.2	/
KDF [-]		0.62	0.60	0.45	/
$KDF_i$ [-]		1.00	0.97	0.73	/

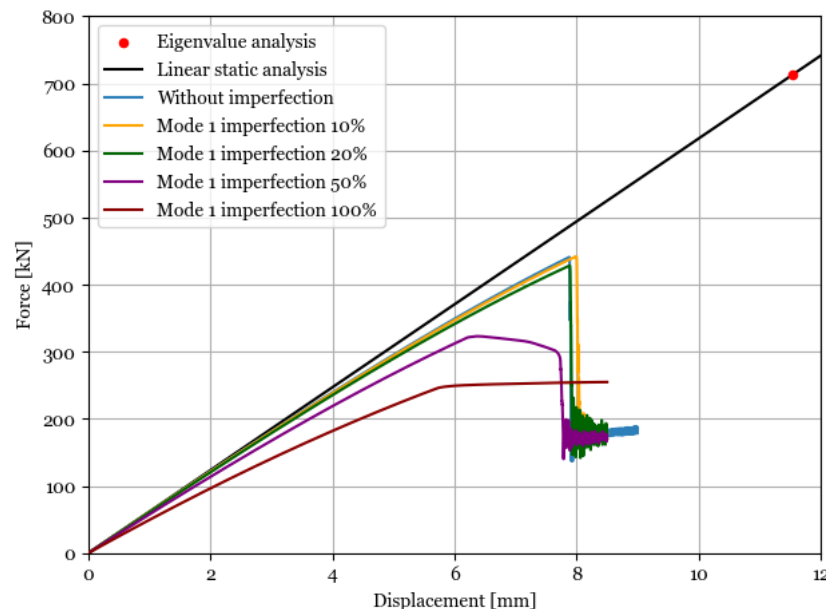


Figure 7.8: Force-displacement graphs of the sandwich composite cylindrical-conical shell with a height of 1600 mm including mode 1 imperfection shape with different amplitudes.

The buckling loads,  $KDF$ , and  $KDF_i$  of the cylindrical-conical shell with a height of 1200 mm including mode 1 imperfection with different amplitudes can be seen in table 7.9. What can be seen is that the  $KDF$  and  $KDF_i$  values are lower compared to the  $KDF$  and  $KDF_i$  values of the 1600 mm shell. When only looking at the  $KDF_i$  values it can be concluded that the cylindrical-conical shell with a height of 1200 mm is more imperfection sensitive to the mode 1 imperfection shape. This can be explained by the fact that the imperfection shape has a deformation closer to the transition. This was not seen for the 1600 mm shell because the deformation was located around the top of the shell. Since the transition area is the weakest part of the structure these results were expected. The force-displacement graphs can be seen in figure 7.9. In the figure it is shown that the stiffness of the models including imperfection amplitudes of 10% and 20% are the same as the stiffness of the model without imperfection. It can also be seen that the post buckling paths of the model without imperfection and the model including imperfection with an amplitude of 10% are similar. Furthermore, for the models with an imperfection amplitude of 50% and 100% the buckling load is less defined and the drop after buckling is not present.

Table 7.9: Buckling loads of the sandwich composite cylindrical conical shell with a height of 1200 mm including mode 1 imperfection shape with different amplitudes.

Imperfection	0%	10%	20%	50%	100%
Buckling load [kN]	442.6	423.2	389.5	300.4	/
$KDF$ [-]		0.56	0.52	0.40	/
$KDF_i$ [-]		0.96	0.88	0.68	/

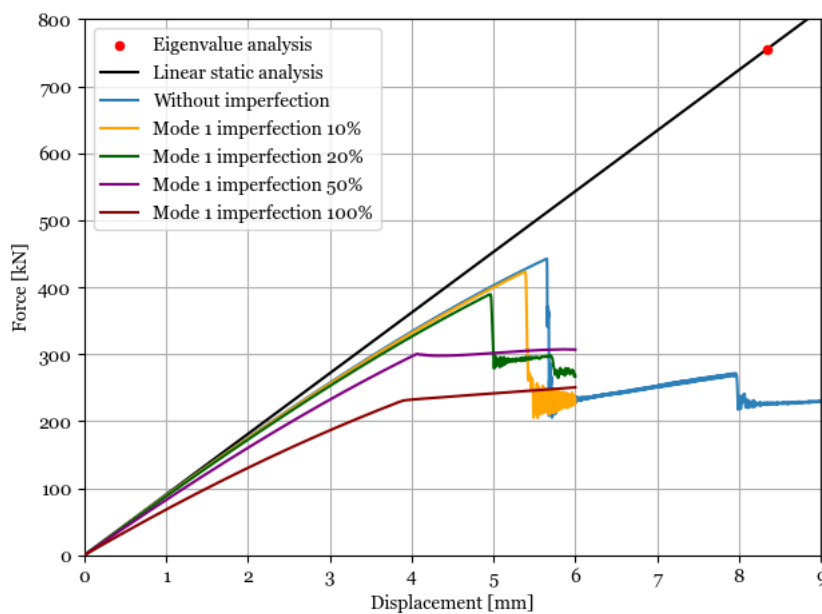


Figure 7.9: Force-displacement graphs of the sandwich composite cylindrical-conical shell with a height of 1200 mm including mode 1 imperfection shape with different amplitudes.

### 7.3.2. Eigenmode imperfection with preload

In order to also use a shape that is more representative as an imperfection for the cylindrical-conical shell the shape obtained by the analysis where a preloading is performed before executing the eigenvalue analysis was used. This is because this mode shape shows a diamond pattern deformation around the intersection and is similar to the deformation shape right before buckling for the dynamic implicit analysis. The shape that was used for this analysis is the mode shape obtained after preloading the structure by -200 kN and can be seen in figure 6.8a.

The buckling loads,  $KDF$ , and  $KDF_i$  of the cylindrical-conical shell with a height of 1600 mm including the mode 1 imperfection obtained after preloading the structure can be seen in table 7.10. It can be seen that the buckling load reduces with increasing imperfection amplitude. Moreover, it can be seen that this imperfec-

tion shape is more effective in decreasing the buckling load when compared to the mode shape imperfection added previously. It can also be observed that a similar imperfection sensitivity is obtained as for the axisymmetric imperfection. This means that the cylindrical-conical shell is not very sensitive to geometrical imperfections. Moreover, it can be concluded that it does not matter if the geometrical imperfection shape is similar to the deformation shape right before buckling of a perfect cylindrical-conical shell since the imperfection sensitivity of adding a mode 1 imperfection is the same as the imperfection sensitivity of adding an axisymmetric imperfection. The results suggest that the non-linear behavior at the intersection is dominating the buckling behavior of the whole shell resulting in that the cylindrical-conical shell not being sensitive to geometrical imperfections.

The force-displacement graphs are shown in figure 7.10. It can be seen that the mode 1 obtained after performing a preload has a bigger effect on the buckling load. It can also be seen that the stiffness of the different amplitude models are similar. Moreover, for all models the same post buckling path is followed. It can also be seen that the difference between the buckling loads and force-displacement graphs obtained by the 50% imperfection amplitude and the 100% imperfection amplitude are very close to each other. This means that the reduction in buckling load converges.

Table 7.10: Buckling loads of sandwich composite cylindrical-conical shell with a height of 1600 mm including mode 1 imperfection shape obtained after performing a preloading of the structure.

Imperfection	0%	10%	20%	50%	100%
Buckling load [kN]	441.5	397.2	371.3	341.15	332.7
KDF [-]		0.56	0.52	0.48	0.47
$KDF_i$ [-]		0.90	0.84	0.77	0.75

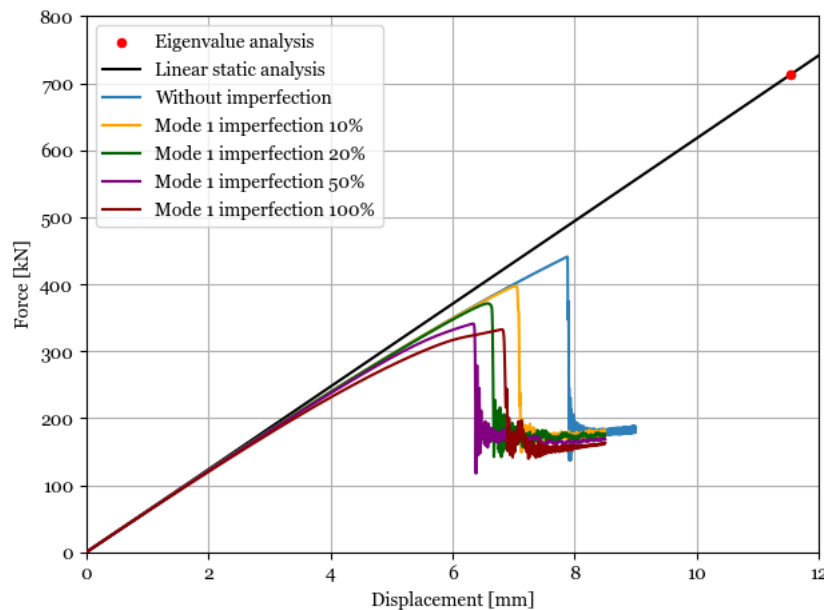


Figure 7.10: Force-displacement graphs of the sandwich composite cylindrical-conical shell with a height of 1600 mm including mode 1 imperfection shape after performing a preloading of the structure.

The buckling loads, KDF, and  $KDF_i$  of the 1200 mm cylindrical-conical shell including mode 1 imperfection after preloading the structure with different imperfection amplitudes can be seen in table 7.11. What can be seen is that the KDF and  $KDF_i$  values are very similar to the KDF and  $KDF_i$  values obtained for the 1600 mm including mode 1 imperfection shape with added preload. This means that both the 1200 mm and 1600 mm shells do not have a large imperfection sensitivity to geometrical imperfection. Moreover, the KDF and  $KDF_i$  value converges which was also seen for the 1600 mm shell.

The load displacement graphs can be seen in figure 7.11. What can be seen is that all the models have similar stiffness for the models without imperfection, imperfection amplitude of 10%, and imperfection amplitude of 20%. It is also interesting to note that the post buckling paths of all models converge to the same value.

Table 7.11: Buckling loads of the sandwich composite cylindrical-conical shell with a height of 1200 mm including mode 1 imperfection shape obtained after preloading of the structure with different amplitudes.

<b>Imperfection</b>	<b>0%</b>	<b>10%</b>	<b>20%</b>	<b>50%</b>	<b>100%</b>
Buckling load [kN]	442.6	397.4	371.9	346.4	340.6
KDF [-]		0.53	0.49	0.46	0.45
KDF <sub>i</sub> [-]		0.90	0.84	0.78	0.77

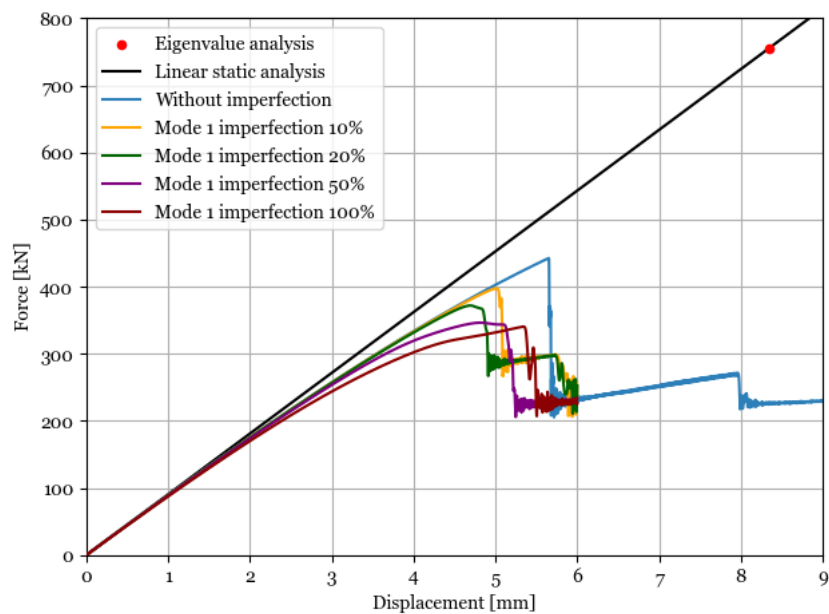
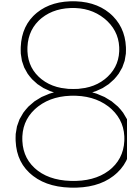


Figure 7.11: Force-displacement graphs of the sandwich composite cylindrical-conical shell with a height of 1200 mm including mode 1 imperfection shape after performing a preload to the structure with different amplitudes.





# Conclusion and recommendations

The purpose of the research was to better understand the buckling behavior of sandwich composite cylindrical, conical, and cylindrical-conical shells. Finite element analyses were used to compare the different shells. Moreover, the imperfection sensitivities of these shells were analysed. This chapter describes the conclusions that can be drawn from these analyses and gives recommendations for future work.

## 8.1. Conclusion

The goal of this thesis was to investigate the buckling behavior and imperfection sensitivity of sandwich composite cylindrical shells, conical shells, and cylindrical-conical shells. From the literature study it became clear that not a lot of research was performed on the buckling behavior of sandwich composite shells and cylindrical-conical shells. This thesis was meant to fill this gap in literature. The focus of this research was based on the numerical modelling of these structures. Three different finite element models were created: A sandwich composite cylindrical shell, a sandwich composite conical shell, and a cylindrical-conical shell. This in order to be able to compare the buckling behavior and imperfection sensitivity of the cylindrical shell and conical shell alone with the buckling behavior and imperfection sensitivity of the cylindrical-conical shell.

First, analyses were performed on the sandwich composite cylindrical and conical shell. The focus of these analyses was to determine which modelling techniques were best to model a sandwich composite shell. A mesh convergence study was performed for both shells and a mesh of 5 mm was considered best in terms of buckling behavior and computational time. Moreover, a comparison was performed on the different elements that can be used to model a sandwich composite shell. This was done by doing an eigenvalue analysis. The elements used were the S4R, SC8R, CSS8, and C3D8R. It should be noted that different models were created; using one element through the thickness or using three elements through the thickness, whereas two elements represent the face sheets and one element represents the core. From the comparison it became clear that the S4R element model and the SC8R element model were best in predicting the buckling behavior of the sandwich composite cylindrical and conical shell. These models gave the lowest computational time and similar buckling behavior compared to the other element models. What also could be observed was that the CSS8 element model gave an inaccurate prediction of the buckling load. The buckling load was about 6% higher compared to the buckling loads of the other element models. Moreover, for the sandwich composite conical shell the CSS8 element was not able to give the right modeshape. However, when 3 CSS8 elements through the thickness were used the results were better but the computational time increased significantly. Therefore, it was chosen to use the SC8R element model for further analyses.

For the sandwich composite cylindrical and conical shell an eigenvalue analysis and a dynamic implicit analysis were performed. For both models the buckling loads predicted by both analyses were close to each other, for the sandwich composite cylindrical shell the difference was 2.9% and for the sandwich composite conical shell the difference was 4.9%. Also the mode shapes and deformation shapes obtained by both analyses were similar. Moreover, the buckling load of the sandwich composite conical shell was lower compared to the sandwich composite cylindrical shell. This was expected due to the semi-vertex angle. For the sandwich composite cylindrical shell also the sensitivity to conical height was investigated. The semi-vertex angle was kept constant and the height was changed, heights between 200 mm and 800 mm were investigated. It could

be seen that the buckling load of the conical shell was independent of the height. Only for the 200 mm height model the buckling load increased but this can be explained by the fact that the structure looks more like a disc than a cone.

An eigenvalue analysis and dynamic implicit analysis were also performed for the sandwich composite cylindrical-conical shell. The buckling load determined by the eigenvalue analysis was the same as for the sandwich composite conical shell. When looking at the mode shape it could be seen that the conical part of the shell was showing deformation similar to the mode shape obtained for the conical shell alone. The cylindrical part was not taking part in the analysis. It looked like the cylindrical part was acting as a boundary condition. When this behavior was compared to the dynamic implicit analysis it could be seen that the buckling load of the dynamic implicit analysis was about 40% lower. Moreover, the shape right before buckling was showing deformation at the transition and no deformation in the conical part. This means that the eigenvalue analysis and dynamic analysis do not show similar results. This was not seen for the separate shells.

In order to investigate when this difference happens, a sensitivity study to conical height and semi-vertex angle was performed for the sandwich composite cylindrical-conical shell. It could be observed that the buckling load of the cylindrical-conical shell is independent of the height. Moreover, the eigenvalue analysis was again showing only deformation at the conical part of the shell and giving a buckling load close to the buckling loads of the conical shells with different heights alone. From these results it can be concluded that the eigenvalue analysis is giving a buckling load and mode shape similar to that of the separate shells, depending on which shell has the lowest buckling load. The difference in buckling load between the eigenvalue analysis and dynamic implicit was around 40% lower for the different height models. This means that the conical height does not play a role in the difference between the eigenvalue analysis and dynamic implicit analysis. Moreover, it could be seen that the sandwich composite cylindrical-conical shell is sensitive to a change in semi-vertex angle. When the semi-vertex angle decreased the difference in buckling loads determined by the eigenvalue analysis and dynamic implicit analysis also decreased. This was expected since for a cylindrical-conical shell with a semi-vertex angle of zero the difference should be negligible.

Since there was a difference between the eigenvalue analysis and dynamic implicit analysis, more research was performed to better understand the behavior that is happening at the transition which cannot be captured by the eigenvalue analysis. From the force-displacement graph of the sandwich composite cylindrical-conical shell it could be seen that there was non-linear behavior before buckling. Since the eigenvalue analysis is not able to capture non-linear effects it is logical that the eigenvalue analysis is giving a different behavior. To better understand what is happening at the transition and why this non-linear behavior happens, the radial displacements and strains were compared at the transition for both analyses. It could be seen that at the transition area the radial displacement for the dynamic implicit analysis was 23% higher compared to the radial displacement by the linear static analysis. It could also be seen that for the dynamic implicit analysis the structure was deforming inward before deforming outward, which was not seen for the linear static analysis. Moreover, the strains for the dynamic implicit analysis were around 30% higher for all plies compared to the linear static analysis. This means that due to the larger deformation and larger strains at the transition for the dynamic implicit analysis the stiffness is much lower compared to the linear analysis resulting in a lower buckling load. This large deformation causes the non-linear behavior seen. In the Abaqus manual it is explained that if there is non-linear behavior present before buckling it can be that the eigenvalue analysis is giving different results when compared to analyses that are able to capture non-linear effects. This is due to the fact that an eigenvalue analysis is linear and is not able to capture non-linear effects. Therefore, it was decided to add a preload to the structure before performing an eigenvalue analysis. This was done in order to show that when the deformation at the transition is present when performing the eigenvalue analysis, a better prediction can be given. This was done by using different values of the preload and it could be seen that the eigenvalue analysis was able to give a better prediction. It could even be observed that the mode shape showed deformation around the transition area and not only at the top of the conical shell. This means that the eigenvalue analysis alone is not able to give accurate results for the sandwich composite cylindrical-conical shell due to the large deformation at the transition.

The model of the sandwich composite cylindrical-conical shell was made by using the separate models of the cylindrical and conical shell and merging the nodes at the transition area. This results in a sharp corner at the transition. Therefore, a model was created including a radius of curvature at the transition to see if this could decrease the non-linear behavior of the sandwich composite cylindrical-conical shell. A radius of curvature of 380 mm was added to the transition and an increase of 20% of the buckling load was obtained. This resulted in a difference between the eigenvalue analysis and dynamic implicit analysis of 26%. The difference



is still large, however, it can be seen that a small radius of curvature already can give a large increase of the buckling load. This means that by using a radius of curvature that is large enough the non-linear behavior can be mitigated and a smaller difference between the eigenvalue analysis and dynamic implicit analysis can be obtained. Next to that the effect of adding a reinforcement to the structure was investigated. When adding a reinforcement of four  $0^\circ$  plies with a length of 300 mm at the transition an increase of the buckling load of 50% can be observed. This results in a difference between the eigenvalue analysis and dynamic implicit analysis of 4.1%. Moreover, the mode shape determined by the eigenvalue analysis and the deformation shape right before buckling for the dynamic implicit analysis show similar behavior. This means that by adding a reinforcement to the transition the radial deformation at the transition can be mitigated and the behavior at the intersection is not dominating the behavior anymore.

The imperfection sensitivities were compared for the sandwich composite cylindrical shell, conical shell, and cylindrical-conical shell models. By adding an axisymmetric imperfection to the structure the sensitivity to geometrical imperfections could be investigated. When an axisymmetric imperfection was added to the models it could be seen that the sandwich composite cylindrical and conical shell have a similar imperfection sensitivity. The sandwich composite cylindrical-conical shell showed a lower imperfection sensitivity. The normalized buckling loads due to an axisymmetric imperfection amplitude of 10% were 0.69, 0.71, and 0.57 for the cylindrical, conical, and cylindrical-conical shell, respectively. However, it should be noted that the effect of the non-linearity causes the small value of the normalized buckling load for the cylindrical-conical shell and is not due to imperfections. It could be seen that for higher imperfection amplitudes the buckling load decreases by a less extend when compared to the separate shell models. This means that the sandwich composite cylindrical-conical shell is not that sensitive to geometrical imperfections as the sandwich composite cylindrical and conical shell. For the sandwich composite cylindrical-conical shell also the effect of adding an eigenmode imperfection to the structure was investigated. The eigenmodes added were the first eigenmode of the eigenvalue analysis and first eigenmode of the eigenvalue analysis performed after a preload. The normalized buckling loads that only take into account imperfections due to the first eigenmode of the eigenvalue analysis and first eigenmode of the eigenvalue analysis performed after a preload using an amplitude of 10% were 1.00 and 0.90, respectively. Moreover, due to the fact that nothing happens with the buckling load of the sandwich composite cylindrical-conical shell when the first eigenmode of the eigenvalue analysis is added to the structure it can be said that the shape obtained by the eigenvalue analysis is not representing the buckling behavior of the shell and should not be used to predict the behavior of these shells. To conclude, the behavior at the intersection is dominating the behavior of the cylindrical-conical shell resulting in not being sensitive to geometrical imperfection.

From this research it can be concluded that a sandwich composite cylindrical-conical shell shows a different buckling behavior than a sandwich composite cylindrical shell and conical shell. This is due to the non-linear behavior happening at the interface for the cylindrical-conical shell, which was not seen for the separate shells. The non-linear behavior results in a large difference between the eigenvalue analysis and the dynamic implicit analysis. From the research done it could be seen that this non-linear behavior could be decreased by adding a radius of curvature at the interface or by reinforcing the structure at the interface using extra composite plies. This resulted in a smaller difference between the eigenvalue analysis and the dynamic implicit analysis. When looking at the imperfection sensitivity it could be seen that the sandwich composite cylindrical shell and conical shell were more sensitive to geometrical imperfections than the sandwich composite cylindrical-conical shell. This can be explained by the fact that the behavior at the interface is dominating the buckling behavior of the sandwich composite cylindrical-conical shell. The results of the thesis stress the importance of including non-linear effects when analysing cylindrical-conical shells.

## 8.2. Recommendations

In this thesis, only finite element analyses were performed to study the buckling behavior of sandwich composite cylindrical, conical, and cylindrical-conical shells. For cylindrical shells and conical shells the buckling behavior and modelling techniques are well known. However, for cylindrical-conical shells the buckling behavior is not studied that much and there are no validated finite element models available. In the thesis more insight was given in the behavior of these shells; however, when only performing finite element analyses the validity of the results are not known. This is very important because in the thesis, it could be seen that the eigenvalue analysis and dynamic implicit analysis showed a different buckling behavior. The results presented suggest that the eigenvalue analysis is not representative for the buckling behavior of these shells; however, this cannot be known without performing tests. Another reason why it is important to perform

buckling tests is that the buckling behavior can be better understood. These reasons stresses the importance of performing buckling tests on cylindrical-conical shells.

However, before the tests can be performed, test articles have to be created. The design proposed in this thesis fails before buckling which is not desired when actual buckling tests are performed. As already stated in the thesis, launch vehicle structures should be designed to fail after buckling. It should be noted that within this thesis the focus lied on sandwich composite cylindrical-conical shells, however, for the design of test articles composite cylindrical-conical shells can also be used.

Another interesting topic for future work is to further investigate the imperfection shapes that influence the buckling load. From this study, it could be seen that for the sandwich composite cylindrical and conical shell the axisymmetric imperfection showed a large reduction in the buckling load. For the sandwich composite cylindrical-conical shell it could be seen that the axisymmetric imperfection showed a small reduction in the buckling load. It could even be seen that the eigenmode shape almost did not influence the buckling load. Due to these differences it can be concluded that different geometrical imperfections result in different buckling loads for different shells. However, it is not yet known why some geometrical imperfections show a larger reduction in buckling load compared to other geometrical imperfections. It is of interest to know why certain imperfection shapes do influence the buckling load of some shells and why some imperfections shape do not influence the buckling load. This in order to know which geometrical imperfections result in the most conservative buckling load prediction.

# Bibliography

- [1] Rohacell® wf. Technical report, Evonik Resource Efficiency GmbH, 2017.
- [2] H. Abramovich. *Stability and vibrations of thin-walled composite structures*. Woodhead Publishing, 2017.
- [3] M. Alfano and C. Bisagni. Probabilistic buckling analysis of composite and sandwich cylindrical shells. In *55th AIAA/ASME/ASCE/AHS/ASC Structures, Structural Dynamics, and Materials Conference AIAA*, number 0166, 2014.
- [4] M. Alfano and C. Bisagni. Probability-based methodology for buckling investigation of sandwich composite shells with and without cut-outs. *International Journal of Computational Methods in Engineering Science and Mechanics*, 18(1):77–90, 2017.
- [5] M. Arbelo, R. Degenhardt, S. Castro, and R. Zimmermann. Numerical characterization of imperfection sensitive composite structures. *Composite Structures*, 108(1):295–303, 2014.
- [6] J. Arbocz and M. W. Hilburger. Towards a probabilistic preliminary design criterion for buckling critical composite shells. *AIAA Journal*, 43(8):1823–1827, 2005.
- [7] E.H. Baker. Experimental investigation of sandwich cylinders and cones subjected to axial compression. *AIAA Journal*, 6(9):1769–1770, 1968.
- [8] M. Baruch, J. Arbocz, and G. Q. Zhang. Laminated conical shells- Considerations for the variations of the stiffness coefficients. In *35th Structures, Structural Dynamics, and Materials Conference*, number 1634, 1992.
- [9] C. Bert, W. Crisman, and G. Nordby. Buckling of cylindrical and conical sandwich shells with orthotropic facings. *AIAA Journal*, 7(2):250–257, 1969.
- [10] C. Bisagni. Numerical analysis and experimental correlation of composite shell buckling and post-buckling. *Composites Part B: Engineering*, 31(8):655–667, 2000.
- [11] C. Bisagni and M. Alfano. Probabilistic buckling analysis of sandwich composite cylindrical shells based on measured imperfections. In *58th AIAA/ASCE/AHS/ASC Structures*, number 0886, 2017.
- [12] S. Castro. Ritz method for the analysis of unstiffened laminated composite cylinders and cones under axial compression. In *54th Israel Annual Conference on Aerospace Sciences*, volume 2, pages 1285–1302, 2014.
- [13] S. Castro, R. Zimmermann, M. Arbelo, R. Khakimova, M. W. Hilburger, and R. Degenhardt. Geometric imperfections and lower-bound methods used to calculate knock-down factors for axially compressed composite cylindrical shells. *Thin-Walled Structures*, 74:118–132, 2014.
- [14] G. Cha and M. R. Schultz. Buckling analysis of a honeycomb-core composite cylinder with initial geometric imperfections. Technical report, 2013.
- [15] C. Chamis. Mechanics of composite materials: past, present, and future. *NASA TM 100793*, 2019.
- [16] E. Clarkson. Hexcel 8552 im7 unidirectional prepreg 190 gsm and 35 percent rc, qualification material property data report. Technical report, National Institute for Aviation Research, Wichita State University, 2017.
- [17] R. Degenhardt, A. Kling, A. Bethge, J. Orf, L. Kärger, R. Zimmermann, K. Rohwer, and A. Calvi. Investigations on imperfection sensitivity and deduction of improved knock-down factors for unstiffened CFRP cylindrical shells. *Composite Structures*, 92(8):1939–1946, 2010.

- [18] Dessault Systems. Abaqus analysis guide, 2019.
- [19] M. Di Pasqua, R. Khakimova, S. Castro, M. Arbelo, A. Riccio, and R. Degenhardt. The influence of geometrical parameters on the buckling behavior of conical shell by the single perturbation load approach. *Applied Composite Materials*, 22(4):405–422, 2015.
- [20] M. F. Di Pasqua, R. Khakimova, S. G.P. Castro, M.A. Arbelo, A. Riccio, A. Raimondo, and R. Degenhardt. Investigation on the geometric imperfections driven local buckling onset in composite conical shells. *Applied Composite Materials*, 23(4):879–897, 2016.
- [21] Y. Goldfeld and J. Arbocz. Buckling of laminated conical shells given the variations of the stiffness coefficients. *AIAA Journal*, 42(3):642–649, 2004.
- [22] G. Henson. Materials for launch vehicle structures. In *Aerospace Materials and Applications, Progress in Astronautics and Aeronautics*, number 504, 2016.
- [23] M. W. Hilburger. High-fidelity buckling analysis of composite cylinders using the STAGS finite element code. In *55TH AIAA/ASME/ASCE/AHS/ASC structures, Structural Dynamics, and materials Conference*, number 0846, 2014.
- [24] M. W. Hilburger and J. H. Starnes. High-fidelity nonlinear analysis of compression-loaded composite shells. In *19th AIAA Applied Aerodynamics Conference*, number 1394, 2001.
- [25] M. W. Hilburger and J. H. Starnes. Effects of imperfections of the buckling response of composite shells. *Thin-Walled Structures*, 42:369–397, 2004.
- [26] M. W. Hilburger, M. P. Nemeth, and J. H. Starnes. Shell buckling design criteria based on manufacturing imperfection signatures. *AIAA Journal*, 44(3):654–663, 2006.
- [27] C. Hühne, R. Rolfes, and J. Tessmer. A new approach for robust design of composite cylindrical shells under axial compression. In *Proceedings of the European Conference on Spacecraft Structures*, number 581, 2005.
- [28] M S Ismail, O Ifayefunmi, and SH S M Fadzullah. Buckling of imperfect cylinder-cone-cylinder transition under axial compression. *Thin Walled Structures*, 144:106–250, 2019. ISSN 0263-8231.
- [29] Christos Kassapoglou. *Design and analysis of composite structures: with applications to aerospace structures*. John Wiley & Sons, 2013.
- [30] J. Kepple, B. G. Prusty, G. Pearce, D. Kelly, R. Thomson, and R. Degenhardt. Influence of imperfections on axial buckling load of composite cylindrical shells. In *19th International Conference on Composite Materials*, number 5332, 2013.
- [31] J. Kepple, M. Herath, G. Pearce, B. Gangadhara Prusty, R. Thomson, and R. Degenhardt. Stochastic analysis of imperfection sensitive unstiffened composite cylinders using realistic imperfection models. *Composite Structures*, 126:159–173, 2015.
- [32] R. Khakimova, C. Warren, R. Zimmermann, S. Castro, M. Arbelo, and R. Degenhardt. The single perturbation load approach applied to imperfection sensitive conical composite structures. *Thin-Walled Structures*, 84:369–377, 2014.
- [33] R. Khakimova, R. Zimmermann, M. Francesca, D. Pascua, S. Castro, M. Arbelo, and R. Degenhardt. Buckling and postbuckling of truncated conical shells with varying semi-vertex angle: the use of the single perturbation load approach. In *54th Israel Annual Conference on Aerospace Sciences*, number 2, 2014.
- [34] R. Khakimova, F. Burau, R. Degenhardt, M. Siebert, and S. G.P. Castro. Design and manufacture of conical shell structures using prepreg laminates. *Applied Composite Materials*, 23(3):289–312, 2016.
- [35] R. Khakimova, D. Wilckens, J. Reichardt, R. Zimmermann, and R. Degenhardt. Buckling of axially compressed CFRP truncated cones: experimental and numerical investigation. *Composite Structures*, 146: 232–247, 2016.

- [36] R. Khakimova, R. Zimmermann, D. Wilckens, K. Rohwer, and R. Degenhardt. Buckling of axially compressed CFRP truncated cones with additional lateral load: Experimental and numerical investigation. *Composite Structures*, 157:436–447, 2016.
- [37] R. Khakimova, S. G.P. Castro, D. Wilckens, K. Rohwer, and R. Degenhardt. Buckling of axially compressed CFRP cylinders with and without additional lateral load: Experimental and numerical investigation. *Thin-Walled Structures*, 119:178–189, 2017.
- [38] D. N. Kosareo, S. T. Oliver, B. A. Bednarczyk, and E. J. Pineda. Buckling design and analysis of a payload fairing 1/6th cylindrical arc-segment panel. In *55th AIAA/ASME/ASCE/AHS/SC Structures, Structural Dynamics, and Materials Conference AIAA*, number 1053, 2014.
- [39] A. C. Orifici and C. Bisagni. Perturbation-based imperfection analysis for composite cylindrical shells buckling in compression. *Composite Structures*, 106:520–528, 2013.
- [40] F. Peña, W.L. Richards, A.R. Parker, A. Piazza, M.R. Schultz, M.T. Rudd, N.W. Gardner, and M.W. Hilburger. Implementation of fiber optic sensing system on sandwich composite cylinder buckling test. In *AIAA/ASCE/AHS/ASC Structures, Structural Dynamics, and Materials Conference*, number 210049, 2018.
- [41] J.P. Peterson. Space vehicle design: buckling of thin-walled truncated cones. Technical report, 1968.
- [42] J.P. Peterson. Space vehicle design: buckling thin-walled circular cylinders. Technical report, 1968.
- [43] A. Przekop, M.R. Schultz, and M.W. Hilburger. Design of buckling-critical large-scale sandwich composite cylinder test articles. In *2018 AIAA/ASCE/AHS/ASC Structures, Structural Dynamics, and Materials Conference*, number 1694, 2018.
- [44] C. D. Reese and C. W. Bert. Simplified design equations for buckling of axially compressed sandwich cylinders with orthotropic facings and core. *Journal of aircraft*, 6(6):515–519, 1969.
- [45] M. Schultz and M. Nemeth. Buckling imperfection sensitivity of axially compressed orthotropic cylinders. In *51st AIAA/ASME/ASCE/AHS/ASC Structures conference*, number 2531, 2010.
- [46] M. Schultz, D. Sleight, D. Myers, P. Allen Waters, W. Jr. Chunchu, A. Lovejoy, and M. W. Hilburger. Buckling design and imperfection sensitivity of sandwich composite launch-vehicle shell structures. In *American Society For Composites 2016 Thirty-First Technical Conference*, number 3505, 2016.
- [47] M. R. Schultz, D. W. Sleight, N. W. Gardner, M.T. Rudd, M. W. Hilburger, T. Palm, and N. J. Oldfield. Test and analysis of a buckling-critical large-scale sandwich composite cylinder. In *2018 AIAA/ASCE/AHS/ASC Structures, Structural Dynamics, and Materials Conference*, number 1693, 2018.
- [48] D. W. Sleight, A. Satyanarayana, and M. R. Schultz. Buckling imperfection sensitivity of conical sandwich composite structures for launch-vehicles. In *2018 AIAA/ASCE/AHS/ASC Structures, Structural Dynamics, and Materials Conference*, number 1696, 2018.
- [49] ASM Aerospace specification metals inc. Aluminum 2024-t4; 2024-t351, 1990. URL <http://asm.matweb.com/search/specificmaterial.asp?bassnum=ma2024t4>.
- [50] A. Tafreshi. Efficient modelling of delamination buckling in composite cylindrical shells under axial compression. *Composite Structures*, 64(3-4):511–520, 2004.
- [51] J G Teng. Elastic buckling of cone-cylinder intersection under localized circumferential compression. *Engineering Structures*, 18(1):41–48, 1996.
- [52] I. Uriol Balbin, C. Bisagni, M. R. Schultz, and M. W. Hilburger. Scaling methodology for buckling of sandwich composite cylindrical structures. In *2018 AIAA/ASCE/AHS/ASC Structures, Structural Dynamics, and Materials Conference*, number 1988, 2018.
- [53] H. N.R. Wagner, C. Hühne, and S. Niemann. Constant single-buckle imperfection principle to determine a lower bound for the buckling load of unstiffened composite cylinders under axial compression. *Composite Structures*, 139:120–129, 2016.

- [54] H. N.R. Wagner, C. Hühne, and S. Niemann. Robust knockdown factors for the design of axially loaded cylindrical and conical composite shells – Development and Validation. *Composite Structures*, 173:281–303, 2017.
- [55] H. N.R. Wagner, C. Hühne, S. Niemann, and R. Khakimova. Robust design criterion for axially loaded cylindrical shells - Simulation and Validation. *Thin-Walled Structures*, 115:154–162, 2017.
- [56] H. N.R. Wagner, C. Hühne, K. Rohwer, S. Niemann, and M. Wiedemann. Stimulating the realistic worst case buckling scenario of axially compressed unstiffened cylindrical composite shells. *Composite Structures*, 160:1095–1104, 2017.
- [57] H. N.R. Wagner, C. Hühne, and R. Khakimova. Towards robust knockdown factors for the design of conical shells under axial compression. *International Journal of Mechanical Sciences*, 146-147:60–80, 2018.
- [58] B. Wang, S. Zhu, P. Hao, X. Bi, K. Du, B. Chen, X. Ma, and Y. Chao. Buckling of quasi-perfect cylindrical shell under axial compression: A combined experimental and numerical investigation. *International Journal of Solids and Structures*, 130-131:232–247, 2018.
- [59] B. Wang, K. Du, P. Hao, K. Tian, Y. J. Chao, L. Jiang, S. Xu, and X. Zhang. Experimental validation of cylindrical shells under axial compression for improved knockdown factors. *International Journal of Solids and Structures*, In Press, 2019.
- [60] B. Wang, X. Ma, P. Hao, Y. Sun, K. Tian, G. Li, K. Zhang, L. Jiang, and J. Guo. Improved knockdown factors for composite cylindrical shells with delamination and geometric imperfections. *Composites Part B: Engineering*, 163:314–323, 2019.
- [61] V. I. Weingarten, E. J. Morgan, and P. Seide. Elastic stability of thin-walled cylindrical and conical shells under axial compression. *AIAA Journal*, 3(3):500–505, 1965.
- [62] Y. Zhao and J. G. Teng. A stability design proposal for cone – cylinder intersections under internal pressure. *international journal of pressure vessels and piping*, 80:297–309, 2003.
- [63] Y. Zhao and J.G. Teng. Buckling experiments on cone-cylinder intersections under internal pressure. *Engineering Mechanics*, 127:1231–1239, 2001.